

POLITECNICO DI TORINO

College of Mechanical Engineering

Master of Science in Mechanical Engineering

Thesis

The Mechanical Characterization of TRM composite materials for structural applications



Supervisor

Prof. Alessia Monaco

Prof. Francesco Tondolo

Candidate

Muhammad Ali

S262588

February 28, 2023

Contents

Chapter 1: Introduction to composites	8
1.1 The use of FRCs for Structural applications.....	8
1.1.1 Types of FRC on basis of Matrix.....	9
1.1.2 Fiber Reinforced Polymers	10
1.1.3 Textile Reinforced Mortars.....	11
1.2 Typical Fibers adopted in TRM systems	12
1.3 Natural Fibers	12
1.4 Synthetic fibers.....	13
1.5 Objectives of the thesis	14
1.6 References	15
Chapter 2: State of the Art on tensile testing of TRM materials	16
2.1 Experimental campaign by Arboleda et al. (2016)	16
2.1.1 TRM composites	17
2.1.2 Fiber reinforcement.....	18
Figure 2. 1 : a) PBO; b) Glass fiber; c) Coated glass fiber; d) Carbon fiber; e) coated carbon fiber	18
2.1.3 Inorganic Matrix	19
2.1.4 Specimen preparation	19
2.1.5 Results	19
2.2 Experimental campaign by Malena et al. (2019).....	22
2.2.1 Tests on Dry fibers	25
2.2.2 Tests on composites	25
2.3 Numerical Modelling by Malena (2019).....	26
2.3.1 Constitutive model	27
2.3.2 Numerical modelling of fiber layer	28
2.3.3 Numerical modelling of mortar layer	28
2.3.4 Numerical modelling of the interface.....	30
2.3.5 Numerical results.....	30
2.4 Numerical Modelling by Monaco et al. (2020).....	32
2.4.1 Perfect Bond	32
2.4.2 Cohesive traction-separation law.....	34
2.4.3 Meshing and boundary conditions.....	35
2.4.4 Mechanical characterization of TRM.....	37
2.4.5 Validation of numerical results against experimental data.....	39
2.5 Experimental campaign by D’Anna et al. (2021)	41
2.5.1 Tensile testing of TRM	42

2.5.2	Testing of fiber specimen	42
2.5.3	Testing of mortar specimen.....	43
2.5.4	Testing of BTRM specimen	44
2.5.5	Results	46
2.6	References	49
Chapter 3: Numerical modeling with ABAQUS.....		51
3.1	Introduction to ABAQUS CAE	51
3.2	Geometry.....	53
3.3	Material Properties.....	55
3.4	Concrete Damage Plasticity.....	55
3.5	Interactions.....	63
3.5.1	Node to surface interactions	64
3.5.2	Surface-to-surface interaction.....	66
3.5.3	Cohesive interaction	68
3.6	Damage initiation criteria	71
3.7	Damage propagation criteria.....	72
3.8	Constraints.....	74
3.8.1	Rigid Body Constraint	75
3.8.2	Embedded region constraint	76
3.9	Step.....	76
3.10	Analysis Procedure	78
3.10.1	Newton's Method.....	79
3.10.2	Quasi-Newton Method	79
3.11	Mesh	80
3.12	Job.....	84
3.13	References	85
Chapter 4: Experimental activity		86
4.1	Preparation of mortar specimens	87
4.2	Experimental tests	89
4.2.1	Flexural tests.....	90
4.2.2	Compression test	91
4.3	Results	92
4.3.1	Results of Flexural test	93
4.3.2	Compression test	94
Chapter 5: Numerical Modelling of tensile behavior		96
5.1	FEM model from experimental data	96

5.2	Development of numerical model.....	97
5.2.1	Part Module	98
5.2.2	Material Properties Module	99
5.2.3	Section Module.....	100
5.2.4	Assembly Module	103
5.2.5	Step Module	104
5.2.6	Constraint Module.....	106
5.2.7	Interaction module	107
Chapter 6: Results and Comparisons		109
6.1	Comparison between experimental and numerical data by Arboleda et al. (2016)	109
6.2	Comparison with S1-PBO-Clamp	110
6.3	Comparison with S1-PBO-Clevis	112
6.4	Comparison with S1-CTRM-Clevis	115
6.5	Comparison with S1-GTRM-Clamp	118
6.6	Comparison with S1-cGTRM-Clamp	120
6.7	Comparison with S1-CTRM-Clamp	122
Chapter 7: Conclusions		126

List of Tables

Table 2. 1 : Mechanical Properties of yarn	18
Table 2. 2 : Properties of inorganic Matrices	19
Table 2. 3 : Experimental Results of tests on each specimen.....	20
Table 2. 4 : Mechanical Parameters of steel	28
Table 2. 5 : Specification of experimental tests	39
Table 2. 6 : Results of BTRM coupon in all stages	47
Table 4. 1 : Data from flexural strength test	94
Table 4. 2 : Data from Compressive tests.....	95
Table 5. 1 : Material Properties of TRM materials	100
Table 6. 1 : Specimen ID	110
Table 6. 2 : Properties of S1-PBO-Clamp	110
Table 6. 3 : Results from Numerical Model of S1-PBO-Clamp.....	111
Table 6. 4 : Data from Numerical model	112
Table 6. 5 : Data From Arboleda et al. along with error.....	112
Table 6. 6 : Properties of S1-PBO-Clevis	113
Table 6. 7 : Results from Numerical Model of S1-PBO-Clevis.....	114
Table 6. 8 : Data from Numerical model	115
Table 6. 9 : Data From Arboleda et al. along with error.....	115
Table 6. 10 : Properties of S1-CTRM-Clevis	115
Table 6. 11: Results from Numerical Model of S1-CTRM-Clevis.....	116
Table 6. 12 : Data from Numerical model	117
Table 6. 13 : Data From Arboleda et al. along with error.....	117
Table 6. 14 : Properties of S1-GTRM-Clevis.....	118
Table 6. 15 : Results from Numerical Model of S1-GTRM-Clamp	118
Table 6. 16 : Data from Numerical model	120
Table 6. 17 : Data From Arboleda et al. along with error.....	120
Table 6. 18 : Properties of S1-cGTRM-Clamp	120
Table 6. 19 : Results from Numerical Model of S1-cGTRM-Clamp.....	121
Table 6. 20 : Data from Numerical model	122
Table 6. 21 : Data From Arboleda et al. along with error.....	122
Table 6. 22 : Properties of S1-CTRM-Clamp	123
Table 6. 23 : Results from Numerical Model of S1-CTRM-Clamp.....	123
Table 6. 24 : Data from Numerical model	125
Table 6. 25 : Data From Arboleda et al. along with error.....	125

List of Figures

Figure 1.1 : Types of FRC	8
Figure 2. 1 : a) PBO; b) Glass fiber; c) Coated glass fiber; d) Carbon fiber; e) coated carbon fiber	17
Figure 2. 2 : Stress strain curve for single layer using Clevis-grip.....	19
Figure 2. 3 : Stress strain curve for single layer using Clamping-grip.....	20
Figure 2. 4 : BPO-TRM Clamping-grip vs Clevis-Grip	20
Figure 2. 5 : C-TRM Clamping-Grip vs Clevis-Grip.....	21
Figure 2. 6 : Experimental setup for direct tensile test on SRG specimens: (a) clamping-grip setup (b) clevis-grip setup.....	22
Figure 2. 7: Experimental test results on dry textile vs composite using Clamping-grip	25
Figure 2. 8 : FEM Mesh a) Clamping-grip setup b) Clevis-grip setup c) clamping-grip mesh d) Clevis-grip mesh	26
Figure 2. 9 : a) Adopted ductile damage constitutive law b) numerical results	27
Figure 2. 10 : CDP Stress-Strain model in tension	28
Figure 2. 11 : Graphical representation of numerical and experimental results a) Clamping-grip b) Clevis-grip.....	30
Figure 2. 12 : Tensile strain in mortar a)crack initiation b) failure point c) direct tensile test	30
Figure 2. 13 : a) Experimental failure mode b) Mortar model failure c) load capacity bs tab length relationship.....	31
Figure 2. 14 : Perfect bond	32
Figure 2. 15 : Orthotropic lamina behavior of fiber	32
Figure 2. 16 : Cohesive model	34
Figure 2. 17 : 1) Perfect Bond 2) Cohesive interaction	34
Figure 2. 18 : TRM Specimen with BCs	35
Figure 2. 19 : Mesh of Fiber and Mortar	35
Figure 2. 20 : Constitutive model A) For compression B) For tension	37
Figure 2. 21 : Damage perimeters of mortar.....	37
Figure 2. 22 : Damage Evolution at interface	38
Figure 2. 23 : Comparison of Numerical model and exoerimental campaign.....	38
Figure 2. 24 : A) Axial stiffness in damage evolution phase B) Ultimate tensile capacity.....	39
Figure 2. 25 : Comparison between crack patterns	40
Figure 2. 26 : Specimen specifications for Basalt fiber testing.....	41
Figure 2. 27 : Tensile test of Basalt grid a) Test setup using DICM b) Specimen installed on testing machine	41
Figure 2. 28 : Positioning of Virtual Extensometer on Fiber specimen	42
Figure 2. 29 : a) Position of virtual extensometer b) Stress-strain curve of SP2_1L c) Stress-strain curve of SP4_1L d) Stress-strain curve of SP4_7L.....	43
Figure 2. 30 : Manufacturing of BTRM Coupon a) Coupon slab b) Curing of specimen	44
Figure 2. 31: BTRM specimen with tabs and speckle pattern	44
Figure 2. 32 : Additional reinforcement in single layer BTRM.....	45
Figure 2. 33 : Stress-strain curve a) Wrap direction b) Weft direction.....	46
Figure 2. 34 : Cracking pattern in a) One-layer reinforced specimen SP8_1L b) Two-layer reinforced specimen SP2_2L c) Three-layered reinforced specimen SP1_3L	47
Figure 2. 35 : Load displacement curves of in a) One-layer reinforced specimen SP8_1L b) Two-layer reinforced specimen SP2_2L c) Three-layered reinforced specimen SP1_3L.....	47

Figure 3. 1 : Stress-Strain curve a) For compression b) For mortar	55
Figure 3. 2 : Mohr-Coulomb criterion a) Mohr circle representation b) Stresses in tangential and normal direction	56
Figure 3. 3 : Material behavior	58
Figure 3. 4 : Material Module, ABAQUS interface	59
Figure 3. 5 : CDP Interface	61
Figure 3. 6 : Interaction Interface	62
Figure 3. 7 : Master and slave nodes, node-to-surface interaction	63
Figure 3. 8 : Node-to-surface interaction, considering first two conditions	64
Figure 3. 9 : Node-to-surface contact, considering the large surface as slave surface.	64
Figure 3. 10 Node-to-surface interaction	65
Figure 3. 11 : Surface-to-surface interaction, smaller surface as masters surface	66
Figure 3. 12 : Master and Slave surface in surface-to-surface contact	66
Figure 3. 13 : Cohesive interaction, ABAQUS interface	67
Figure 3. 14 : Cohesive interaction, ABAQUS interface	68
Figure 3. 15 : Linear elastic traction separation law	69
Figure 3. 16: Damage evolution, Separation based	70
Figure 3. 17 : Damage evolution, Separation based	72
Figure 3. 18 : Damage evolution criteria, energy based	73
Figure 3. 19: Rigid body constraint, ABAQUS Dialogue Box	74
Figure 3. 20: Embedded constraint, ABAQUS Dialogue box	75
Figure 3. 21: Step Dialogue Box	77
Figure 3. 22 : Step Module, Newton's and quasi-Newton's method	79
Figure 3. 23 : Element type, Mesh ABAQUS interface	80
Figure 3. 24 : Element shape, mesh module	81
Figure 3. 25 : Remeshing rule, mesh module	82
Figure 3. 26 : Verify mesh, mesh module	83
Figure 4. 1 : Weight Balance	86
Figure 4. 2 : Graduated cylinder	87
Figure 4. 3 : Mortar specimen mold Figure 4. 4: Filled mold	87
Figure 4. 5 : Mold mounted on the tamper machine	88
Figure 4. 6 : Mortar specimen	89
Figure 4. 7: Flexural testing machine	90
Figure 4. 8: Specimen of compression test	90
Figure 4. 9 : Universal tensile testing machine	91
Figure 4. 10 : Specimen failed under compressive load	91
Figure 4. 11: Force displacement Curves from M2 to M12 specimen	92
Figure 4. 12 : Trend under compressive load	94
Figure 5. 1 : Fiber Part module Figure 5. 2 : Meshed Fiber	97
Figure 5. 3 : Mortar part module Figure 5. 4 : Meshed mortar	98
Figure 5. 5: Section module of fiber, ABAQUS interface	100
Figure 5. 6 : Section plane on mortar	100
Figure 5. 7 : Mortar Section assignment	101
Figure 5. 8 : Aluminum Tabs section assignment	101
Figure 5. 9 : Fiber Section assignment	101
Figure 5. 10 : ABAQUS assembly Module	102
Figure 5. 11 : Material orientation of Fiber Figure 5. 12 : Material orientation of mortar	103

Figure 5. 13 : Encaster Boundary condition	103
Figure 5. 14 : Displacement BC.....	104
Figure 5. 15 : Displacement BC.....	104
Figure 5. 16 : Rigid body constraint.....	105
Figure 5. 17 : Interaction-Cohesive law	106
Figure 5. 18 : Cohesive Interaction properties	107
Figure 6. 1 : Stress vs strain comparison for S1-PBO-Clamp	111
Figure 6. 2 : Stress vs strain comparison for S1-PBO-Clevis	113
Figure 6. 3 : Stress vs strain comparison for S1-CTRM-Clevis	116
Figure 6. 4 : Stress vs strain comparison for S1-GTRM-Clamp	118
Figure 6. 5 : Stress vs strain comparison for S1-cGTRM-Clamp.....	121
Figure 6. 6 : Stress vs strain comparison for S1-CTRM-Clamp.....	123

Chapter 1: Introduction to composites

Composites are artificially prepared materials which comprise of at least two different components mainly a matrix and reinforcing agent. Their physical properties as well as chemical properties are quite different from one another. These properties are not altered during the manufacturing process, and they remain unchanged even in the finished composite product. Most of the composites comprise of matrices which have weaker mechanical properties as compared to the fiber which is relatively strong in term of mechanical properties like tensile behaviour and strength etc. The main goal is to get a finished product with high strength-to-weight ratio as well as other benefits like corrosion resistance and water proofing. Most widely used commercial materials usually consist of glass fibers couples with various types of polymeric matrices, mostly thermoplastics and thermosetting plastics.

Currently, in the literature many researchers have recommended thermoplastics due to their mouldability characteristics. But on the other hand, thermoplastics have high manufacturing cost, that has made them less preferable. In addition to this, thermoplastics are incarnated with specific problems of wear, fracture toughness and many more.

Composite materials have a lot of applications related to engineering, construction and manufacturing. Now, fiber reinforced composites with natural or synthetic fiber layers are gaining more and more importance and demand in the market due to their light weight and high strength.

1.1 The use of FRCs for Structural applications

A Fiber Reinforced Composites (FRC) basically consist of two components: the fibers and the matrix and between them there is a thin interphase region [1][2].

Among FRC, Fiber-Reinforced Polymers (FRPs) have high strength to weight ratio and exhibit exceptional properties such as high durability, stiffness, flexural strength, and resistance to corrosion, wear, impact, and fire. Due to these widespread and unique features, the FRP have a lot of applications in mechanical, construction, automobile, aerospace, biomedical and many other manufacturing and engineering industries.

Performance of these composites depend on the type and properties of matrix, fiber and the interface as well as manufacturing techniques. Therefore, the properties of various

fibers, interfaces, layout patterns, their classifications and the manufacturing techniques need to be deeply investigated in order to optimize the characteristics which are essential for the specific applications [3].

1.1.1 Types of FRC on basis of Matrix

FRC can be classified into five groups according to their matrices.

- metal matrix composites (MMCs)
- ceramic matrix composites (CMCs)
- carbon/carbon composites (C/C)
- polymer matrix composites or Fiber Reinforced Polymers (FRP)
- Textile Reinforced Mortar

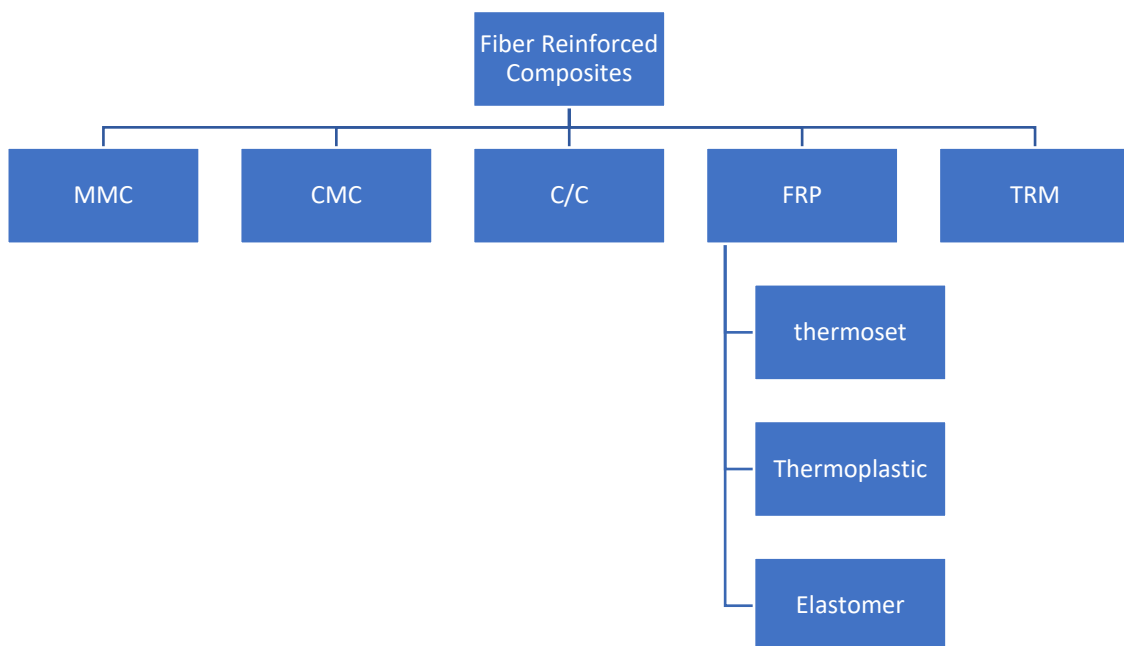


Figure 1.1 : Types of FRC

Primary role of matrix is to hold the reinforcement. In the case of polymers, it is considered as resin. The FRC are extensively being used as an enhancement and replacement for infrastructure components or systems that are constructed of conventional construction and building materials, like concrete and steel. FRP composites are lightweight, corrosion resistant, having high strength to weight ratio and specific stiffness,

are easily manufactured, and can be altered according to the application requirements. Due to these beneficial characteristics, FRC have not only been implemented in new construction but also rehabilitation of already built structures acting as reinforcement in concrete, bridges and underpasses, modular structures, and as an external reinforcement for strengthening and seismic upgrading of structures.

1.1.2 Fiber Reinforced Polymers

Fiber reinforced polymers or fiber reinforced plastics (FRP) are composite material based on a polymer or plastic matrix which is reinforced with fibers. Fiber can be of any type ranging from natural fibers (jute, sisal and basalt etc.) to synthetic fibers (carbon and glass etc.). Often, some fibers like wood asbestos or paper can also be used[4].

FRPs stand out as an excellent subcategory of composites because of their light weight. FRPs are further classified into 3 categories depending on the type of matrix. These are thermoset, thermoplastic, and elastomeric composites. Thermosets cannot be remolded and reused. They have polymers in the form of crosslinked chains at the curing stage. At the end of curing, we get a tough and rigid phase product which can't be remolded. Fiber reinforced composites have now emerged as a new domain of structural materials which is used as a replacement for metals and steels in several critically sensitive components in space applications, automotive sector, marine industries etc. because of their high strength to weight ratio, fatigue and corrosion resistance and low manufacturing costs etc. Because of these large number of applications, FRCs can be clearly regarded as a material having a big potential to be implemented in a wide range of different engineering domains with some extra benefits of high specific strength, and resistance to corrosion compared to other commonly used metallic and ceramic composites. Some common examples for thermosetting plastic matrices are polyester, vinyl ester, polyimide, epoxy, cyanate ester, polyurethane, and bismaleimide etc.

Thermoplastics have an extra advantage of being able to be reused. Thermoplastics can be heated and melted and later on, remolded into new desired products. Thus, they have ability to be recycled more broadly as compared to thermosetting plastics. Thermosetting plastics have an ability of not losing structural rigidity at high temperatures so they can be used in elevated temperature applications. Some of the common thermoplastic matrices are polyamide, polypropylene, polyethylene, PEEK, thermoplastic polyurethane, thermoplastic polyimide, polycarbonate, PLA, polysulfide, polyphenylene sulphide.

In the case of elastomers, we undergo the process of vulcanization which results in crosslinking of chains. Rubber is a widely used elastomer which is produced as a result of vulcanization. Elastomers have advantage over thermosets and thermoplastics matrices because of their highly elastic mechanical characteristics. Some of the applications of elastomeric composites include polyester fiber reinforced hoses, aramid fiber-reinforced automobile tires, steel-wire, or mesh-reinforced heavy-duty truck tires [9].

1.1.3 Textile Reinforced Mortars

During the last few decades, the use of composites for the purpose of strengthening has become very common. Although TRM composites can guarantee a high strength-to-weight ratio, good corrosion resistance and ease of application, several issues are involved with this technique, particularly in the case of masonry: lack of breathability and compatibility, sensitivity to debonding phenomena at the interface and low resistance to fire and high temperatures.

The compatibility with the substrate and the reversibility of the intervention are required, as in case of cultural heritage buildings, or specific exposition conditions may compromise the long-term effectiveness of the reinforcement, as in presence of high temperature and humidity

Aiming to overcome these drawbacks, Textile Reinforced matrix (TRM) composites have started to be adopted during the last few years and have proved to be suitable for the strengthening of masonry and reinforced concrete structures [6].

TRM composites are made using a cementitious matrix combined with different types of fabric meshes with different geometries[7]. The most common materials used for the fabric are glass, steel, PBO, carbon and other natural fibers like basalt, sisal, jute, hemp etc.

The use of a lime-based mortar as inorganic matrix is particularly suitable for masonry substrates, as it can offer better chemical and mechanical compatibility with the porous, uneven and rough masonry substrate than organic matrices, and can ensure vapor permeability and improved durability. More efficient in enhancing bearing capacity against both in-plane and out-of-plane actions.

TRM provide a more sustainable solution against cementitious matrices (predominantly used in TRM systems), can accommodate masonry movements during the hardening phase, and relies on materials readily available in most countries. However, the mechanical properties and behaviours of these matrices are not yet studied in depth with a lot of areas still depriving of in-depth research. The use of inorganic matrices needs to be validated with extensive research activities; their mechanical properties are significantly weaker compared to those of epoxy adhesives. In particular, in the case of dry fiber grids the type of matrix and its thickness may greatly influence the mechanical performance of the composites [8].

1.2 Typical Fibers adopted in TRM systems

Two type of fibers are mainly adopted and investigated in TRM systems: synthetic fibers such as steel, PBO, glass, polyester, carbon, and natural fibers which are instead fully or partially green (biodegradable). Among the latter, flax, hemp, jute, and sisal are today the most widely adopted.

The main purpose of the fiber grid inside the matrix is to provide the necessary reinforcement to the material which significantly enhance its mechanical properties. Recent advancements in research on natural fiber-based composites revealed that the mechanical properties linked to the composites with natural fibers are nearly comparable to those with the reinforcement with glass fibers[9].

1.3 Natural Fibers

Natural fiber reinforced composites or green composites, in terms of their biodegradability, are of two basic types which are fully green composites and partially green composites. Fully green composites contain grid of natural fibers within matrix with a suitable resin which is renewable. However partially green composites are not fully recyclable. They can be recycled only to some extent depending upon the ability of the fiber to be reused[10].

Natural fiber reinforced composites have a lot of benefits, due to their biodegradability, recyclability and other notable environmental benefits as compared to synthetic FRC. For example, the FRC with the natural jute fiber could provide an environmentally sustainable, lightweight and cost effective replacement to synthetic FRCs.

Natural fibers provide some extra features such as lesser cost, biodegradability, higher availability, and significant physical and mechanical properties. FRCs have fascinated a large number of manufacturer and developers due to sustainability and biodegradability properties of natural fiber reinforced composites (FRC), due to their lower environmental, lower cost, including lower carbon emission and lower fossil fuel consumption, and lesser density, and a relative ease in the fabrication. As a result of application of these fibers, we get a combination of various desired properties like stiffness, strength, toughness and lower density etc. As discussed before, that natural fibers exhibit nearly same level of mechanical and physical characteristics as other enormously used fibers but are relatively abundant and cheap. Natural fibers provide improvement in ductile behaviour, toughness properties, flexural strength, and impact resistance properties of a material when coupled with various matrices.

1.4 Synthetic fibers

Synthetic fibers are artificially made fibers based on chemicals such as petrochemicals and synthetic fibers derived mostly from nylon, polyester, acrylic polymer and polyacrylonitrile fibers used to make fiberglass. Synthetic fibers are usually manufactured from synthetic polymers with small molecule chains which have an origin derived from petroleum-based chemicals or petrochemicals. These materials undergo polymerization process to form a chemical which have two adjacent carbon atoms bonded together. Different these chemical compounds are used to produce wide range of synthetic fibers.

Use of synthetic Fiber Reinforced composites has increased many folds throughout the construction industry as builders and constructors started to recognize its many benefits. It is also gaining a greater interest among the concrete sector due to the reduced construction time span and lesser labor costs. Besides the cost issues, quality matters are of significant importance for the construction and Synthetic Fiber Reinforced composites fulfils these requirements.

Synthetic Fibers has a major benefit that these Reinforced composite Fiber are more durable than most of the natural fibers and readily pick-up various dyes. Most of the synthetic fibers offer some extra benefits like stretching, waterproofing and resistance to corrosion, sunlight, moisture, and damaging effects of oils from human skin because they cause fibers to break down and wear away. Natural fibers are much more prone to the effects of these impacts as compared to synthetic fibers. This is mainly due to the reason

that nature always offer biodegradable characteristics. One of the problems with natural fibers is that natural fibers are prone to larva insect's infestation while synthetic fibers are safe from this damaging effect. Natural fibers are also more corrosion resistant and water resistant as compared to natural fibers. Some extra advantages associated with synthetic fibers are lessen the gravity of plastic shrinkage cracking

- Reduces segregation phenomenon and bleeding in the matrix
- Provides resistance against micro cracking
- Increases the durability of surface
- Reduction of in-place cost versus wire mesh for temperature/shrinkage crack control
- Can be added to concrete mixture easily at any time prior to mixing
- More durable due to higher strength of mortar
- No Dampness and leakage
- Increase the abrasion resistance of concrete floor against moving loads
- Increase impact resistance against point loads [11]

1.5 Objectives of the thesis

Although a lot of research is already done on the mechanical characterization of TRM composites, the knowledge is still incomplete and several research data are still unavailable. The context of this thesis involves the mechanical characterization under traction of TRM systems based on natural and synthetic fibers. In particular, within the thesis, experimental and numerical activities have been developed:

- experimental characterization of mortar specimens, involving compression tests and 3-point bending tests;
- numerical modelling of the tensile behavior of TRM coupons tested by several authors and available in the technical literature.

The experimental characterization of mortar prisms has been conducted at the Laboratory of Materials and Structures (MASTRLAB) of Politecnico di Torino. The numerical simulations have been conducted using the finite element software Abaqus 2019.

In the following chapters, firstly, the state of the art will be proposed, then the experimental and numerical activities conducted within the thesis will be presented and the main results and conclusions will be described.

1.6 References

- [1] W. J. Cantwell and J. Morton, “The impact resistance of composite materials — a review,” *Composites*, vol. 22, no. 5, pp. 347–362, Sep. 1991, doi: 10.1016/0010-4361(91)90549-V.
- [2] M. J. Horton and S. R. Schmid, “Library of Congress Cataloging-in-Publication Data Kalpakjian, Serope, 1928-Manufacturing engineering and technology / Serope Kalpakjian.” [Online]. Available: www.pearsonhighed.com/permissions/.
- [3] D. K. Rajak, D. D. Pagar, P. L. Menezes, and E. Linul, “polymers Fiber-Reinforced Polymer Composites: Manufacturing, Properties, and Applications”, doi: 10.3390/polym11101667.
- [4] “Fibre-reinforced plastic,” https://en.wikipedia.org/wiki/Fibre-reinforced_plastic.
- [5] J. Njuguna, K. Pielichowski, and J. Fan, “Polymer nanocomposites for aerospace applications,” *Advances in Polymer Nanocomposites: Types and Applications*, pp. 472–539, 2012, doi: 10.1533/9780857096241.3.472.
- [6] J. D’anna, G. Amato, J. Chen, G. Minafò, and L. la Mendola, “Effects of different test setups on the experimental tensile behaviour of basalt fibre bidirectional grids for TRM composites,” *Fibers*, vol. 8, no. 11, pp. 1–18, Nov. 2020, doi: 10.3390/fib8110068.
- [7] J. D’anna, G. Amato, J. Chen, G. Minafò, and L. la Mendola, “Effects of different test setups on the experimental tensile behaviour of basalt fibre bidirectional grids for TRM composites,” *Fibers*, vol. 8, no. 11, pp. 1–18, Nov. 2020, doi: 10.3390/fib8110068.
- [8] “MECHANICAL CHARACTERISATION OF FLAX AND JUTE TEXTILE-REINFORCED MORTARS,” <https://cee.sheffield.ac.uk/?q=news/mechanical-characterisation-flax-and-jute-textile-reinforced-mortars>.
- [9] M. Jawaaid and H. P. S. Abdul Khalil, “Cellulosic/synthetic fibre reinforced polymer hybrid composites: A review,” *Carbohydrate Polymers*, vol. 86, no. 1, pp. 1–18, Aug. 2011, doi: 10.1016/J.CARBPOL.2011.04.043.
- [10] B. Madsen and E. K. Gamstedt, “Wood versus Plant Fibers: Similarities and Differences in Composite Applications,” *Advances in Materials Science and Engineering*, vol. 2013, p. 14, 2013, doi: 10.1155/2013/564346.
- [11] Constro Facilitator, “Synthetic Fiber Reinforced Concrete – Types and Advantages,” <https://www.constrofacilitator.com/synthetic-fiber-reinforced-concrete-types-and-advantages/>.
- [12] N. Saba, M. Jawaaid, and M. T. H. Sultan, “An overview of mechanical and physical testing of composite materials,” in *Mechanical and Physical Testing of Biocomposites, Fibre-Reinforced Composites and Hybrid Composites*, Elsevier, 2018, pp. 1–12. doi: 10.1016/B978-0-08-102292-4.00001-1

Chapter 2: State of the Art on tensile testing of TRM materials

In Recent years, TRMs have been considered as one of the most important and widely considered materials for the reinforcement and rehabilitation of existing structures. Numerous research have already been done on the mechanical characterization and analytical behavior of TRM materials, but still a lot of TRMs are yet to be tested and analyzed.

Tensile testing is one of the most common and basic tests for the characterization of TRM materials. The tensile behavior of TRM materials is a bit complex because it is affected not only by the characters of fiber and the mortar, but also by the mechanical properties at the interface between the two.

The tensile characterization of TRM materials can be carried out by two main approaches:

- firstly, the experimental characterization of TRM materials under pure traction;
- secondly, the numerical modelling of tensile response.

Several authors have conducted both laboratory tests and finite element modeling of the behavior under traction of TRM coupons. In the following, the research results obtained by Arboleda et al. (2016) [6], Malena et al. (2019) [20], Monaco et al. (2020) [18] and D'Anna et al. (2021) [19] will be described.

2.1 Experimental campaign by Arboleda et al. (2016)

The experimental technique adopted by Arboleda et al. (2016) in the research work [6] basically uses two types of test setups depending on the clamping method that is being used for the load transfer between the specimen and the testing machine. As there are a few problems related to standardization of various clamping mechanisms used for various applications, in the scope of this research. The author used clevis-grip for application of load on specimen at the point where the specimen is provided with the aluminum tabs. In case of testing with the clevis grip, the metal tabs of 3mm thickness are provided to be attached to the shear grips implementing the adhesive tension. In the case of the clevis gripping, pinned end provides with multiple degree of freedom. However, in the case of

clamping grips, aluminum tabs were provided at the extreme ends of the specimen which is gripped by the tensile testing machine to evenly distribute the load to the specimen. In the case of glass fiber coupons, a protective coating of epoxy resins is provided to ensure proper and balanced loading and to avoid any damage.

And the clamping grip is used to apply compressive stress orthogonal to the plane of specimen. Thus, in the case of clevis-grip, the shear stresses play an important role. The problem with clevis-grip is the slippage between the two surfaces. This clamping mechanism doesn't provide with enough clamping force to keep the two layers together, so the specimen usually fails by the slippage. But still, specimens are tested using the clevis grip because it better represents the field applications in which the ends are not gripped. However, in the case of clamping mechanism, the ends are anchored so we get a final brittle failure instead of the slippage. The observation of the effect of load on the specimen (the elongation) was observed using the extensometer of 50 mm base length. Dimension of the specimen in all cases are 100 mm x 40 mm x 10 mm. The dimensions for the tabs are 60mm x 40mm x 2mm.

For the test using the clevis-gripping, the universal testing machine of 130kN testing capacity is used implementing 0.25 mm/min displacement control. Elongation was observed using an extensometer of gauge length of 100 mm. In the case of the clamping grips, universal testing machine of 100 kN was used with displacement control load of 0.1 mm/min. However, during the 2nd stage, the crack initiation phase, the displacement control load is increased to 0.3 mm/min. The extensometer used in this case is same as in the case of clevis gripping. Glass fibers and coated glass fiber composite specimen, namely G-TRM and cG-TRM were not tested with the clevis-grip.

2.1.1 TRM composites

Following TRM specimens are investigated in the research work done by [1].

- Dry fibers of Polyparaphenylene benzobisoxazole (BPO)
- Carbon fiber with dry fibers and carbon fiber having with protective coating on dry fibers.
- Glass fiber with dry fibers and glass fibers with protective coating of styrene butadiene

Each of these fibers are used to form the TRM specimen which is tested.

2.1.2 Fiber reinforcement

Fiber reinforcement is inserted in TRM specimen in a number of layouts. Each layout mechanism has different properties. A detailed experimental characterization is needed to determine the effect of various fiber layout on the tensile properties of the corresponding TRM. These fiber layouts differ on the basis of number of yarns, the nominal width of yarns and the spacing between fibers. As far as the scope of the thesis is concerned, following are the fiber geometries being investigated.

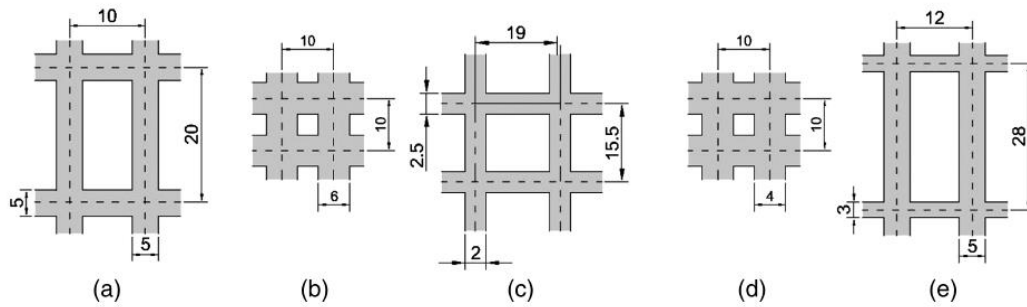


Figure 2. 1 : a) PBO; b) Glass fiber; c) Coated glass fiber; d) Carbon fiber; e) coated carbon fiber

In the case of PBO the fiber layout dimensions are 0.046mm in wrap direction and 0.011mm in weft direction, which shows its unbalanced nature. The Carbon fiber has a balanced layout in wrap and weft direction with 0.047mm dimensions. Coated carbon fiber is also balanced fiber with 0.175mm equivalent thickness in both directions. For the case of glass fiber. Equivalent thickness is 0.036mm and for coated glass fiber, the thickness is 0.05mm. Ends of coupons specimens of Glass fiber reinforced polymers are supported by epoxy resins to provide anchor to the fibers in matrix.

All these fiber specimens were individually tested as a single yarn as well as a specimen of 40mm width using universal testing machines of loading capacities of 2 to 100 kN following the EN ISO 10618/2005 standards. The details of mechanical properties obtained as a result of experimentation is shown in the form of table as follows.

Table 2. 1 : Mechanical Properties of yarn

Fabric	Number of yarns	Cross section area (mm ²)	Number of tests	Average stress at failure (GPa)	COV (%)	Elastic modulus (GPa)	COV (%)
PBO fiber	1 yarn	0.41	6	3.9	3.2	216	20.8
	4 yarns	1.64	4	3.4	7.3	—	—
C fiber	1 yarn	0.42	3	1.9	14.9	203	9.8
	4 yarns	1.68	3	1.9	10.4	—	—
cC fiber	1 yarn	2.68	3	1.3	9.2	263	11.2
G fiber	1 yarn	0.24	4	1.4	11.4	49	—
cG fiber	1 yarn	0.90	5	1.2	2.7	56	30.5
	3 yarns	2.70	5	1.1	1.3	—	—

2.1.3 Inorganic Matrix

In the research work done by Arboleda et al. (2016) [6], the inorganic matrix is used for the preparation of the specimens. For the case of each individual type of fiber, the inorganic matrix selected is different, depending upon the compatibility with the fiber, workability properties and to form a near perfect bond between two phases. The details of properties of the mortar used for each specific fiber is given in the form of table.

Table 2. 2 : Properties of inorganic Matrices

Matrix type	Tensile EN 12390-6 (BS EN 2009)		Compressive EN 1015-11 (BS EN 1999)		Flexural EN 1015-11 (BS EN 1999)		Elastic modulus EN 14580 (GPa) (BS EN 2005b)
	Strength (MPa)	COV (%)	Strength (MPa)	COV (%)	Strength (MPa)	COV (%)	
Mortar used with PBO fabric	4.75 (7) ^a	4.05	33.90 (5)	10	>2 (ds)	—	>6 (ds)
Mortar used with C fabric	3.30 (5)	3.6	24.02 (5)	2.5	3.5 (ds)	—	>7 (ds)
Mortar used with cC fabric	3–5 (ei)	—	>45 (ds)	—	7 (ei)	—	7 (ei)
Mortar used with G fabric	2–4 (ei)	—	10 (ds)	—	3 (ei)	—	5 (ei)
Mortar used with cG fabric	3–5 (ei)	—	27.13 (7)	4.1	8.4 (14)	13.15	8 (ds)

^aWithin brackets, number of tested coupons or source of data (ds = data sheet; ei = estimated interval).

2.1.4 Specimen preparation

For the preparation of specimen, a flat rectangular mold was used. Mortar is manually poured forming a layer of matrix of thickness of 5mm. Then the fiber layer is introduced and is pressed in the matrix. Then the 2nd layer is applied in the mold, covering the fiber layer, and is spread evenly by using a trowel. After the preparation of specimen, the specimens were seasoned at 20°C and 60 % relative humidity in ambient conditions for a period of 28 days.

2.1.5 Results

As a result of the experimentation. Stress strain curves are obtained from the testing machine. Now a proper analysis and data management of the curve data is required. In order to summarize the results and to get a consistency between experiments on various specimens. The region of 0.9 f_{fu} and 0.6 f_{fu} and the corresponding strain range is selected in order to get the values of the Elastic strains in all directions.

$$E_f = \frac{\Delta f}{\Delta \varepsilon} = \frac{0.9f_{fu} - 0.6f_{fu}}{\varepsilon_{@0.9f_{fu}} - \varepsilon_{@0.6f_{fu}}}$$

Table 2. 3 : Experimental Results of tests on each specimen

Material	Grip type (number) ^a	Value type	E_1 (GPa)	E_2 (GPa)	E_3 (GPa)	σ_{i1} (MPa)	σ_{i2} (MPa)	σ_u (MPa)	ε_{i1} (%)	ε_{i2} (%)	ε_u (%)	E_1^* (GPa)	σ_{i1}^* (MPa)
PBO-FRCM 4 yarns	Clevis (10)	Average	1,805	128	—	375	—	1,664	0.017	—	1.756	—	—
		CoV (%)	25	12	—	22	—	5	25	—	8	—	—
C-FRCM 4 yarn	Clevis (5)	Average	512	80	—	458	—	1,031	0.102	—	0.996	—	—
		CoV (%)	25	23	—	10	—	5	44	—	14	—	—
cC-FRCM 3 yarns	Clevis (9)	Average	1,570	56	—	381	—	1,296	0.023	—	1.641	—	—
		CoV (%)	55	14	—	36	—	12	33	—	14	—	—
cC-FRCM 2-PLY	Clevis (5)	Average	465	52	—	149	—	1,133	0.025	—	1.79	8	3
		CoV (%)	24	17	—	24	—	10	37	—	25	15	22
PBO-FRCM 4 yarns	Clamp (34)	Average	1,181	76	216	890	1,100	3,316	0.082	0.5	1.69	5	4
		CoV (%)	20	33	9	15	13	14	31	34	18	20	15
C-FRCM 4 yarns	Clamp (10)	Average	1,102	68	186	482	620	1,492	0.06	0.24	0.74	5	2
		CoV (%)	18	28	22	21	19	19	13	20	21	18	21
G-FRCM 4 yarns	Clamp (8)	Average	1,029	41	56	545	691	1,292	0.064	0.44	1.82	2	2
		CoV (%)	31	59	36	25	7	8	25	28	47	31	25
cG-FRCM 3 yarns	Clamp (17)	Average	1,310	32	64	460	431	872	0.045	0.38	0.69	6	2
		CoV (%)	33	34	17	30	20	21	41	13	38	34	30

^aWithin brackets, number of tested coupons.

The stress strain curves for BPO-TRM, C-TRM and cC-TRM are shown in the following graph using the clevis-grip mechanism. Usual trilinear behavior is observed for each specimen.

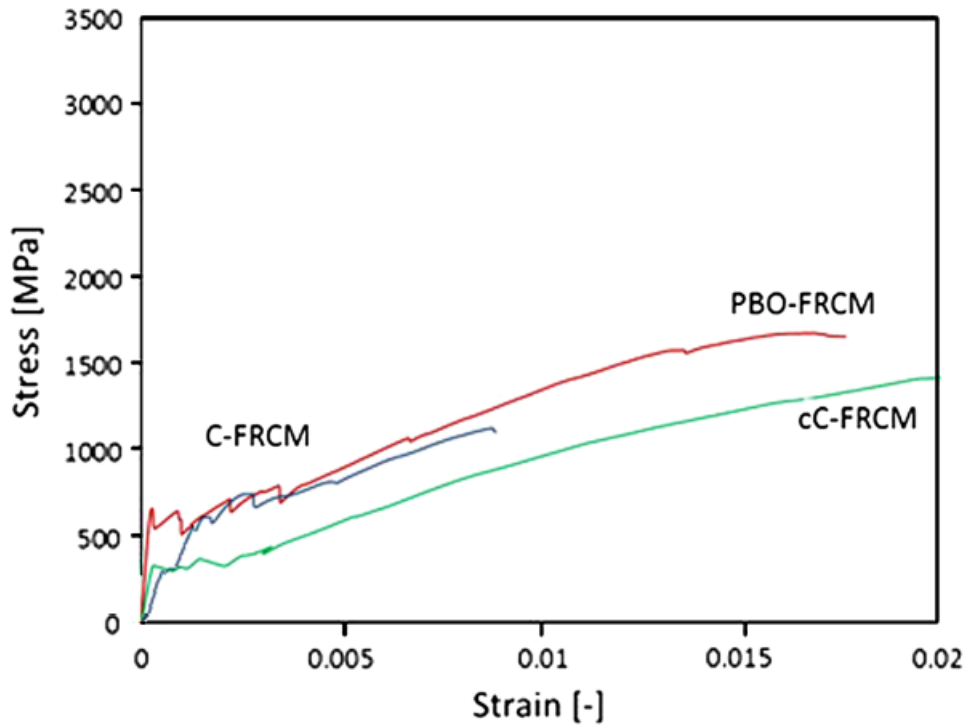


Figure 2. 1 : Stress strain curve for single layer using Clevis-grip

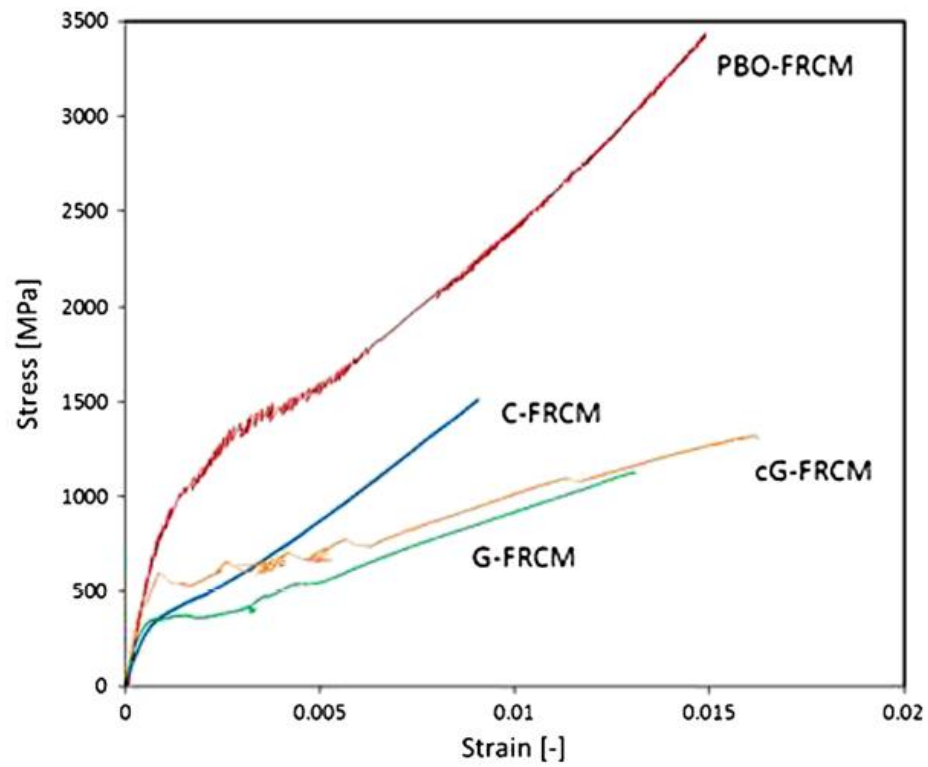


Figure 2. 3 : Stress strain curve for single layer using Clamping-grip

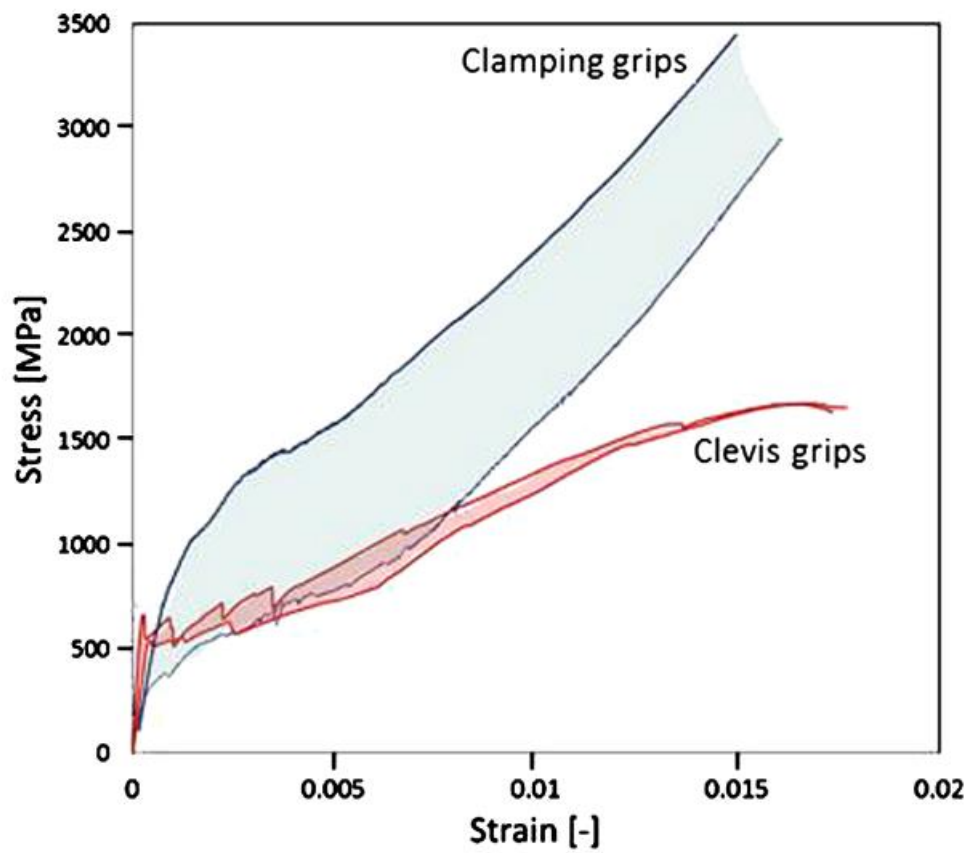


Figure 2. 4: BPO-TRM Clamping-grip vs Clevis-Grip

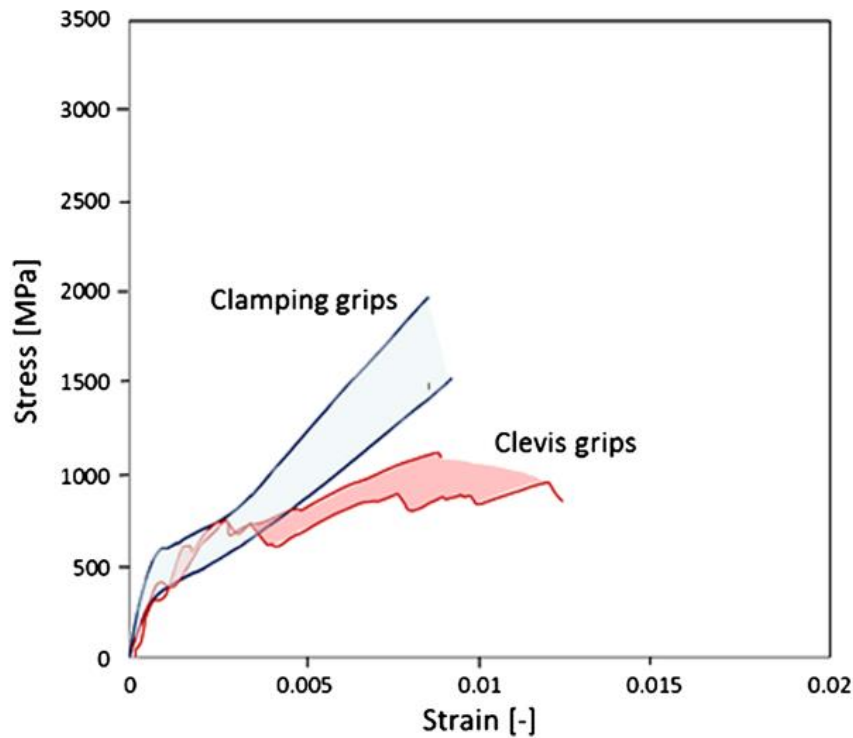


Figure 2. 5 : C-TRM Clamping-Grip vs Clevis-Grip

2.2 Experimental campaign by Malena et al. (2019)

In the research work by Malena et al. (2019) [20], the composite material under investigation is steel reinforced grouts. Steel reinforced grouts basically consist of Ultra high strength fibers suspended in inorganic matrix. Already some research work is present for these materials. But an in-depth study related to the individual properties of fibers as well as mortar, for example ductile behavior of fibers, brittle behavior of mortar matrix, still need to be investigated properly. The bonding interaction between the mortar and fiber interface also needs to be investigated. Individual as well as combined mechanical characterization of fibers and mortar is important because mechanical response of individual elements is different from the composite form. The reason for this deviation of properties is the slippage between the two layers, multiple cracking of mortar and individual fracture of fiber layers.

First part of mechanical characterization consists of an experimental campaign to determine the properties of composite material as well as the individual layers. A complete experimental strategy needs to be defined for that purpose including the experimental equipment, composite specimen preparation, planning of experimental strategy.

The experimental setup mainly consists of a tensile testing machine which is equipped with clamping mechanism to transfer the load from the machine to specimen. Different clamping mechanism cause different stress transfer which conclusively cause failure of specimen in different manners. So, for each case, the clamping mechanism is chosen accordingly. The two clampings used in the case of mentioned research are:

- clamping grips.
- clevis grips.

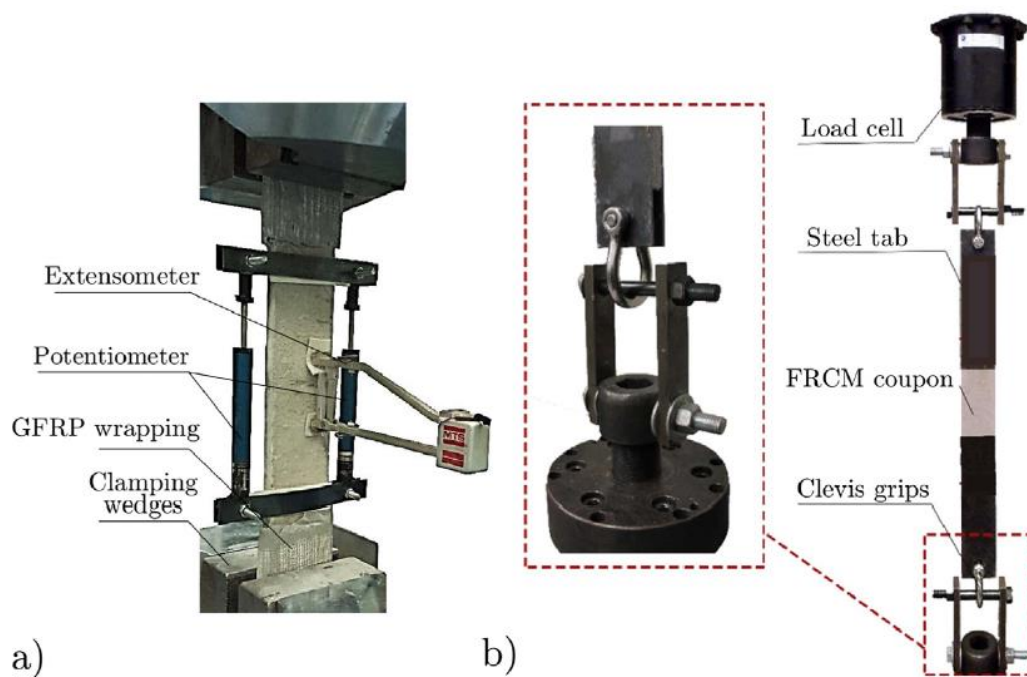


Figure 2. 6 : Experimental setup for direct tensile test on SRG specimens: (a) clamping-grip setup (b) clevis-grip setup

In the case of clamping grip setup. The specimen is mounted in such a way that both ends of the specimen are actually fastened to the testing machine as a result of lateral pressure applied by the clamping wedge. As a result of such clamping, the compression stress as well as the shear stresses are properly transferred from equipment to the specimen. As a result, the experimental results are way more reliable. Clevis grip setup are more reliable for the representation of the behavior of specimen in its idle installation phase when the composite is without any prestress (lateral pressure). The failure mode of the specimen needs to be understood. The composite material is prone to slippage between the two layers. The strength of both layers is of higher orders as compared to bonding strength between the two layers so because of application of traction load. The slippage between the two layers is the most common failure mode. During the application of the load on the

specimen, the shear stress acts between the two layers which acts to tear the bond apart. The resistance created by the bonds at interface is broken and the material fails by slippage.

For the mechanical characterization of TRM, the most widely adopted testing reference standards is RILEM TC 232-TDT Recommendation [7]. The standards described by the mentioned research work are followed in the scope of research by Malena. The mortar specimens are prepared in such a way that mortar is molded as prismatic layers. In between every two layers of mortar, a fiber layer is sandwiched. Textile is composed of Ultra High Tensile Stress Steel cords. In which case two wires are wound around three rectilinear wires by twisting them around. In this way, a better interlocking is obtained.

Preparation of specimen also requires strategic planning because the fiber needs to be embedded between the two mortar layers accurately and evenly in the longitudinal direction. The specimen is created and seasoned to be ready for experimentation. Another important factor in the preparation of the test specimen is the mold, which is used to prepare the specimen. Wood, plastic, steels and many other materials can be used to manufacture the mold. While preparation of specimen in the mold, special attention must be paid in order to avoid the misalignment between the layers. A perfectly aligned specimen with parallel layers can guarantee a reliable result.

After the preparation of specimen, the specimen is introduced in the testing machine and is clamped via clamping mechanism. The clamping grip setup consists of wedges to clamp the specimen to the machine. The clamps are pressed against the specimen and clamping load grips the specimen by hydraulic mechanism. The tensile tests are mostly displacement control tests with a predefined displacement rate value. The values are usually very low to allow uniform stress distribution among layers and to avoid any inertial damage. Values of axial loads are measured for the characterization of specimen. These values correspond to the failure stresses of the specimen. The measurement of effects of load on the specimen can be measured by several ways like Digital image correlation or by use of transducers etc. but in the scope of this experiment, the strains are measured using the extensometer.

2.2.1 Tests on Dry fibers

According to research work done by Malena, the experimental campaign consists of several tests on dry fibers, mortar prismatic specimens and composite specimens. For dry textile specimen, the dimensions are 50.8mm x 436mm. Aluminum tabs were chosen at lateral edges to provide a proper gripping. Clamping gripping mechanism is used for the load transfer between the specimen and testing machine. Total of 6 specimen were created with 8 fiber cords each. Loading conditions of 0.3mm/min are applied.

As a result of displacement control load, we get two phases.

- Linear phase, having a proportional relationship between stress and strain. This curve is obtained involves almost 60-80% of the region and gives an idea about the tensile strength of fibers.
- A hardening phase with nonlinear relationship between stress and strain, which finally leads to brittle failure.

2.2.2 Tests on composites

Experimental campaign consists of two basic tests. In both experiments, the difference lies in the clamping mechanism in order to judge the effect of clamping mechanism. The detail of experimental strategy is as follows.

First test consists of 5 prismatic specimens. The dimension off the specimen are 600 mm length, 40 mm width and 10 mm thickness. The fiber layer consists of 5 cords in each specimen with length same as specimen, 31.75mm width and area equal to 2.67mm^2 . Clamping grip clamping setup was considered for the testing. The loading conditions are displacement control load of 0.3mm/min. The stress strain curve is obtained by using extensometer.

The 2nd experimental campaign on composite specimen involves the use of clevis-grip clamping mechanism. The dimension of specimen for this experiment is 500 mm length, 50 mm width and 13 mm thickness. Loading conditions are 0.25 mm/min displacement control load, with a loading capacity of 130kN.

In the case of clamping grip test, we get the same 3 phase. First phase is as usual the linear curve between stress and strain. 2nd phase is the crack initiation phase, where the micro cracks appear on the specimen and the stress and strain are no longer proportional but

show a plastic behavior. 3rd phase involves the propagation and evolution of the cracks, which finally leads to brittle failure. Experimental investigation has shown a relative increase of 10% in tensile strength of composite as compared to the tensile strength of bare fibers.

In the case of clevis-gripping, we observe a very obvious slippage between the fiber layer and the mortar layer although all the composite specimens are provided with the twist interlocking layout in the textile. Initially, we obtain the same linear behavior but in this case the portion of linear behavior is relatively too short. Then the cracks start to appear near the clamped region which corresponds to 2nd phase. These cracks then keep on evolving until the final failure. The comparison of all three experiments is expressed in the form of following graph.

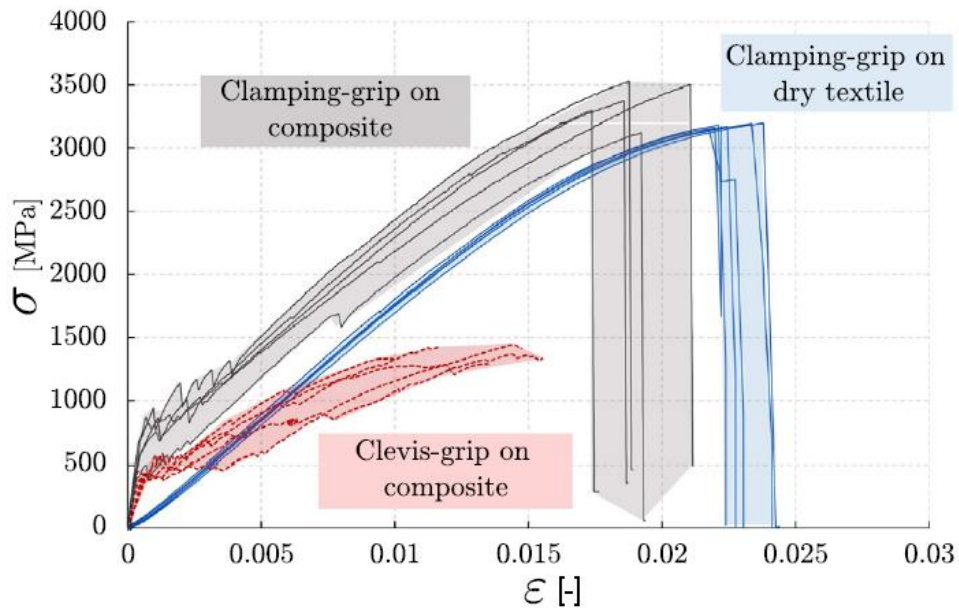


Figure 2. 7 : Experimental test results on dry textile vs composite using Clamping-grip

2.3 Numerical Modelling by Malena (2019)

The creation of numerical model was performed implementing FEM using ABAQUS. All the above-mentioned experimental campaign is replicated numerically using proper tools and modules present in ABAQUS. Proper definition of geometry is required for each type of experiment. So all the experimental techniques must be efficiently realized in the form of numerical model. After the definition of geometry and preparation assembly as a combination of the two layers, the specimen

must be meshed properly. So, a meshing technique of 3D hexahedral mesh elements is chosen for both, mortar and fiber. Then the interface between the fiber and the mortar needs to be modelled. As mentioned before, the interface modelling is done using two techniques, namely the perfect bond and the cohesive interaction. Various restraints and boundary conditions are applied to the specimen in order to simulate the experimental test as numerical model. Finally, the load is applied to perform the simulation. Load is applied in vicinity of the clamping area and the exact location of the application of the load depends on the type of clamping being replicated.

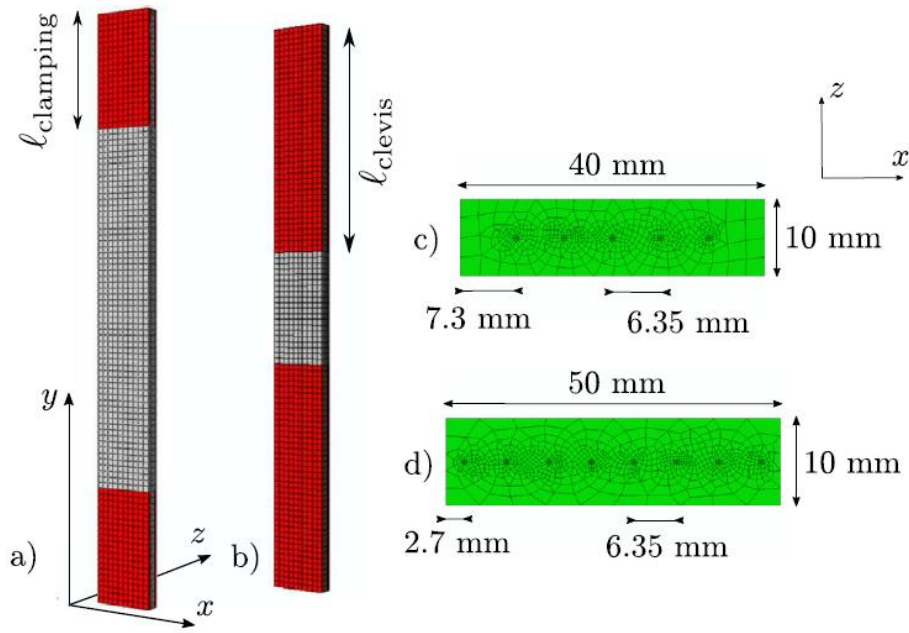


Figure 2. 8: : FEM Mesh a) Clamping-grip setup b) Clevis-grip setup c) clamping-grip mesh d) Clevis-grip mesh

2.3.1 Constitutive model

The preparation of a complete and reliable constitutive model requires a proper realization of the constituents of the composite as numerical model. So, three important aspects that needed to be taken in account while modelling are as follows.

- Modelling of the fiber layer
- Modelling of the mortar layer
- Modelling of the interface between the two layers

2.3.2 Numerical modelling of fiber layer

In order to numerically define the fiber layer, its numerical properties as well as the physical properties and phases needs to be defined. Elastic phase of the response of the fiber is modelled by introduction of damage initiation criterion, which represents the domain of 1st stage and the initiation of the 2nd phase. In the elastic phase the young modulus needs to be defined along with the yielding stress f_0 . This data is obtained from the experimental campaign. The strength f_{st} characterizes the initiation of the cracks thus it defines the initiation of 2nd phase.

The fracture energy plays an important role in reducing the mesh dependency issues and is defined as characteristic length of 10mm. Then the damage evolution law is used to numerically model the post elastic phase of the fiber layer.

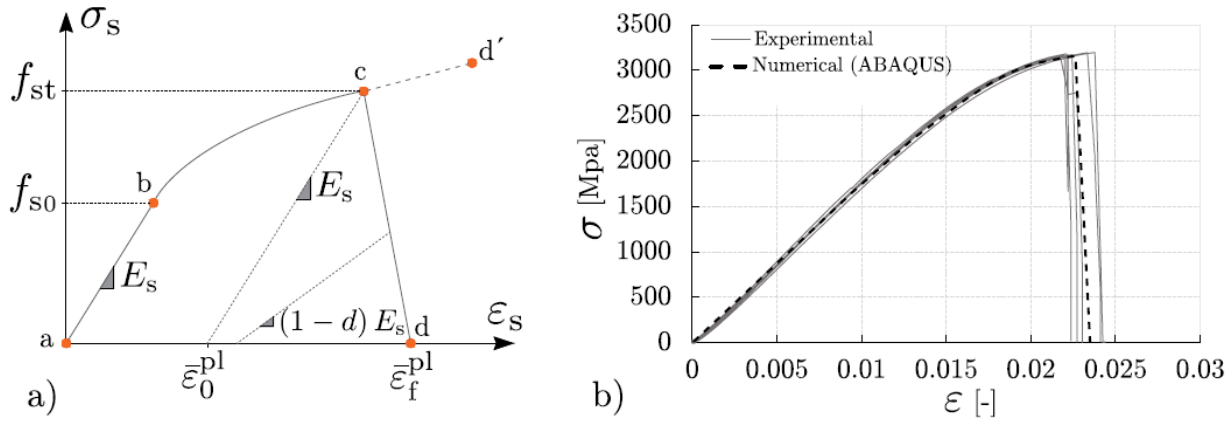


Figure 2. 9 : a) Adopted ductile damage constitutive law b) numerical results

Table 2. 4 : Mechanical Parameters of steel

Steel parameters.

E_s [GPa]	f_{s0} [MPa]	f_{st} [MPa]	ϵ_0^{pl}	ϵ_f^{pl}	G_f [N/mm]
182	1820	3157	0.0045	0.0234	9.57

2.3.3 Numerical modelling of mortar layer

Mortar layer is a little bit complex to model because of its complex nonlinear behavior and different response in tension as well as compression. However, the response in the compression phase does not play an important role in the numerical modelling. However, the tensile behaviour is significant as it

explains the phases, the elastic and plastic response, the crack initiation and propagation etc. The mechanism of non-linearity in the mortar layer is defined using the concrete damage plasticity model [8]. CDP is defining the damage parameters d_t and d_c and the evolution law explained as follows

$$\sigma_{mc} = (1 - d_c) E_m (\varepsilon_c - \tilde{\varepsilon}_c^{pl})$$

$$\sigma_{mt} = (1 - d_t) E_m (\varepsilon_t - \tilde{\varepsilon}_t^{pl})$$

These two expressions define the CDP model in tension as well as compression. A graphical representation of the CDP is as follows.

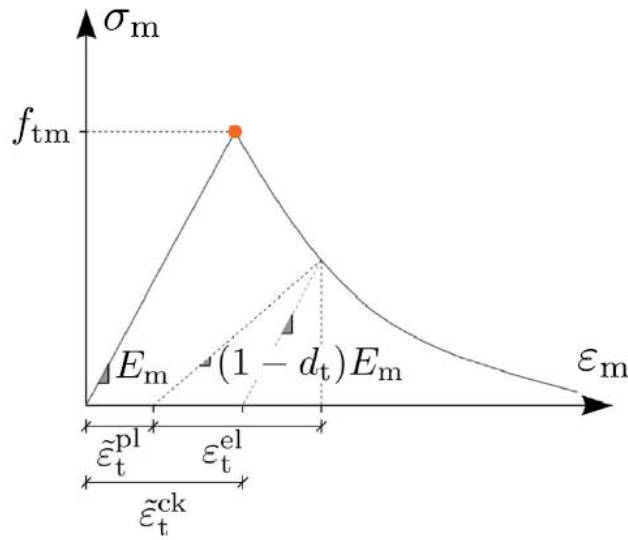


Figure 2.10 : CDP Stress-Strain model in tension

In order to define the elastic behavior of the mortar layer, the most important parameters are E_m , the elastic modulus of mortar and f_{mt} the tensile strength of fiber. If we ideally assume that the response is elastic and no slippage occurs between the two layers then we get the following governing equation to replicate the response in elastic phase.

$$E_s A_s \varepsilon_l + E_m A_m \varepsilon_l = N_l$$

Where A are the corresponding areas and ε are the strains. In order to define the elastic modulus of the mortar we use following equation.

$$E_m = \frac{N_l - E_s A_s \varepsilon_l}{A_m \varepsilon_l}$$

An important factor is the stress contribution of the fiber on the mortar in the composite and is governed by the following equation.

$$\sigma_m(\varepsilon) = \frac{N_c - E_s A_s \varepsilon}{A_m}$$

Where N_c is the compression load. In order to define the CDP, the value of δ_m is measured at various strain levels between the cracking of the mortar and the steel yielding.

$$\tilde{\varepsilon}_t^{pl} = \tilde{\varepsilon}_t^{ck} - \frac{d_t}{1 - d_t} \frac{f_t}{E_0}$$

The above-mentioned equation defines the post cracking behavior of the mortar in CPD where ε_t^{pl} is the plastic strain in tension and ε_t^{ck} is the cracking strain.

2.3.4 Numerical modelling of the interface

The interface between the two layers is modelled by bilinear bond-slip cohesive law. For this law, two most important parameters are tangential stress τ and the slip s . In order to completely define the cohesive interface, the maximum tangential stress τ_m and its relative slip s as well as the debonding slip s_{db} needs to be determined. Values of the slips were taken from previous research work done by [9,10]. The value of τ_m is obtained by results of the bond test Experiments [11,12].

We determine the load at the debonding using two assumptions. Firstly, the steel cord is assumed to be behaving elastically and secondly the matrix is rigid.

$$P_{deb} = \frac{n}{2} \pi d \sqrt{2E_s G_f d}$$

Where d is the number of cords G_f is the fracture energy. Finally, the tangential stress is defined as

$$\tau_m = \frac{4P_{deb}}{n^2 \pi^2 d^3 E_s s_{deb}}$$

Which is the relationship between the tangential stress, the debonding pressures, the number of cords and the relative slip. Thus, after the calculation of the parameters, all the constituents of numerical model are defined properly.

2.3.5 Numerical results

Some graphical representations of the obtained results from ABAQUS model are shown as

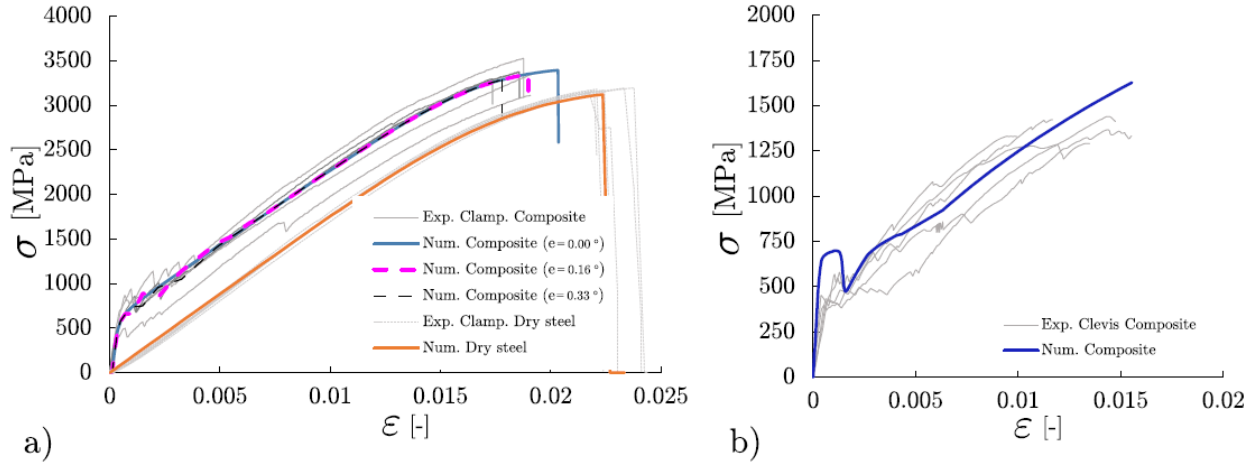


Figure 2. 11: Graphical representation of numerical and experimental results a) Clamping-grip b) Clevis-grip

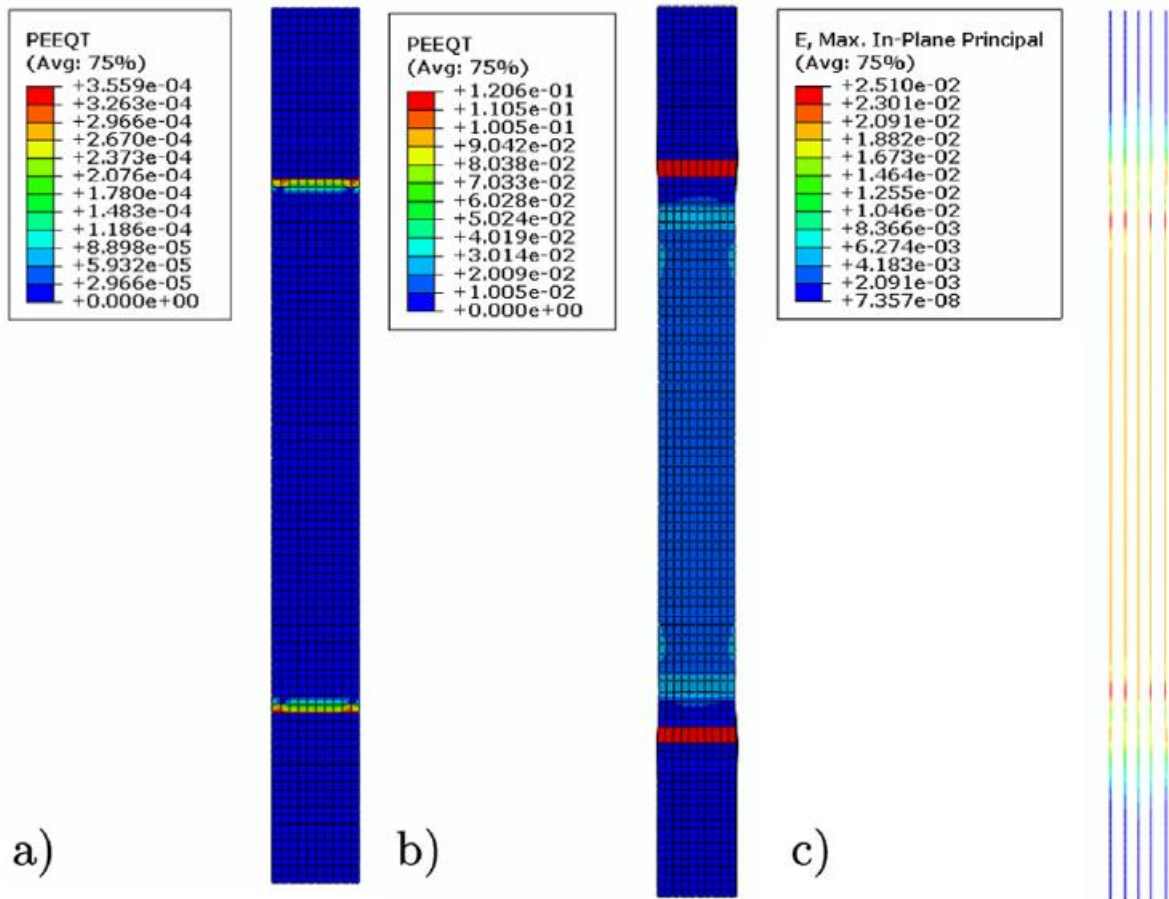


Figure 2. 12: tensile strain in mortar a) crack initiation b) failure point c) direct tensile test

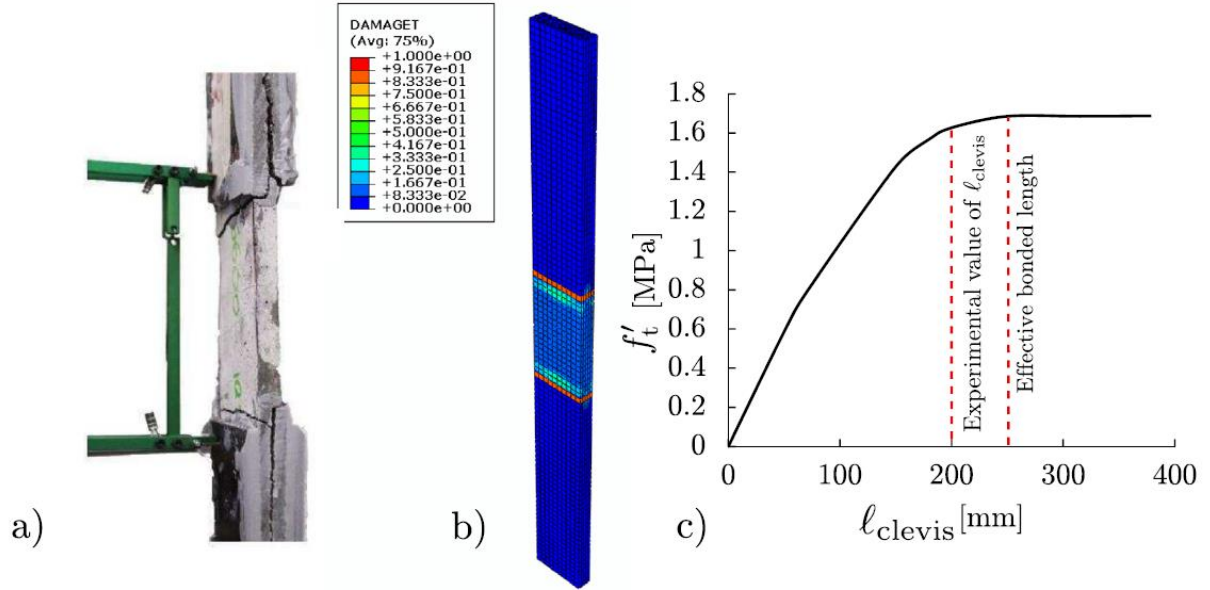


Figure 2.13: a) Experimental failure mode b) Mortar model failure c) load capacity vs tab length relationship

2.4 Numerical Modelling by Monaco et al. (2020)

The numerical modelling technique implemented in the research “Constitutive Numerical Model of TRM Strips Under Traction” by Alessia Monaco, Giovanni Minafò, Jennifer D’Anna, M. Concetta Oddo and Lidia La Mendola (2020) [18] presents the model for traction behavior of TRM materials. Along with the individual mechanical properties of both mortar and the fiber, the properties related to the interface between the two are of great significance due to above mentioned issues related to cohesive failure and sliding phenomenon. So, there are multiple ways to model the interface between the two materials. In the research article mentioned above, two different techniques are mentioned.

2.4.1 Perfect Bond

The first technique to model the interface is the “perfect bond” between the fiber and mortar layer. It is a relatively simpler technique based on the concept of embedded structures. In this technique, a group of elements from one material are considered embedded to the elements of other material considered as host elements. The embedded and the host elements are thus geometrically linked to one another so as a result, the degree of freedom of two type of elements are linked to one another via interpolation. The perfect bond technique replicates the interface based on the method that embedded nodes

and the host nodes are linked to each other such that the maximum distance between the two is predefined by the specific geometric tolerance.

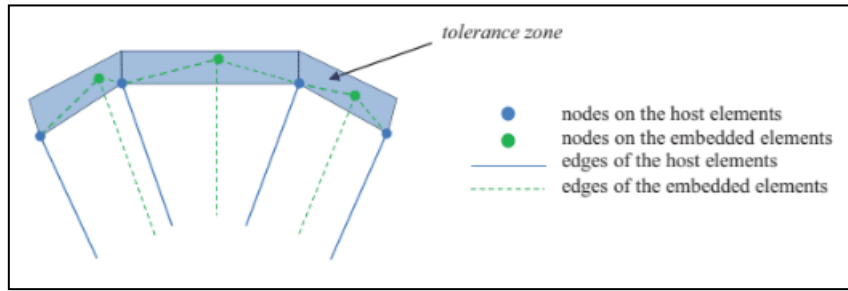


Figure 2. 14: Perfect Bond

In this technique, a region is defined in between the host nodes (as shown as blue shaded region). This region is surrounded and bounded by the host nodes and is called the tolerance zone. The green nodes represent the embedded nodes. If the embedded node lies in the tolerance zone, then it is numerically linked to the corresponding host elements and their degree of freedom will be linked to each other. In this technique, we model the fiber elements as shell elements and the mortar elements as 3D deformable structure. So in this case, the nodes of fiber (modelled as shell) will be linked to the nodes of mortar and their degree of freedom will be linked to one another.

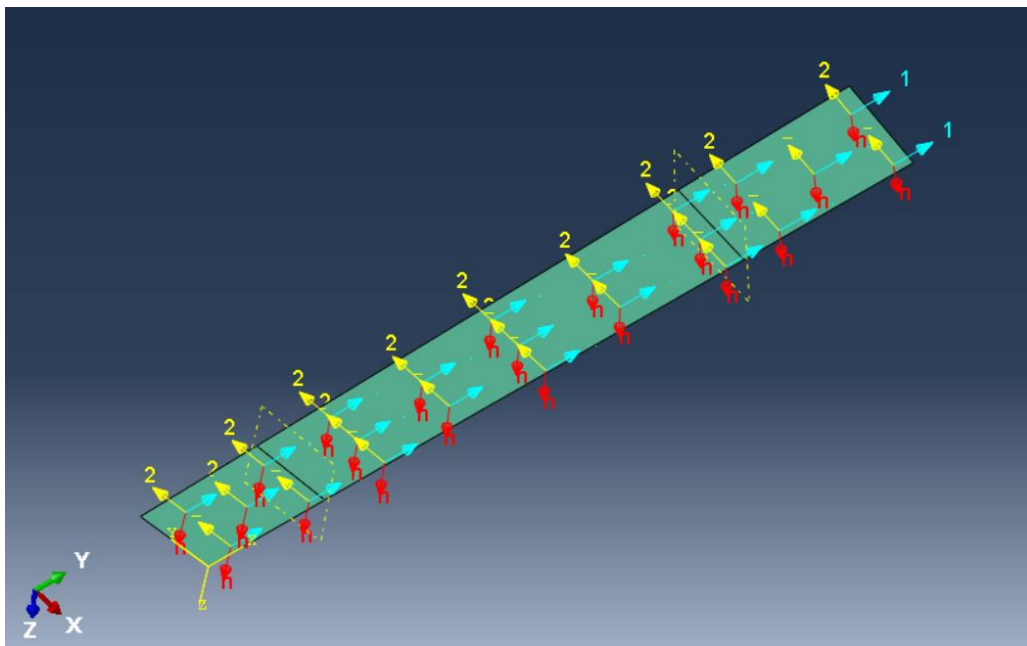


Figure 2. 15 : Orthotropic lamina behavior of fiber

2.4.2 Cohesive traction-separation law

This is a relatively complex and more realistic approach. The implementation of Cohesive traction-separation model suggests the dependence of contact stresses on the elastic stiffness of the interface. However, the interface is constrained by the limitation of negligible thickness to avoid further complications in the model. Thus, the nodes related to the two layers in FEM numerical model are not fixed to one another but actually linked based on the predefined stiffness of the interface. Thus, the interface no longer consists of a linear elastic phase only. The three phases observed by the cohesive model are as follows.

- Elastic linear phase with linear traction separation relationship (elastic), similar to Perfect Bond.
- Damage initiation phase
- Non-linear damage evolution phase (plastic).

The interface in the first phase is governed by the stiffness matrix.

$$\mathbf{t} = \begin{Bmatrix} t_n \\ t_s \\ t_t \end{Bmatrix} = \begin{bmatrix} K_{nn} & K_{ns} & K_{nt} \\ K_{ns} & K_{ss} & K_{st} \\ K_{nt} & K_{st} & K_{tt} \end{bmatrix} \begin{Bmatrix} \delta_n \\ \delta_s \\ \delta_t \end{Bmatrix} = \mathbf{K} \delta$$

Where the t_n is the nominal traction stress vector, t_s and t_t are the two tangential stress vectors, orthogonal to the nominal stress vector. In order to determine the end of first phase and the start of damage evolution phase, a damage criterion is defined. When the damage criterion is reached, the initiation of damage starts, and the interaction is no longer linear. The damage criteria is defined as

$$\max \left\{ \frac{t_n}{t_n^0}, \frac{t_s}{t_s^0}, \frac{t_t}{t_t^0} \right\} = 1$$

Where the values in the denominator are the corresponding peak values of the stresses. After the initiation of damage, the damage evolution law is adopted to describe the rate of degradation of cohesive stiffness in the interface.

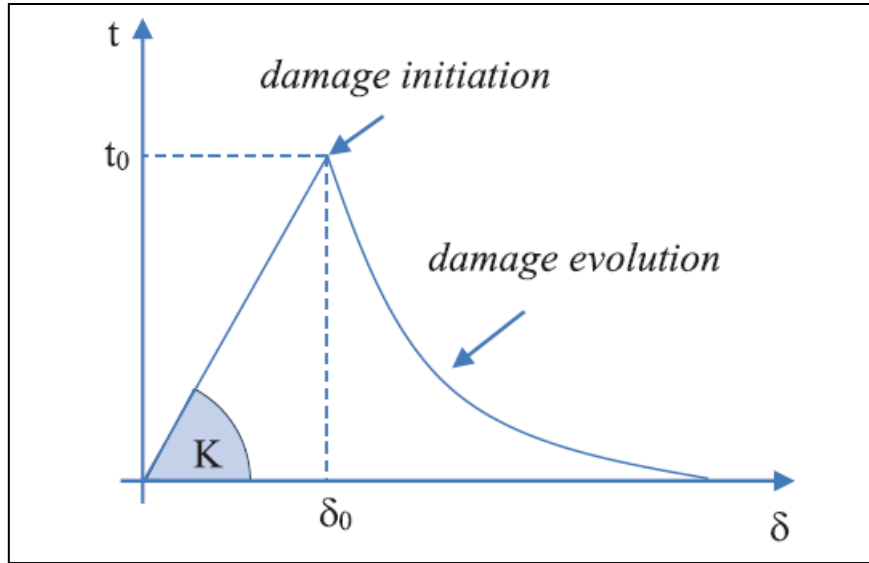


Figure 2. 16 : Cohesive model

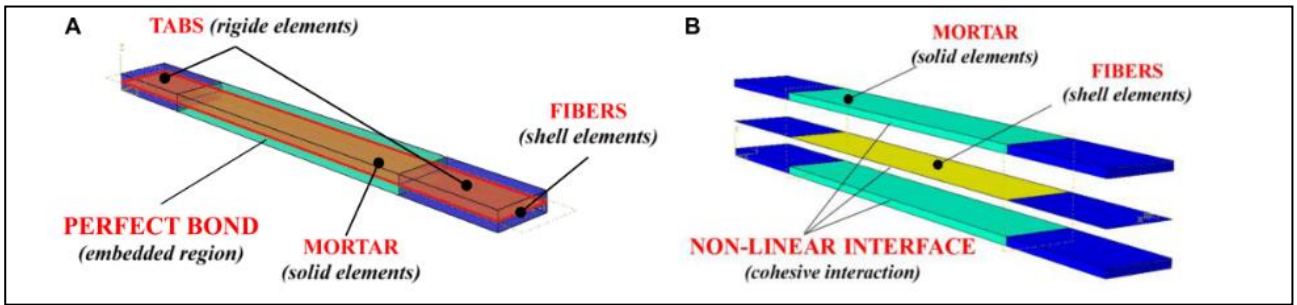


Figure 2. 17 : 1) Perfect Bond 2) Cohesive interaction

2.4.3 Meshing and boundary conditions

In order to simulate the numerical model of the TRM specimen, the boundary conditions are implemented in such a way that rigid tabs are provided at top and bottom ends to avoid the slippage between the mortar and the fiber. Thus, the nodes in this region are fixed by rigid boundary condition. A reference point is attached to one end which is linked to the region governed by rigid boundary condition. Thus, the tie nodes belonging to the rigid boundary condition are attached to reference point such that their degree of freedom is linked with each other. According to the practice adopted by mentioned research article, the displacement is applied to the reference point at the bottom and the encaster boundary condition is applied to the top. The encaster boundary conditions constraints the tie nodes.

Thus, the specimen is fixed at the top by encaster BC and displacement BC is applied at the bottom.

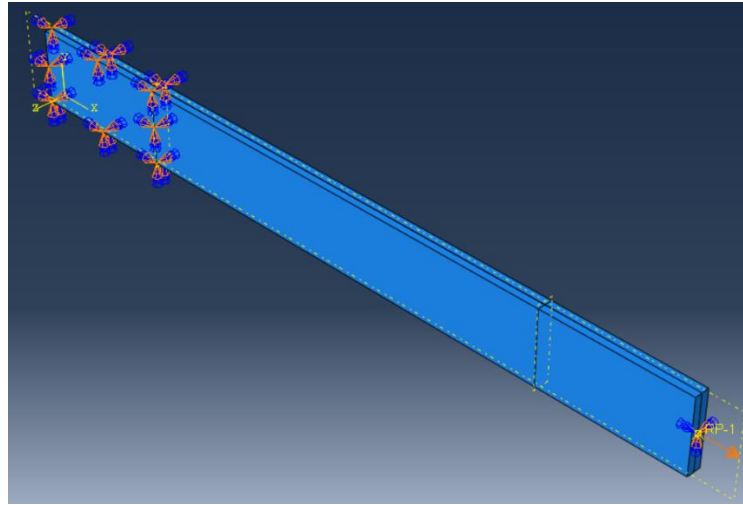


Figure 2. 18 : TRM Specimen with BCs

Meshing for the TRM specimen is done in such a manner that first order hexahedral elements were chosen for the mortar layer (CD3D8R) and the meshing for fiber layer was carried out using linear quadrilateral shell elements (S4R). Mesh size of 4mm was adopted, depending on the computational time. Mesh type and size are actually a tradeoff between the authenticity of results and computational time. So, mesh sensitivity analysis was done to choose the proper mesh.

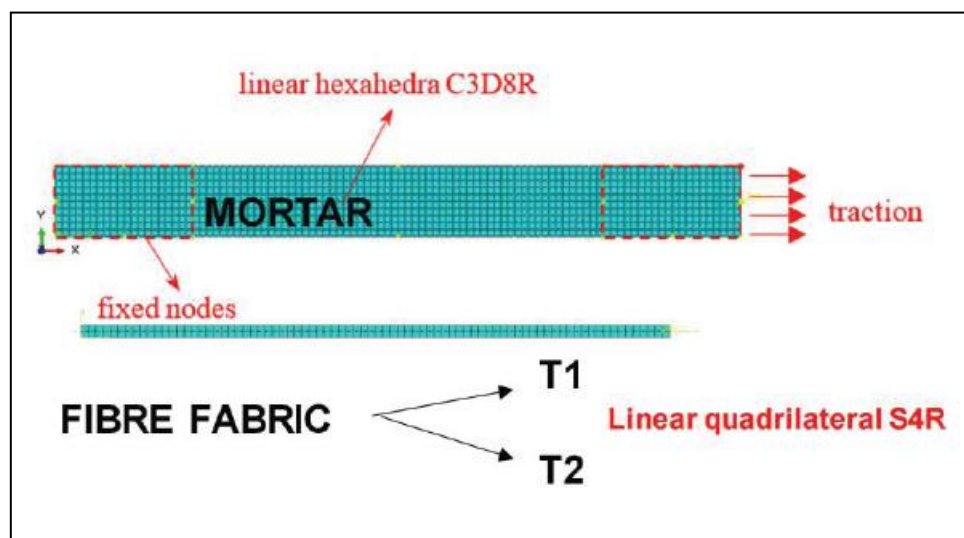


Figure 2. 19 : Mesh of Fiber and Mortar

2.4.4 Mechanical characterization of TRM

In order to characterize the TRM specimen, some mechanical variables need to be determined. In the research, for the fiber part, considered as lamina, these mechanical properties are defined across two orthogonal planes, the longitudinal and the transverse direction. The mechanical properties are deduced from the experimental results obtained by experimentation. Following are the mechanical parameters that need to be determined

- The elastic modulus E_1 in the longitudinal direction and E_2 in the transverse direction. In the case of the mentioned research, the E_2 is considered as 0.4% of E_1 .
- The poisson's ratio is set to be 0.35 along both orthogonal planes v_1 and v_2 .
- The shear modulus along all three planes G_{12} G_{23} and G_{13} depends on the respective poisson's ratio value.

$$G_{12} = \frac{E_1}{2 \cdot (1 + v_{12})};$$

$$G_{13} = \frac{E_1}{2 \cdot (1 + v_{13})};$$

$$G_{23} = \frac{E_2}{2 \cdot (1 + v_{23})}$$

- The value of Nusselt number Nu_{12} is adjusted as 0.35.
- Values of plastic strain and yield stress are obtained from experimental results and are different for each type of fiber element used.

The mechanical parameters for mortar in the case of perfect bond approach are the poisson's ratio and young's modulus. As before, they are obtained from experimental results. But in case of the cohesive approach, a proper mechanism for the post elastic region needs to be defined. So for this purpose, in the case of mentioned research, the constitutive model proposed by Sargin (1971) [1] was implemented. For the simulation of tensile behavior, the average of stress strain curves obtained by a series of experiments was used. For determination of damage variable for tensile and compressive behavior, following equation proposed by Mazzucco were considered.

$$d_c = 1 - (1 - A_c) \frac{\lambda_c}{\varepsilon_{eq}^p} - A_c e^{[-B_c(\varepsilon_c - \lambda_c)]};$$

$$d_t = 1 - (1 - A_t) \frac{\lambda_t}{\varepsilon_{eq}^p} - A_t e^{[-B_t(\varepsilon_t - \lambda_t)]}$$

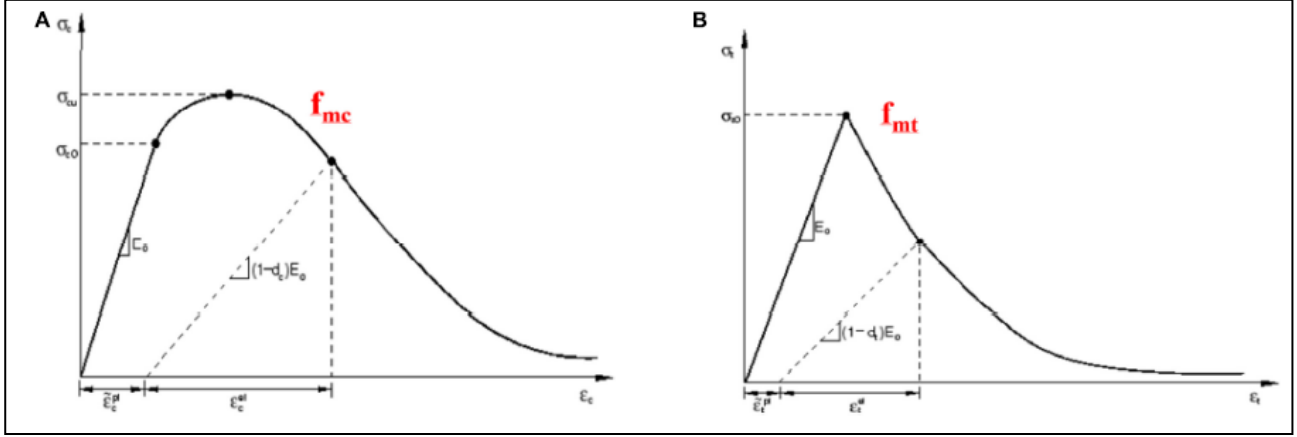


Figure 2. 20: Constitutive model A) For compression B) For tension

Traction	Compression
$A_t = 1.00$	$A_c = 0.95$
$B_t = 1100$	$B_c = 500$
$\lambda_t = 0.00001$	$\lambda_c = 0.002$

Figure 2. 21: Damage perimeters of mortar

For the simulation of interface between the fiber and mortar in the case of cohesive approach, is done using the surface-to-surface interaction tool in the ABAQUS. The fiber is taken as master surface and mortar as slave surface. These surfaces are linked with each other using uncoupled traction-separation response concept proposed by (Monaco, 2016; Carozzi et al., 2016; Malena et al., 2019; Monaco et al., 2019) [2]. In this approach, the stiffness matrix needs to be defined with normal direction k_{nn} , tangential direction k_{tt} and longitudinal direction k_{ss} . All the extra diagonal terms in the stiffness matrix are set to be zero.

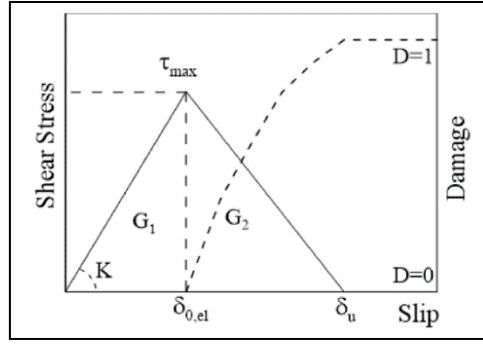


Figure 2. 22: Damage Evolution at interface

2.4.5 Validation of numerical results against experimental data

For the purpose of comparison and validation of numerical results, experimental data available in research literature by Arboleda[6], D'Antino [4] and D'Anna [6] are taken into account. For the sake of simplicity and effectiveness, for validation, only single fiber layer models were analyzed in all approaches. Some experimental details for each experimental campaign is expressed as follows.

Table 2. 5 : Specification of experimental tests

	Mortar	Fibers	No. of layers	f_t (MPa)	E_f (GPa)	f_m (MPa)	E_m (GPa)
Arboleda et al., 2016	Cementitious enriched with short fibers (<5%)	PBO	1	3,400	216	4.75	>6
D'Antino and Papanicolaou, 2018	Cement-based	Coated-carbon	1	1,890	219	6.7	15
D'Anna et al., 2019	Cement-based, reinforced with short glass fibers	Basalt	1	2,045	82	8	10

f_t = tensile strength of the fiber; E_f = elastic modulus of the fiber; f_m = tensile-bending strength of the mortar; E_m = elastic modulus of the mortar in compression.

A graphical representation of the comparison of results obtained from numerical modelling and the experimental campaign are shown below.

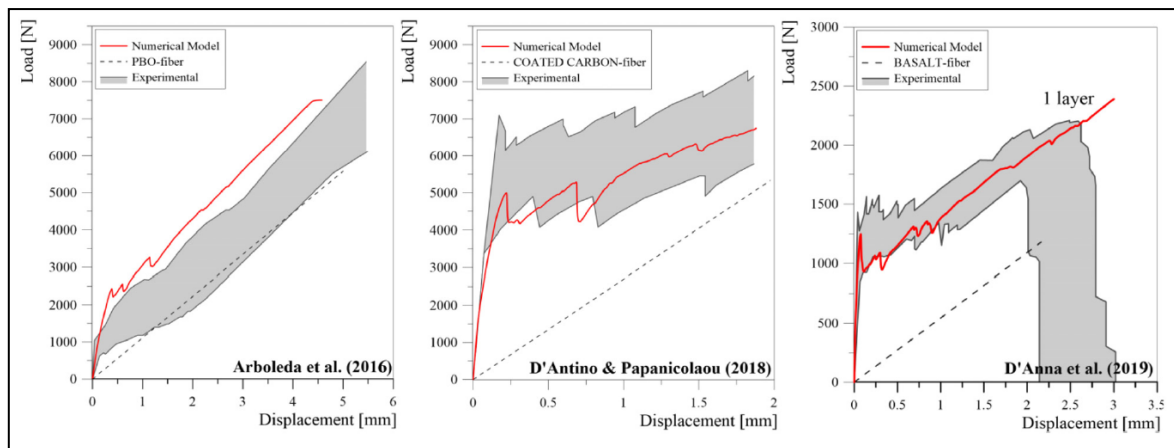


Figure 2. 23: Comparison of Numerical model and experimental campaign

The above graphs represent the cohesive approach which exhibits quite good results. The trend of the graph is in correspondence with the experimental data. The elastic region is determined very effectively by the numerical model, and the trend in the crack initiation and crack evolution stage is also within range of experimental values. However, the slope of damage evolution phase is not always in correspondence with the trend exhibited by axial stiffness of bare fiber.

In order to express the results of parametric analysis, graphs are represented which depict the stiffness values in the last stage normalized in comparison to the axial stiffness of the fiber layer by varying the mechanical ratio of fiber layer in the matrix. As a result of this variation, it is observed that we get a non-linear curve that slopes downwards (uptrend). The fiber ratio is refined as ω and is defined as

$$\omega = \frac{A_f f_f}{b t f_{mc}}$$

where A_f is the total are of the fiber layer, f_f is the tensile strength of fiber f_{mc} is the compressive strength. b and t are the two lengths of fiber. Thus, axial stiffness values do not increase in same amount as the mechanical ratio of fiber is increased. Finally, the effect of variation of ω becomes negligible. In 2nd graph, the trend of mechanical ratio of fiber is observed in accordance with the ratio of ultimate tensile capacity F_u and the capacity of fiber F_f . Now we obtain a downtrend with decreasing slope. So the effect of variation of ω becomes negligible as the ω is kept increasing.

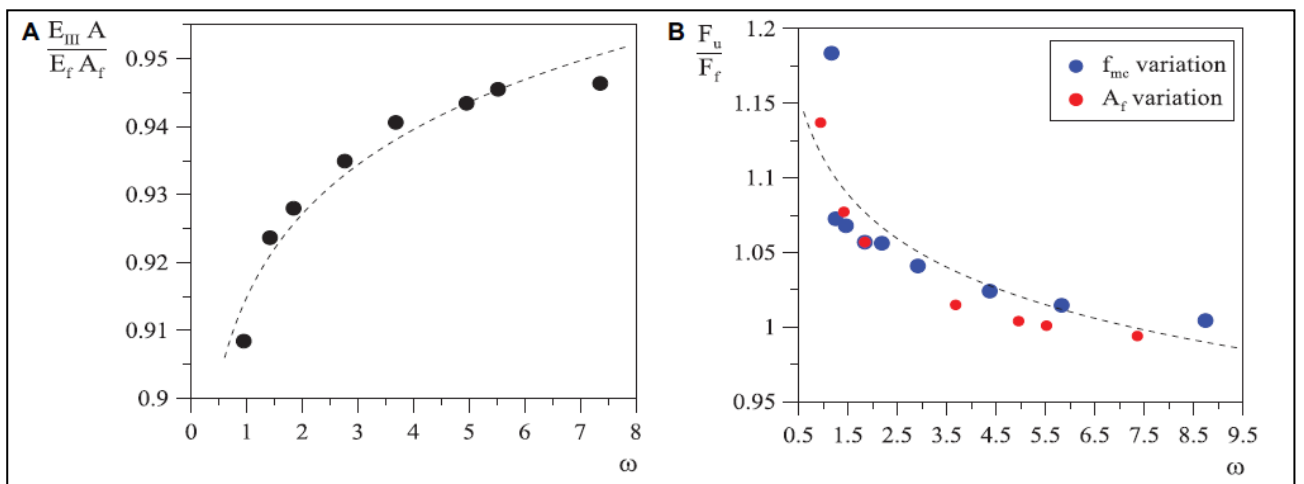


Figure 2. 24: A) Axial stiffness in damage evolution phase B) Ultimate tensile capacity

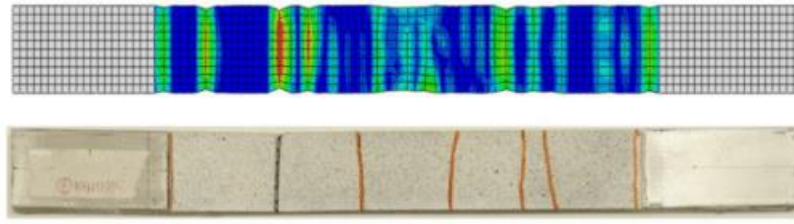


Figure 2. 25 : Comparison between crack patterns

2.5 Experimental campaign by D'Anna et al. (2021)

Experimental campaign by D'Anna et al. (2021) [19], as in the case of previously mentioned research, involves the experimental characterization of TRM materials. In order to justify the application of TRM materials in masonry applications, the properties and experimental behavior of each and every TRM material needs to be defined in order to justify the reliability of corresponding material in the particular application. Research by D'Anna involves the characterization of Primed alkali-resistant bi-directional Basalt fiber (organic fiber) TRM using Digital image correlation. Basalt TRM includes the organic matrix whose mechanical behavior is quite complex because when the TRM material is tested, the mechanical properties depend not only on the properties of individual elements, but also on the interface between the two layers and also in the number of layers.

The difference in experimental campaign between D'Anna and previous researchers is that D'Anna tested the TRM material using experimental standards set by [13] using Digital image correlation in order to judge the behavior of specimen under traction.

The application of DICM technique involves the illumination of the specimen from behind using a light source. Linear targets or contrast marks are applied on the specimen in order to observe the behavior under traction. These marks are observed using video-extensometers. Video-extensometers provide contactless detection of the behavior of specimen under the action of load. DICM technique is based on the principle that specific contrast markers are set on the specimen having predetermined distance between them. Using the extensometer, the change in distance between the markers is observed. This data is analyzed using the DICM software.

2.5.1 Tensile testing of TRM

Experimental characterization in this research involved more in detail and precise testing of TRM material under traction load, using DICM. The experimentation involves 3 steps.

- First step is the experimental testing on bare fibers.
- Second step involves the testing of mortar specimens.
- The last stage involves the mechanical characterization of the TRM specimen.

2.5.2 Testing of fiber specimen

In order to carry out the mechanical characterization of constitutive elements of basalt TRM, the basalt fiber strips are tested via monotonic tensile tests following the standards set by [14]. The Fiber specimen taken for the experimentation have a wrap length of 260 mm and weft length of 13.5 mm. These fibers were glued to aluminum tabs in order to mount the fiber to 100 kN universal testing machine at a loading rate of 2 mm/min. The aluminum tabs were 80mm long and 2mm thick and were installed on both sides of each fiber. Fiber specimen is installed inside the testing machine using the aluminum tabs at both ends and the gripping of machine clamps on the aluminum tabs is of 50mm. The reason for having aluminum tabs longer than the gripped area is to reduce the stress concentration inside the fiber.

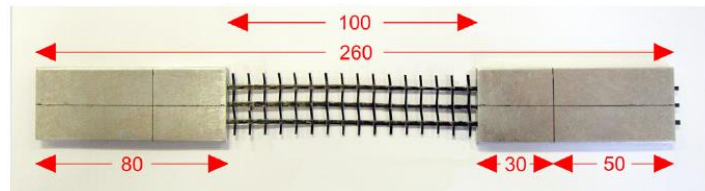


Figure 2. 26 : Specimen specifications for Basalt fiber testing

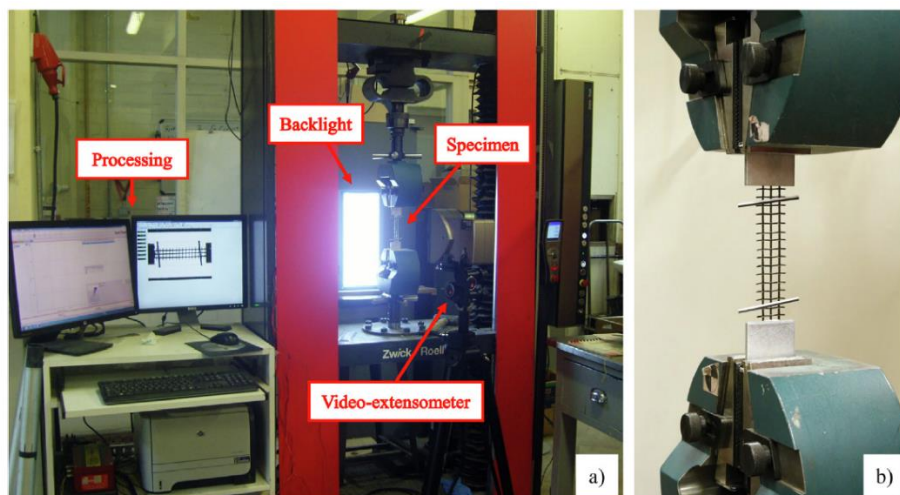


Figure 2. 27: Tensile test of Basalt grid a) Test setup using DICM b) Specimen installed on testing machine

One of the most important aspect to be decided in the characterization of tensile behavior using DICM technique is the position of the virtual extensometer. The position of extensometer must be adjusted in such a way that it depicts properly, the elongation of the specimen. In order to do so, the virtual extensometers are places along the edges where the aluminum tab is glued. The exact layout of virtual extensometers on the specimen is explained in following figure.

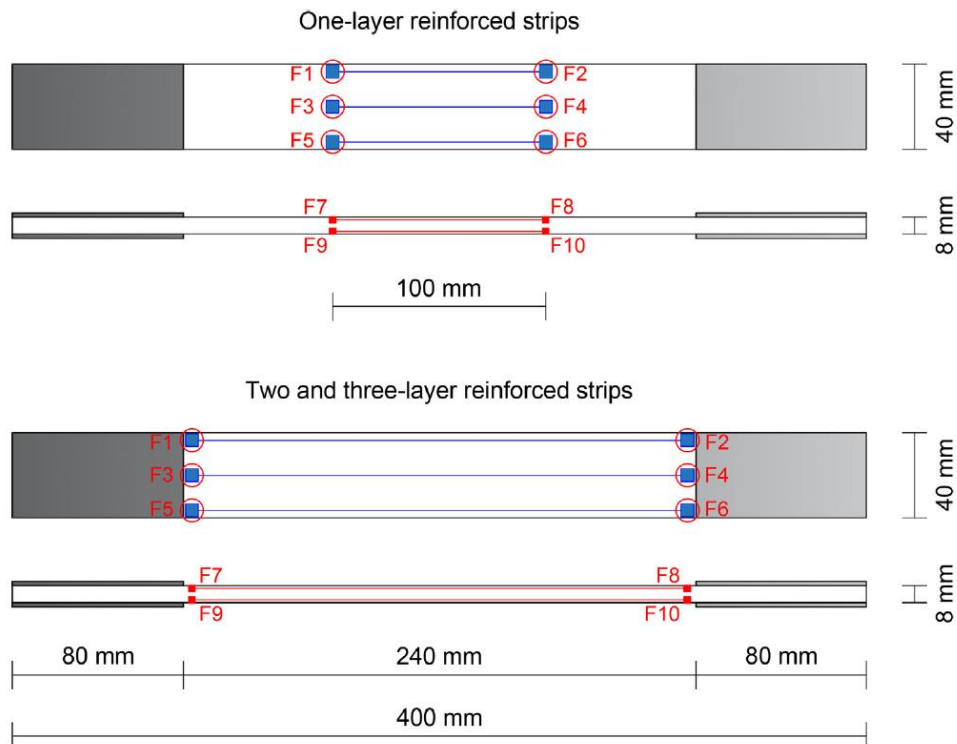


Figure 2. 28 : Positioning of Virtual Extensometer on Fiber specimen

2.5.3 Testing of mortar specimen

Mortar inside the basalt TRM basically consists of two components.

- Cement based high strength mixture of hydraulic natural lime, special additives and sand.
- Polymers reinforces with short glass fibers.

This mixture promises better compatibility with basalt fiber and better breathability properties in masonry applications of the TRM specimen. However, in this step of experimentation, the mortar mixture is tested individually, following the standards.

The mortar specimen prepared for the testing is basically prismatic, with a dimension of 40mm x 40mm x 160mm. Initially three-point bending tests were performed on the

specimen in order to determine the flexural strength of the specimen. As done before, DICM technique is used in the testing phase in such a way that contrast markers were sprinkled in the specimen surface and then the specimen is illuminated using a illumination source and the results are detected using the extensometer. As discussed before, the results depend on the positioning of virtual extensometer. The layout of the specimen and the result from each extensometer is as shown in figure.

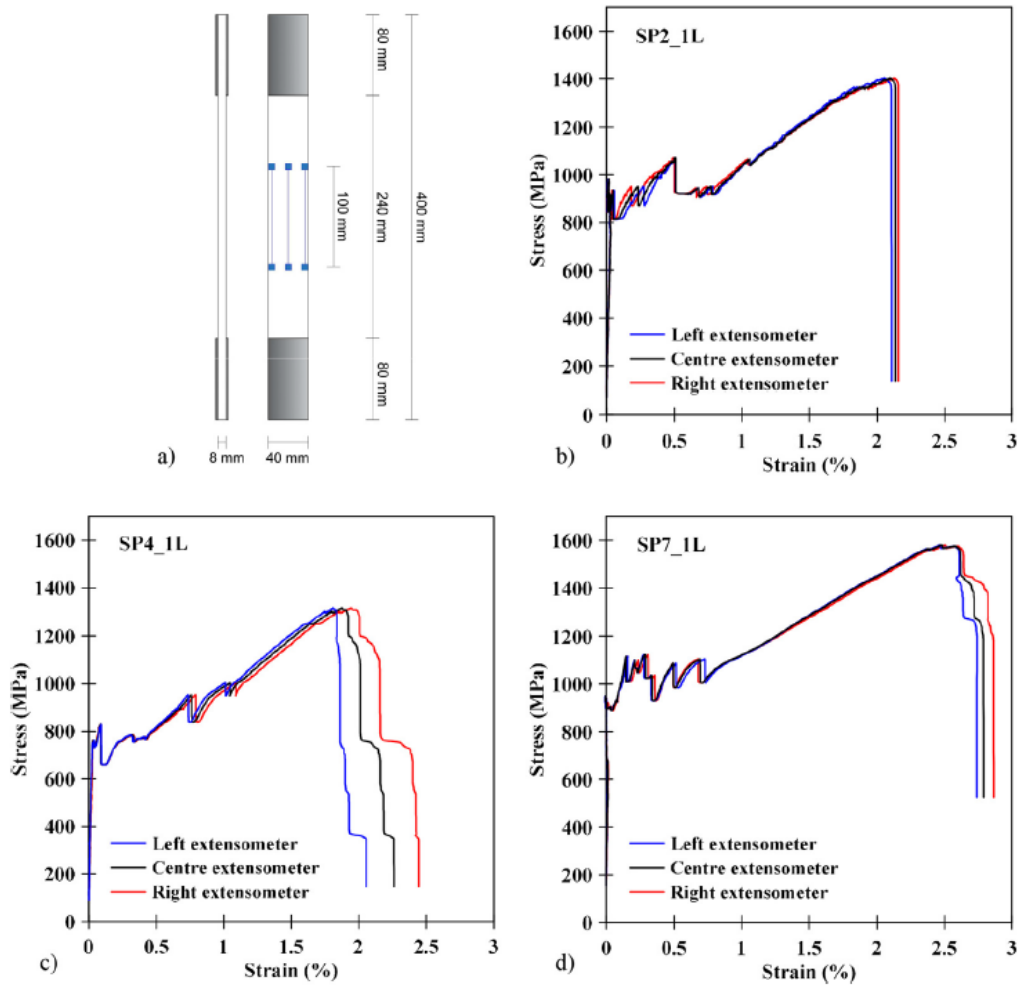


Figure 2. 29 : a) Position of virtual extensometer b) Stress-strain curve of SP2_1L c) Stress-strain curve of SP4_1L d) Stress-strain curve of SP4_7L

2.5.4 Testing of BTRM specimen

For the mechanical characterization of Basalt TRM, test setup is identical to that of the previous testing i.e 100kN universal testing machine with a load rate of 2 mm/min. The specimen for BTRM basically consists of two layers, mortar and the fiber. The number of layers depends on the tensile behavior of the BTRM specimen. The interface between the two layers is not provided with some extra bonding agent to avoid slipping of the two

layers. Instead, the mortar and the fiber layers are seasoned together as a result of which a cohesive interface is automatically developed between the two phases.

The preparation of BRFCM specimen is done following the standards already suggested by various research works [15,16,17]. The BTRM specimens are prepared in such a way that for single layer BTRM specimen, the mortar layers are 4mm thick. The fiber layer is sandwiched between two mortar layers. But for the specimen with multiple layers, the mortar layer is of 2 or 3 mm, to avoid over thickening of the specimen. The cross-sectional area of the BTRM specimen is thus 40mm X 8mm and a unclamped length of 400mm. Aluminum tabs are provided at each end of the specimen in order to ensure a proper gripping with the clamping mechanism of the test setup and to ensure proper load transfer from machine to the specimen. The aluminum tabs are 80mm long and 40mm wide. In order to avoid the stress concentration at the most loaded point, the clamping area is less than the length of the aluminum tabs.

After the preparation of specimen, the specimen is seasoned at 20°C and 70% relative humidity for 30 days.

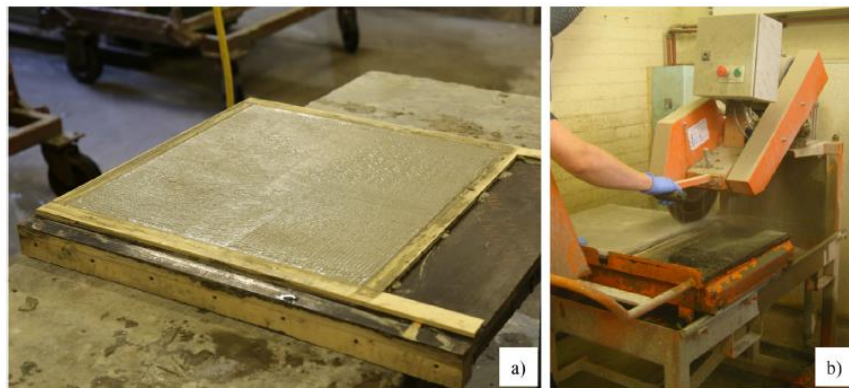


Figure 2. 30: Manufacturing of BTRM Coupon a) Coupon slab b) Curing of specimen

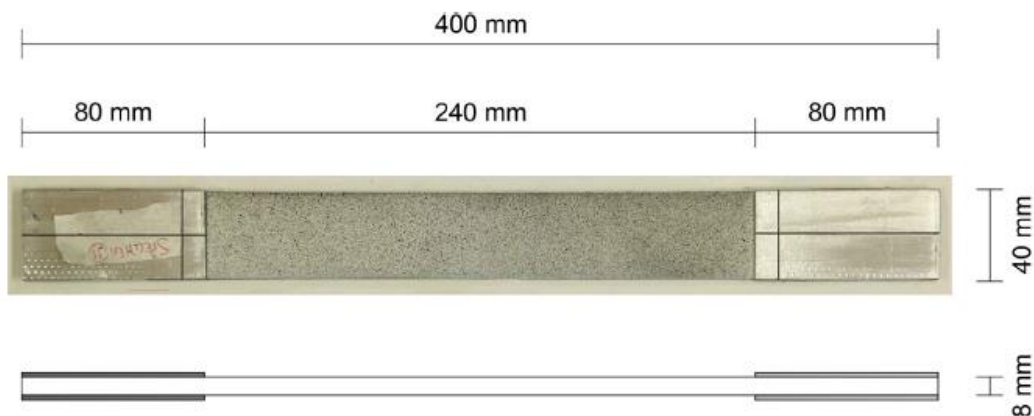


Figure 2. 31 : BTRM specimen with tabs and speckle pattern

One of the major problems with the specimen with single layer is that the failure often occurs at highly concentrated point other than the middle fiber region where the failure needs to occur in order to have a perfectly performed experiment. However, in order to resolve this issue, an additional reinforcement of the fiber layer is implemented with a dimension of 150mm X 40mm. However, the specimen with multiple layers is not provided with the extra reinforcement because that would increase the thickness.

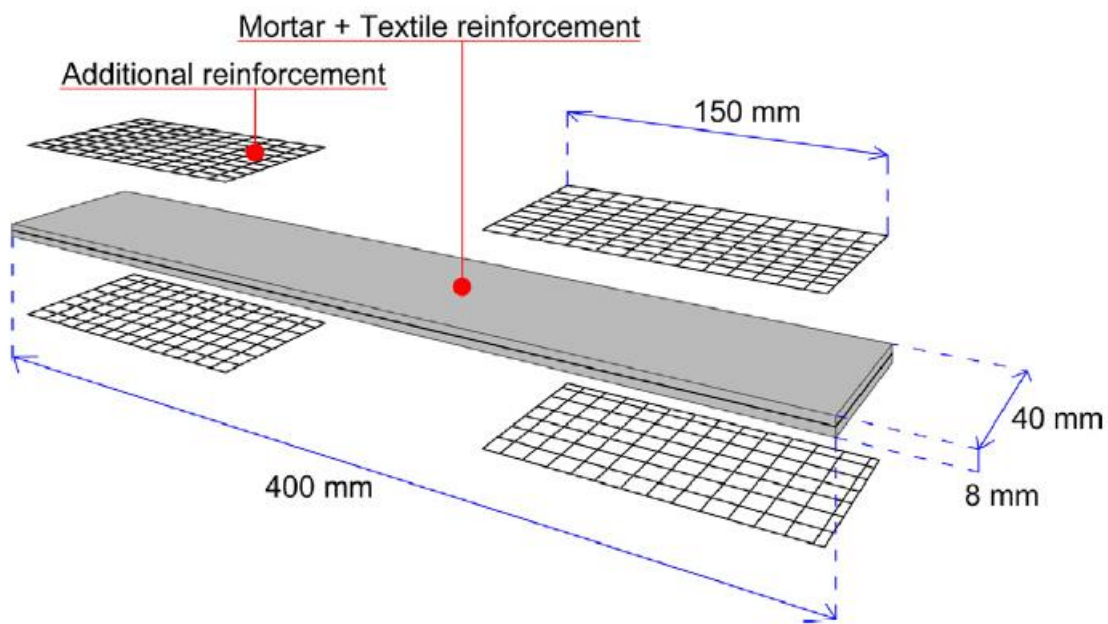


Figure 2. 32 : Additional reinforcement in single layer BTRM

2.5.5 Results

Experimental campaign adopted by D'Anna involves the testing of Fiber, mortar and the composite material. Individual tests were performed using the same testing strategy as well as the same testing equipment. Test on bare fibers included the tests on Basalt fiber in wrap and weft direction. Basalt fiber is a bi-Directional fiber with mechanical properties different in both directions. The results obtained as a result of experimentation are shown below in the form of following graph.

As a result of testing on fiber specimen, the average of peak stress in wrap direction for all specimen under observation was 2045 MPa, average strain was 2.55% and the average of elastic modulus was 81.91 GPa. In the case of testing on fiber in weft direction, the average of peak stress, strain and Elastic modulus was 1983 MPa, 2.4% and 81.88 GPa respectively.

In the case of composite specimen, the stress strain relationship is extended over three phases. It is observed that the scatter of strain at peak stress point ranges from 0.44% to 4% which shows that the bending effects are negligible in the plane of the specimen. The experimental results are shown in the form of table as follows.

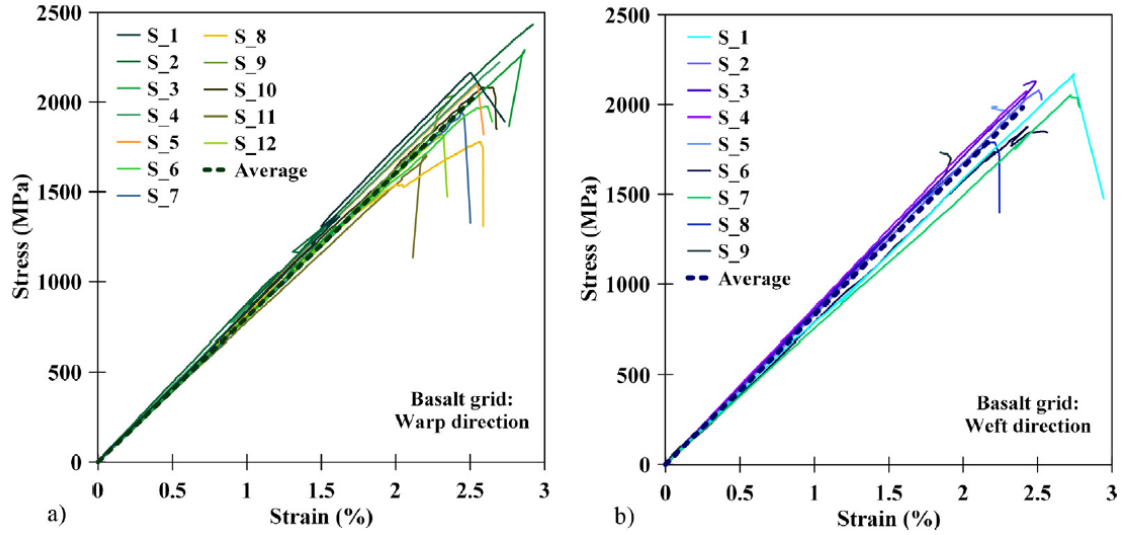


Figure 2. 33: Stress-strain curve a) Wrap direction b) Weft direction

Table 2. 6 : Results of BTRM coupon in all stages

	Samples	Peak load [N]	Peak stress [MPa]	Strain [%]	Tangent modulus [GPa]
Stage I		F_I	$\sigma_I = F_I/A_f$	ϵ_I	E_I
	SP1_1L*	–	–	–	–
	SP2_1L	1306.85	933.46	0.048	1947.14
	SP3_1L	756.24	540.17	0.015	3684.67
	SP4_1L	1067.87	762.76	0.034	2233.56
	SP5_1L	1427.38	1019.56	0.042	2432.16
	SP6_1L	1446.39	1033.13	0.018	5739.64
	SP7_1L	1315.78	939.84	0.021	4475.45
	SP8_1L	1318.24	941.60	0.035	2653.89
	Average (COV %)	1234.11 (19.8%)	881.50 (19.8%)	0.030 (41.8%)	3309.50 (42%)
	SP1_2L	1788.57	638.77	0.038	1690.90
	SP2_2L	1491.68	532.74	0.031	1722.97
	SP3_2L	1063.47	379.81	0.015	2566.29
	SP4_2L	1331.08	475.39	0.048	987.92
	SP5_2L	1566.32	559.40	0.041	1353.67
	Average (COV %)	1448.22 (18.7%)	517.22 (18.7%)	0.035 (36.7%)	1664.35 (35.2%)
	SP1_3L	1437.38	342.23	0.044	786.74
Stage II		F_{II}	$\sigma_{II} = F_{II}/A_f$	ϵ_{II}	E_{II}
	SP1_1L*	–	–	–	–
	SP2_1L	1318.42	941.73	0.826	9.33
	SP3_1L	1264.24	903.03	0.862	38.57
	SP4_1L	1426.55	1018.96	1.145	26.33
	SP5_1L	1517.34	1083.82	1.202	6.05
	SP6_1L	1430.40	1021.71	0.979	18.55
	SP7_1L	1523.73	1088.38	0.874	11.53
	SP8_1L	1305.57	932.55	1.242	8.70
	Average (COV %)	1398.03 (7.4%)	998.60 (7.4%)	1.019 (17.2%)	17.01 (69.2%)
	SP1_2L	1973.63	704.87	0.458	18.66
	SP2_2L	1693.58	604.85	0.383	31.07
	SP3_2L	1896.52	677.33	0.411	65.45
	SP4_2L	1885.00	673.21	0.531	40.87
	SP5_2L	1827.60	652.71	0.460	26.48
	Average (COV %)	1855.26 (5.6%)	662.59 (5.6%)	0.448 (12.5%)	36.51 (49.5%)
	SP1_3L	1821.68	433.73	0.229	43.78
Stage III		F_{III}	$\sigma_{III} = F_{III}/A_f$	ϵ_{III}	E_{III}
	SP1_1L	2080.92	1482.14	2.463	–
	SP2_1L	1964.19	1402.99	2.096	36.31
	SP3_1L	2132.64	1523.32	2.028	53.22
	SP4_1L	1841.98	1315.70	1.876	40.61
	SP5_1L	2134.09	1524.35	2.503	33.86
	SP6_1L	2083.79	1488.42	2.392	33.01

Samples	Peak load [N]	Peak stress [MPa]	Strain [%]	Tangent modulus [GPa]
SP7_1L	2211.45	1579.61	2.577	28.84
SP8_1L	1990.37	1421.69	2.643	34.93
Average (COV %)	2054.93 (5.7%)	1467.28 (5.7%)	2.322 (12.2%)	37.25 (21.2%)
SP1_2L	3847.49	1374.10	2.151	39.53
SP2_2L	4149.43	1481.94	2.405	43.38
SP3_2L	3295.68	1177.03	1.549	43.89
SP4_2L	3328.44	1188.73	1.815	40.14
SP5_2L	3069.95	1096.41	1.641	37.56
Average (COV %)	3538.20 (12.6%)	1263.64 (12.6%)	1.912 (18.8%)	40.90 (6.6%)
SP1_3L	4633.19	1103.14	1.466	54.13

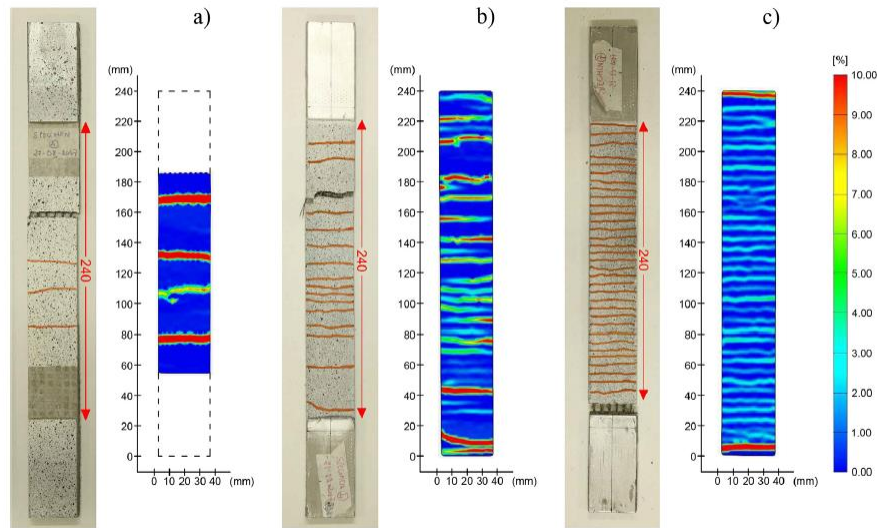


Figure 2. 34 : Cracking pattern in a) One-layer reinforced specimen SP8_1L b) Two-layer reinforced specimen SP2_2L c) Three-layered reinforced specimen SP1_3L

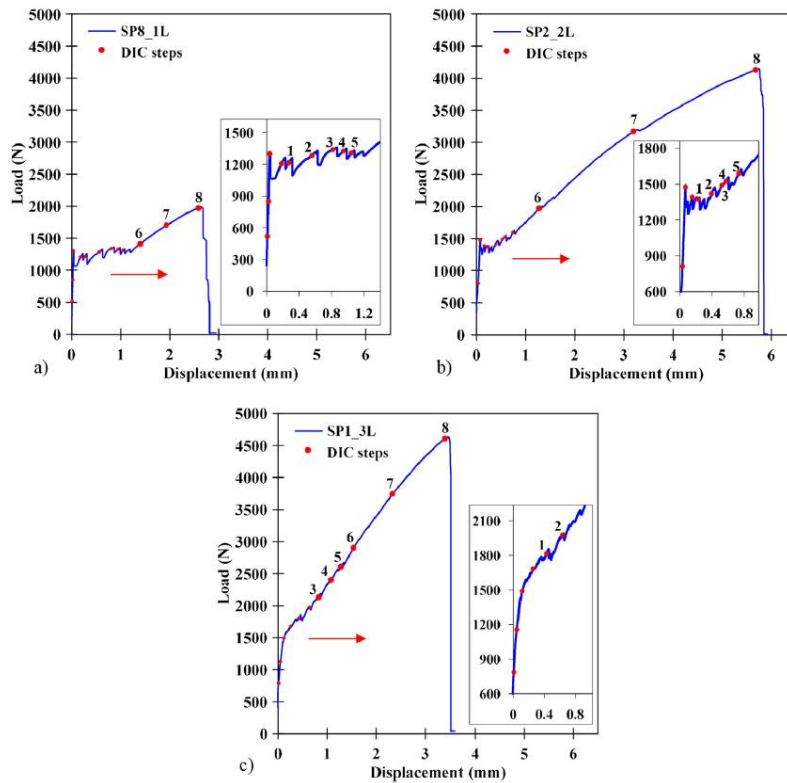


Figure 2. 35 : Load displacement curves of in a) One-layer reinforced specimen SP8_1L b) Two-layer reinforced specimen SP2_2L c) Three-layered reinforced specimen SP1_3L

Under the scope of this thesis, the main results that need to be compared between the experimental campaign performed by the author of research and the numerical model created by the thesis writer involves the stress-strain comparison and the load-displacement comparison between the two. For this purpose, only the stress-strain and the load-displacement graphs are discussed in this section.

2.6 References

- [1] Sargin, M. (1971). Stress-Strain Relationship for Concrete and the Analysis of Structural Concrete Sections. Study 4, Solid Mechanics Division. Waterloo: University of Waterloo.
- [2] Monaco, A. (2016). Numerical prediction of the shear response of semiprefabricated steel-concrete trussed beams. *Constr. Build. Mater.* 124, 462–474.
- [3] Marianovella Leonea,*, Maria Antonietta Aielloa, Alberto Balsamob, Francesca Giulia Carozzic, Francesca Ceronid, Marco Corradie, f, Matija Gamsg, Enrico Garbinh, Natalino Gattescoi, Piotr Krajewskij, Claudio Mazzottik, Daniel Oliveiral, Catherine Papanicolaoum, Giovanna Ranocchiai, Francesca Roscinio, Dorothea Saenge T. D’Antino Glass fabric reinforced cementitious matrix: Tensile properties and bond performance on masonry substrate.
- [4] D’Antino, T., and Papanicolaou, C. (2018). Comparison between different tensile test set-ups for the mechanical characterization of inorganic-matrix composites. *Constr. Build. Mater.* 171, 140–151.
- [5] D’Anna, J., Amato, G., Chen, J. F., Minafò, G., and La Mendola, L. (2019). On the use of Digital Image Correlation (DIC) for evaluating the tensile behavior of BTRM strips. *Key Eng. Mater.* 817, 377–384.
- [6] Arboleda, D., Carozzi, F. G., Nanni, A., and Poggi, C. (2016). Testing procedures for the uniaxial tensile characterization of fabric-reinforced cementitious matrix composites. *J. Compos. Constr.* 20:04015063
- [7] RILEM Technical Committee 232-TDT (Wolfgang Brameshuber) brameshuber@ibac.rwth-aachen.de, 2016. Recommendation of RILEM TC 232-TDT: test methods and design of textile reinforced concrete: Uniaxial tensile test: test method to determine the load bearing behavior of tensile specimens made of textile reinforced concrete. *Materials and Structures*, 49, 4923–4927. .
- [8] J. Lee, G.L. Fenves, Plastic-damage model for cyclic loading of concrete structures, *J. Eng. Mech.* 124 (8) (1998) 892–900.
- [9] M. Malena, G. de Felice, Debonding of composites on a curved masonry substrate: experimental results and analytical formulation, *Compos. Struct.* 112 (2014) 194–206, <https://doi.org/10.1016/j.compstruct.2014.02.004>.

- [10] M. Malena, Closed-form solution to the debonding of mortar based composites on curved substrates, *Compos. Part B: Eng.* 139 (2018) 249–258, <https://doi.org/10.1016/j.compositesb.2017.11.044>.
- [11] De Santis, F. Ceroni, G. de Felice, M. Fagone, B. Ghiassi, A. Kwiecie, G.P. Lignola, M. Morganti, M. Santandrea, M.R. Valluzzi, A. Viskovic, Round robin test on tensile and bond behaviour of steel reinforced grout systems, *Compos. Part B: Eng.* 127 (2017) 100–120.
- [12] S. De Santis, H.A. Hadad, F. De Caso y Basalo, G. De Felice, A. Nanni, Acceptance criteria for tensile characterization of fabric-reinforced cementitious matrix systems for concrete and masonry repair, *J. Compos. Constr.* 22 (6) (2018) 04018048.
- [13] EN 1015-11. Methods of test for mortar for masonry – Part 11: Determination of flexural and compressive strength of hardened mortar. 1999.
- [14] ISO 13934-1. Textiles – Tensile properties of fabrics – Part 1: Determination of maximum force and elongation at maximum force using the strip method. CEN – European Committee for Standardization. April 2013.
- [15] ICC. AC434. Proposed Acceptance Criteria for Masonry and Concrete Strengthening Using Fibre-reinforced Cementitious Matrix (TRM) and Steel Reinforced Grout (SRG) Composite Systems. Whittier, CA: ICC-Evaluation Service, 2016.
- [16] RILEM Technical Committee 232-TDT (Wolfgang Brameshuber) *Mater Struct* 2016, 49: 4923. doi:10. 1617/s115270160839z.
- [17] G.P. Lignola, C. Caggegi, F. Ceroni, S. De Santis, P. Krajewski, P.B. Lourenço, L. Zuccarino, Performance assessment of basalt TRM for retrofit applications on masonry, *Compos. Part B-Eng.* 128 (2017).
- [18] Monaco, A., Minafò, G., D’Anna, J., Oddo, M. C., & La Mendola, L. (2020). Constitutive numerical model of FRCM strips under traction. *Frontiers in Built Environment*, 6, 60.
- [19] D’Anna, J., Amato, G., Chen, J. F., Minafò, G., & La Mendola, L. (2021). Experimental application of digital image correlation for the tensile characterization of basalt FRCM composites. *Construction and Building Materials*, 271, 121770.
- [20] Malena, M., Sangirardi, M., & de Felice, G. (2019). Steel Reinforced Grout under uniaxial load: Experimental evidences and numerical modelling. *Construction and Building Materials*, 227, 116808.

Chapter 3: Numerical modeling with ABAQUS

The concept of numerical modeling was developed in order to reduce the dependence research on experimentation. There are numerous drawbacks to practical experimentation such as high costs, time consumption and various factors that affect the accuracy of experimental results. Numerical modeling provides with a cost effective and time saving as well as effective alternative to experimentation. There are numerous techniques for numerical modeling such as Finite Volume Method (FVM), Finite Element Method (FEM) and Finite Differential Method (FDM). A little comparison between these three is as follows.

FDM is relatively older technique. It requires less computational time but the accuracy of FDM is lower. In the case of FDM, the solution of partial differential equations is obtained at each node.

FVM is also easier to perform and usually provides us with better conservation properties. Computational time required for FVM is still lower than FEM. Partial differential equations are solved for a given finite volume. These finite volumes are actually infinitesimal volumes obtained by space discretization.

FEM is the most accurate technique but requires high computational time. Accuracy of results depends a lot on the mesh quality. In case of FEM, the entire computational domain is split in smaller domains called finite elements, by space discretization. In case of FEM, we get algebraic equations for steady state problem and partial differential equations for transient problems. These equations are solved on each finite element. FEM can easily handle complex geometries.

So, in our case we use FEM using ABAQUS.

3.1 Introduction to ABAQUS CAE

ABAQUS CAE (Complete ABAQUS Environment) is a software application used for construction of model, application and implementation of FEM and finally proper visualization of results using appropriate interactive graphical techniques. ABAQUS CAE is contains the mechanism for solution of FEM method on constructed model as well as ABAQUS Viewer for post processing, accessed through module visualization which

manages the results obtained by simulation in output database file (ODB). The results from ODB are further post processed as various visual graphics. ABAQUS CAE has also the advantage of being able to accept the models which are imported from various modelling platforms. ABAQUS CAE offers complete freedom of customization of material and physical properties for the model. Mechanical and material properties of model as well as environment can be adjusted together with the loads and the boundary conditions. ABAQUS CAE allows you to build models quickly and easily. After the completion of the model, the model is submitted for simulation and the results can be monitored. There are various modules included in the ABAQUS CAE interface, in order to determine all the required inputs. Following are the modules.

Part: In the part module, the user defines the geometry of individual elements of the model.

Property: In the property module, the user defines the mechanical and physical properties of all the materials included in the model. After creating the materials by defining properties, the user determines various sections of the model and assigns material to every section.

Assembly: In this module, the user defines the assembly by connecting and mating various parts created in the part module. Users can define various sets and surfaces according to need.

Step: In the step module, the user defines the time aspect of the model by determining the time period, the number of increments, and related increment sizes.

Interaction: In the interaction module, the user defines the interaction between various parts on the basis of contacting surface between them. Various interactions can be set between parts like surface-to-surface contact, self-contact, pressure penetration etc

Load: In the load domain, the user defines the load and the loading conditions on the model. The boundary conditions are also set in the load module.

Mesh: In the mesh module, the user defines the mesh, each part is seeded according to meshing criteria and then meshed.

Optimization: In the optimization module, users refine the model to get accurate simulation results. There are two basic ways of optimization, topology optimization and shape optimization.

Job: In the job module, the user defines the type of analysis done on the model.

Visualization: In the visualization module, the users get the result of the simulation. This module is provided with various graphical tools for better visualization of results.

So, the user defines the model in ABAQUS CAE which is submitted to ABAQUS Explicit or ABAQUS Standard for computation, and the simulation results are later post-processed in the ABAQUS.

3.2 Geometry

When defining each part of the model, user needs to determine if it is intended to construct a three-dimensional or plane geometry, as well as to indicate whether the part is deformable or rigid elements. A deformable part is an element which can deform under the action of a load that can be of the type mechanical, thermal, electrical, etc., while a rigid part represents a non-deformable part which is very often used in contact analyzes to model bodies that cannot be deformed. It is then possible to draw the geometry with solid shapes, shell, wire or point. The definition of the geometry and, in particular, the choice of element is functional to the type of analysis needed to be performed. If three-dimensional geometry is chosen, definition of the method of extrusion of the plane geometry is also performed for example Extrusion, Revolution and Sweep commands. All this is performed using the initial window that appears when part is created.

After that, the modelling interface appears just like any other CAD software interface, that allows the user to creation of any two-dimensional geometry using the sketching tools. Another facility provided by ABAQUS is the ability to import the pre-constructed model (eg on AutoCAD, SolidWorks etc) into ABAQUS. In order to model bodies that cannot be deformed, it is possible to draw the geometry with solid shapes, shell, wire or point, depending on the selection. The definition of the geometry and, in particular, the choice element is functional to the type of analysis needed to be implemented. The model may be described using different type of external conditions.

- **Initial conditions**, with which are specified in the initial step, where various initial conditions are defined depending upon the type of fluid dynamic problem under investigation.

- **Boundary conditions**, which refer to variables of the problem, such as displacements or rotations in a static fluid dynamic analysis or temperatures in a heat transfer analysis, in case of Thermal problem.
- **Loads**, of various kinds and dependent on the analysis, can be contracted loads and distributed, which may or may not follow the rotation of nodes or surfaces to which they are referred, in case of FD problem.

It is essential for the analysis that the correct definition of the type of element to be associated with each part or region and the type of integration is performed. It is possible to choose between a linear or quadratic integration using the ABAQUS interface.

Following are the four techniques of meshing.

- **Structured:** this type of mesh generates structured meshes using simple predetermined shapes such as squares or cubes. The element used with this technique is a hexahedron (HEX) in three-dimensional parts.
- **Swept:** this meshing technique is used for complex surfaces. The meshing technique consists of two steps. ABAQUS CAE initially creates a mesh on one side of the region (called the source side), then copies the nodes of the mesh created one layer of element at a time, until it reaches the final side, this path is called sweep path. This technique is frequent in elements with circular sections or in perforated elements. The element used with this technique is a hexahedron (HEX) for three-dimensional parts, while TRI or QUAD for two-dimensional parts.
- **Free:** Unlike structured mesh, this technique does not use pre-established templates but allows for greater flexibility. The resulting meshes can be very complex. The element used with this technique is a tetrahedron (TEX) for three-dimensional parts, while TRI or QUAD for two-dimensional parts.
- **Bottom up:** This is a completely manual meshing procedure that allows you to construct a hexahedral mesh in any region of solid part. While all other techniques are constrained in some way by geometry. While this type of mesh can ignore some geometric constraints.

3.3 Material Properties

Material properties is the module where the composition of the geometry is defined. Each and every material, which is constituent of the geometry, is defined in this section. In order to define the material, various physical and mechanical properties need to be defined. To completely define a material inside ABAQUS interface, following domains and orientations of material properties must be determined.

- The **section assignment**, after defining the material. In the case of beam and truss elements, assignment of the profile.
- Defining the **orientation of the section** for the elements. Orientation is defined on all sections individually.
- A **local reference system** to define the characteristics and orientation of the material (Datum System of coordinates). if isotropic materials are not used. Material orientation is defined individually on all parts.
- The **normal direction** for shell or membrane elements.
- The **tangent direction** for the tangent beam truss elements.

As discussed before, the definition of a material depends on various physical and mechanical properties. These physical properties are obtained using the experimentation techniques. The modeling of a material passes through the definition of its characteristics, each of which associated with a specific fundamental mechanical or physical behavior.

3.4 Concrete Damage Plasticity

In order to completely realize and simulate a material in ABAQUS, the physical or mechanical properties are utilized in the form of individual characteristics or models. These models actually represent the behavior of material under the action of loadings. In the case of the model developed under the scope of this thesis, the CDP is used to model the mortar layer. In order to practice simplicity and to reduce the computation power and time, the material definition of mortar layer can be done using simple yield strength and tensile strength values corresponding to the specific strains produced as a result of experimentation.

However, in order to model the mortar layer more precisely, a complete and stepwise behavior of mortar under the action of loading can be considered. Using this method, one

can model the behavior of mortar layer in the plastic phase. This is the basis of Concrete Damage Plasticity. CPD is usually used to determine the behavior of materials under simple static loads and also under the action of complex loads like cyclic loads and dynamic loads. Like all plastic bonds, the Concrete Damaged Plasticity Model assumes that the material has a strength limit beyond which permanent deformations are formed. Thus, the response of material under the effect of load, depends on two phases, the elastic phase and the plastic phase (defined using CPD).

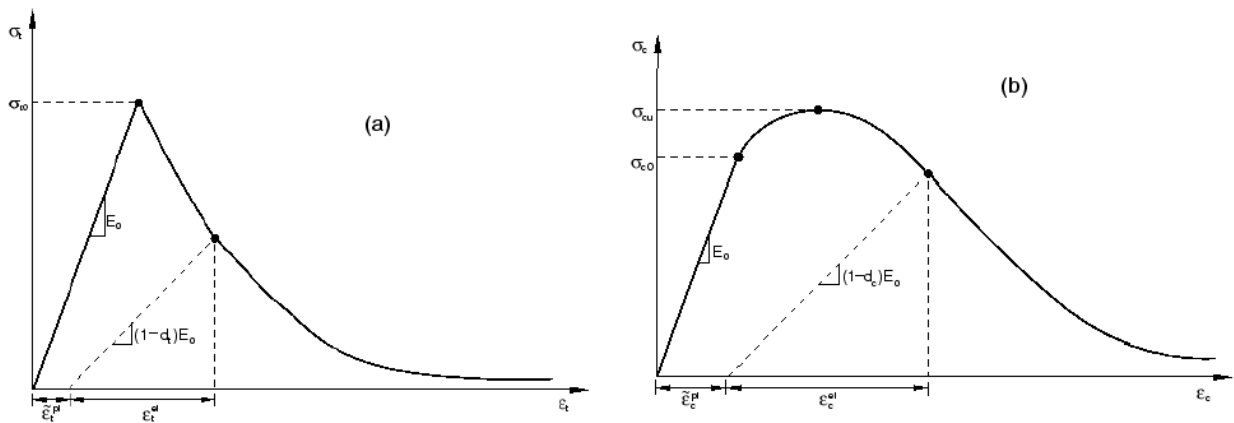


Figure 3. 1 : Stress-Strain curve a) For compression b) For mortar

Due to the dissipative nature of the elastic stiffness matrix, it does not undergo any modification during the load history. On the other hand, the plastic deformation process depends on the value of the applied stress as well as on the load path. Therefore no one-to-one correspondence between the applied stress and the plastic deformation is present. As a result, the relationships that correspond the stresses to the strains have to be written in incremental or differential form. In the development phase of plastic deformation, once the yielding is achieved, the stress-strain relationship can be of three types, namely hardening, softening or perfect relationship. The constitutive equation that defines this section is called the sliding law. In the case of complex stress states, as in the case of mortar, a function must be established that determines all the points of initiation of plastic strains, that means a yield criterion must be defined. When a stress state is found on the surface defined by the yield function, the slip law takes over to define the link between incremental stresses and strains. This law can be of two types:

- **Associated**, which is applied if the direction of the plastic strain is orthogonal to the surface.
- **Non associated**, which is applied if the direction of plastic strain is other than orthogonal to surface.

In order to express the evolution of yielding behavior (Plastic Potential function), in case of materials that do not exhibit a perfectly plastic behavior, it is necessary to completely define all the required parameters and the evolution equation. Hydrostatic pressures play vital role in the case of brittle materials or the materials that exhibit near brittle behavior, like mortar and other masonry materials. Thus, in order to define the yield criteria, the hydrostatic effects must be taken into account. These include the Drucker – Prager criterion and the Mohr – Coulomb criterion for isotropic materials.

The mohr-Coulomb acts such that it estimates the failure pattern in one plane when the predetermined upper limit of combination of Normal and Tangential forces is achieved. This law is a general form of Friction failure hypothesis. Mathematically it is expressed as

$$\tau = c - \sigma_n \cdot \tan\phi$$

where τ is the value of the shear stress on the failure plane, c is the cohesion, σ_n is the normal stress on the failure plane and ϕ is the internal friction angle. In the case of Mohr-Coulomb criterion, as in the law of friction failure, the yield stress not only relates to the maximum stress in tangential direction, but also to the normal stress applied on the shear plane. As discussed before, the Mohr-Coulomb criterion is a General or particular case of Mohr Criterion. Following figures graphically represent the application of Mohr-Coulomb criterion.

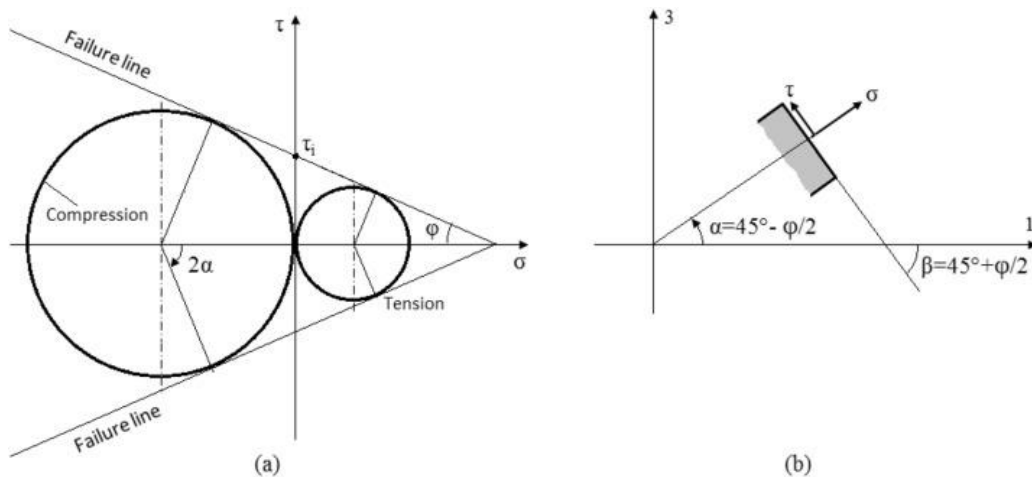


Figure 3. 2 : Mohr-Coulomb criterion a) Mohr circle representation b) Stresses in tangential and normal direction

The graphical representation of the Mohr's plane shows that in the principal planes σ_1 and σ_2 , the yield stress is prismatic. Beyond that prismatic region we get the plastic region. However, the tension compression yield region in the Mohr's criteria is of hexagonal nature. The material properties of material exhibiting the CDP expresses a high compressive strength as compared to tensile strengths. However there may be some exception in the case of composites like fiber glass where tensile strength is more than compressive strengths. But in the case of majority of brittle materials like concrete etc, the compressive strength is significantly higher than the tensile strength. CPD model is designed in accordance with the tensile as well as compressive nature of the material.

Another criterion that needs to be defined here is the Drucker and Prager criterion. Main significance of this criteria is that the concrete damage plasticity in ABAQUS is based on this criterion. Drucker and Prager criterion provides excellent CDP representation of the material behavior of concrete, masonry materials and mortars etc. Drucker and Prager criterion is based on the modification of Von Mises yield criterion, which was one of the pioneers theoretical formulations for combining the tensile and shear stresses. The modified form of Von Mises criteria suggests that the hydrostatic compressive stress components do not take part in plastic deformation. The Drucker and Prager criterion is represented as shown in the figure below.

Using the Drucker-Prager criterion the issue of calculating the increases in plastic deformation at the edges of the elastic domain in the Mohr-Coulomb material is resolved. An elliptical domain is defined in the plane of the principal stresses (in conditions of plane effort). However, this domain is not centered in the origin, which makes the determination of the increment in plastic deformation simpler. The linear behavior is easy to model, and this can be carried using simpler approaches, but the Abaqus CDP constitutive model actually models the non-linear behavior of mortars, i.e beyond the elastic phase, including fracture region, in both, traction and compression, on the basis of theory of plasticity expressed as various criteria. CPD model is applied to mortar and other masonry substrates, which are later anchored with various fibers to form composite materials on which the ABAQUS simulations are carried out, according to the scope of the thesis.

In order to complete the pre-requisites of the simulations, material properties need to be inserted into the ABAQUS material properties dialogue box. In the case of elastic

materials, the two properties that need to be defined are the poisson's ratio and the young's modulus.

Material Behaviors

Elastic
Concrete Damaged Plasticity

General Mechanical Thermal Electrical/Magnetic Other

Elastic

Type: Isotropic ▼ Suboptions

☐ Use temperature-dependent data

Number of field variables: 0

Moduli time scale (for viscoelasticity): Long-term

☐ No compression

☐ No tension

Data

	Young's Modulus	Poisson's Ratio
1	6000	0.19

Figure 3. 3 : Material behavior

In the case of materials, where the behavior is expressed on the basis of three phases, including the post elastic ductile phase, the Concrete damage plasticity needs to be defined. For this purpose, some specific material properties to completely define the CPD are.

- **Dilation angle Ψ :** value is set to be in between 30° and 40° . The value in the case of our thesis is set to be 31° .
- **Eccentricity:** it is the displacement between the line of action of tensile or compressive loading and the line of action of a uniform stress across the cross-section [2]. In the case of the thesis research, value is assumed to be 0.1.

- **fb0/fc0:** it is the ratio between the strength(stress) in compression or tension in biaxial state versus the uniaxial state. In the case of the scope of thesis research, value is taken to be 1.16.
- **K:** is the ratio of the plastic strain associated with stiffness degradation (ϵ_p^-) versus that without stiffness degradation (ϵ_p). The ratio K is directly proportional to the ratio of cohesive forces to the maximum cohesion interaction of the specimen [3]. Its value is assumed to be 0.667.
- **Viscosity parameter:** this parameter helps in convergence of results. For the simulation of constitutive bond of concrete specimen, this parameter regularizes the viscoplastic behavior. the value is assumed to be 0.0001.

Edit Material [X]

Name: Mortar

Description: [Text Box]

Material Behaviors

- Elastic
- Concrete Damaged Plasticity**
- Concrete Tension Damage

General Mechanical Thermal Electrical/Magnetic Other

Concrete Damaged Plasticity

Plasticity Compressive Behavior Tensile Behavior

☐ Use temperature-dependent data

Number of field variables: 0

Data

	Dilation Angle	Eccentricity	fb0/fc0	K	Viscosity Parameter
1	31	0.1	1.12	0.667	0.0001

OK Cancel

Figure 3. 4 : Material Module, ABAQUS interface

After the definition of the parameters that define the CPD model, the in detail and in-depth study of concrete damage plasticity requires the investigation of compressive and tensile behavior of materials under the action of a loading whose effects are beyond the elastic phase. The diverse and comprehensive study of all three phases (elastic phase and the two post elastic phases) is required.

In order to define the compressive side of the Concrete damage plasticity, the yield stress and compressive deformation parameters are needed to be defined, as per the requirements of ABAQUS. This gives birth to the necessity of a governing system in order to determine the relationship between yield stress and inelastic strain (which is the strain obtained in 2nd and 3rd phase of the damage initiation and propagation). The ABAQUS converts the inelastic strain values into the plastic strain values using the following equation and later uses them against the yield stress values for numerical calculations.

$$\epsilon_c^{pl} = \epsilon_c^{in} - \frac{d_c}{1-d_c} \cdot \frac{\sigma_c}{E_0}$$

Where the d_c is the above-mentioned damage variable in compression.

Now the tensile behavior in the initiation and propagation phase of crack is generally defined in ABAQUS CPD by the help of yield stress and the cracking strain. After the initial elastic strain phase, the material specimen starts exhibiting the necking phenomenon until it breaks, right after the Ultimate tensile stress point.

By the use of above-mentioned system, the tensile and compressive behavior is completely defined in ABAQUS CPD.

In numerical form, this damage model can be expressed using the Mazars model [4] of uniaxial compression and tension using the scalar damage variables defined as d . The evolution of damage is governed using the following equations.

$$d_t = 1 - \frac{\kappa_0(1 - A_t)}{\kappa} - \frac{A_t}{\exp[B_t(\kappa - \kappa_0)]}$$

$$d_c = 1 - \frac{\kappa_0(1 - A_c)}{\kappa} - \frac{A_c}{\exp[B_c(\kappa - \kappa_0)]}$$

Where A_t , A_c , B_t and B_c are scalar material parameters that define the nonlinear response in tension and compression in CPD. These values are obtained using the experimental results. K is the maximum of ε_{\sim} and K_0 . This strain is obtained from the strain tensor and is taken as the equivalent strain obtained while loading.

Edit Material [X]

Name: Mortar

Description: [Text Box]

Material Behaviors

- Elastic
- Concrete Damaged Plasticity**
- Concrete Tension Damage

General Mechanical Thermal Electrical/Magnetic Other

Concrete Damaged Plasticity

Plasticity Compressive Behavior **Tensile Behavior**

Type: Strain [Dropdown]

☐ Use strain-rate-dependent data

☐ Use temperature-dependent data

Number of field variables: 0 [Spin Box]

Data

	Yield Stress	Cracking Strain
1	1.24966184	0
2	1.78575069	2E-05
3	2.260126272	4E-05
4	2.665352751	6E-05
5	2.99896042	8E-05
6	3.262669422	0.0001
7	3.461292359	0.00012

OK Cancel

Figure 3. 5 : CDP Interface

3.5 Interactions

After the determination of material properties, the construction of each individual part and the section assignment of each part, these individual parts are combined using the assembly module. After the completion of assembly, various assembly surfaces and points (thus nodes) interact with each other. Interactions are the properties that define the behavior of two surfaces in contact. Usually, their interaction with each other is defined by perfect bond as default, in which the nodes are tied against each other constraining their degree of freedoms with each other. However, in real conditions, there may be effect of friction and sliding among the interaction surfaces. Surfaces in contact are prone to slide against each other depending on the static friction coefficients. So, a user defined interaction between surfaces or nodes depends on these slipping and friction factors.

The surfaces in contact are deformable bodies, as a result of the application of loading, deformities can be observed. The effect of these deformities can be translated as a result of contact between various surfaces. So, the interaction of surfaces must be simulated precisely. So, the user needs to provide ABAQUS with appropriate numerical parameter values such as friction coefficients etc. ABAQUS provides user with a number of interaction tools such as surface-to-surface contact, self-contact, model change etc.

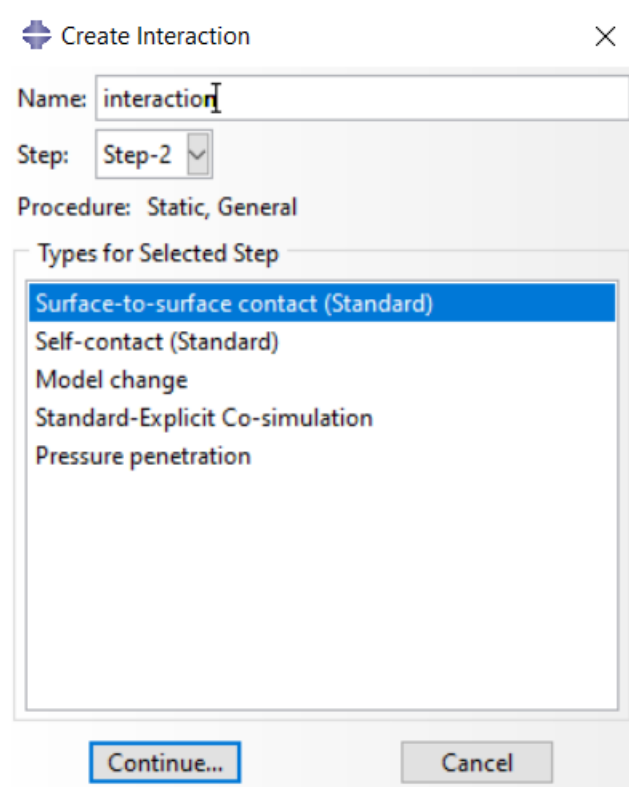


Figure 3. 6 : Interaction Interface

3.5.1 Node to surface interactions

In the node to surface interaction, the nodes of slave surface interact with the nearby master surface nodes however the master surface nodes do not interact with the slave surface nodes. The master surface nodes may penetrate the slave mesh as it can be observed by following figure. However, this problem arises mostly when the slave surface is allocated to the larger and less dense surface.

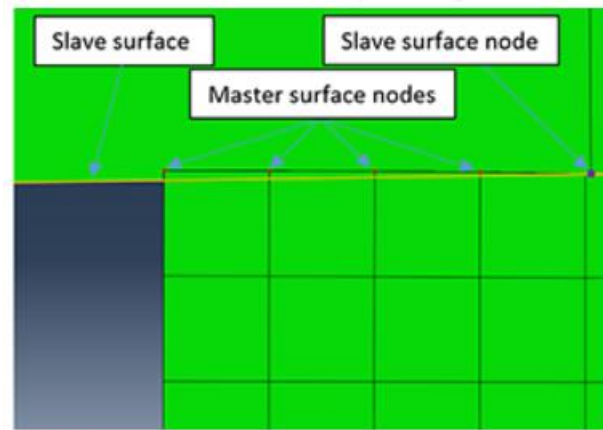


Figure 3. 7 : Master and slave nodes, node-to-surface interaction

In order to avoid this issue of nodes penetration in node-to-surface interactions, ABAQUS manual suggests that.

- Slave surface should be allocated to the smaller of the two surfaces in contact.
- Slave surface must be allocated to the surface with higher mesh density.
- Slave surface should be allocated to the surface which is stiffer (both geometrically and materially)

Among these 3 conditions, if it is not possible to meet all three conditions, it is advisable to meet first two conditions. Figure shown below expresses the results of above problem if master surface is stiffer than the slave surface.

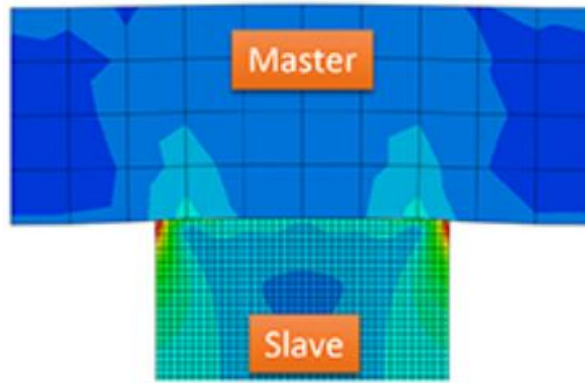


Figure 3. 8: Node-to-surface interaction, considering first two conditions

As it can be observed from the figure that the results are quite satisfactory, we get no penetration of nodes. High stress concentration at the edges is also visible so the node-to-surface interaction gives reliable results if at least 2 conditions are met. However, if we reverse the masters and slave surface in the above example, then the slave surface becomes larger, and we no longer respect the first condition. The results can be seen in the following figure.

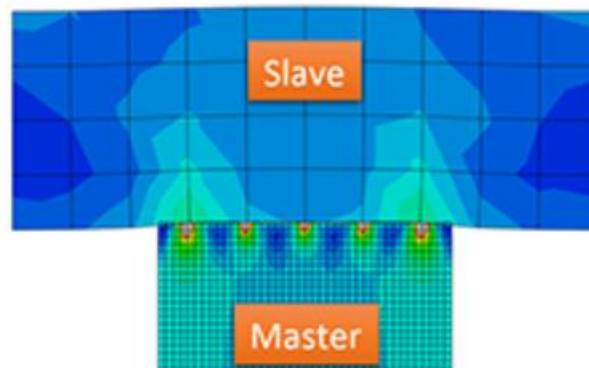


Figure 3. 9 : Node-to-surface contact, considering the large surface as slave surface.

These results are not satisfactory because we get unnecessary concentrated loads at various contact points which have no logical reason. Five concentrated loading points are obtained instead of two at the edges. This gives rise to some mathematical singularities which exaggerate the results. The penetration of nodes can also be observed all along the contact and is specifically observable near the edges.

In order to make the simulation results reliable, it is advisable to make modifications with the master's surface mesh. Mesh size must be reduced in such a manner that it is lower

than the slave surface. The larger of the two surfaces should be the masters surface. Following figure shows the correct application of node-to-surface interaction respecting all the three conditions.

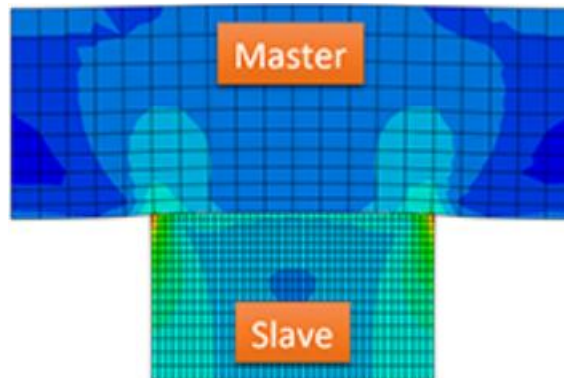


Figure 3. 10 : Node-to-surface interaction

As it is observed that the concentrated loads have been shifted to the edges which ensure no exaggeration of results. No node penetration is observable along the contact surface neither at the edges.

3.5.2 Surface-to-surface interaction

The surface-to-surface contact is one of the options to define the interaction between two surfaces. In this type of interaction, one surface among the surfaces in contact, acts as master surface as the other acts as slave surface. Surface nodes of both, master and slave surface interact with each other to define the interaction.

In the surface-to-surface contact method, the interaction between surface acts in such a way that average position of each slave node is considered to constraint each contact. Every contact is enforced to closest slave node but also other nearby slave nodes. Each node of slave surface is virtually connected to a cluster of nearby nodes of master's surface.

As in the previous case of node-to-surface interactions, in order to achieve reliable results, the mesh density of the slave surface must be higher, and the master's surface must be geometrically larger than the slave surface. In the surface-to-surface interaction, considering the masters surface to be smaller than slave surface, is expressed by following figure.

However, this type of interaction ensures that there is no penetration between the nodes of master and slave surface. This method can be illustrated by the following figure.

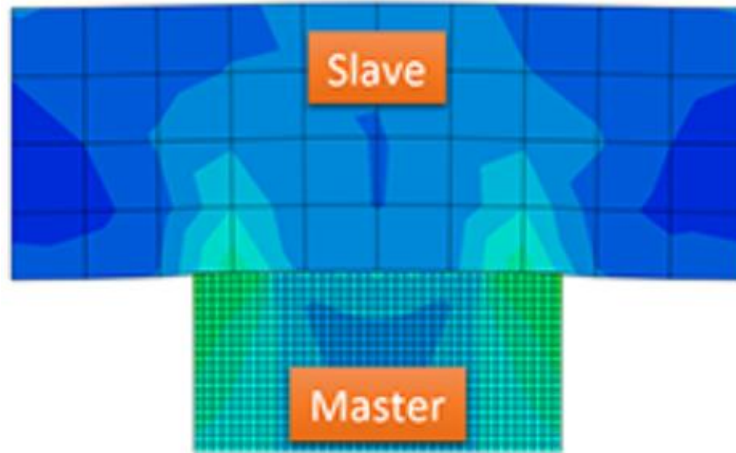


Figure 3.11 : Surface-to-surface interaction, smaller surface as master's surface

The acceptance criteria of results for this type of case are the formation of appropriate concentrated stress loadings at the edges of contact and no penetration of nodes between the master surface and the slave surface. However, in this case both conditions are not met. So, the results are utterly unreliable. Now we modify the model and make the larger surface, a master surface.

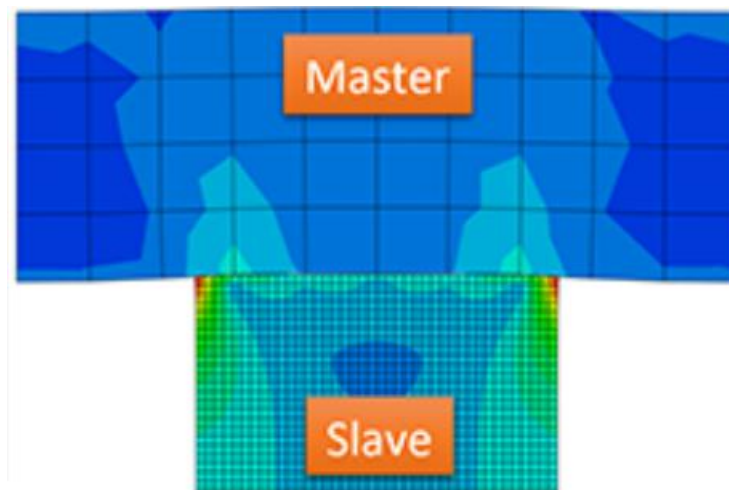


Figure 3.12 : Master and Slave surface in surface-to-surface contact

Now both acceptance criteria are met properly. A proper surface-to-surface contact between the master and slave surface ensures a high stress load at the edges of contact between two surfaces (which should be present). In order to get more efficient results, it is

advisable to use the smaller and denser (according to mesh density) part as the slave surface and the other as master surface [5].

3.5.3 Cohesive interaction

Cohesive interaction is one of the applications of surface-to-surface interaction. Traction-separation constitutive model is implemented in order to model the interface between two surfaces. The interface thickness is negligibly small.

The interface between two surfaces in contact is modelled in such a way that the bond between elements is modelled up to the elastic limit of the tension slip curve.

One of the advantages of cohesive interaction is that it can be used to model the sticky surfaces where two surfaces which are not in contact initially, come in contact with each other and exhibit cohesive contact behavior. The cohesive contact modelling can be used in order to simulate general contacts between two surfaces. However, this technique is not applicable for finite-sliding and surface-to-surface formulation.

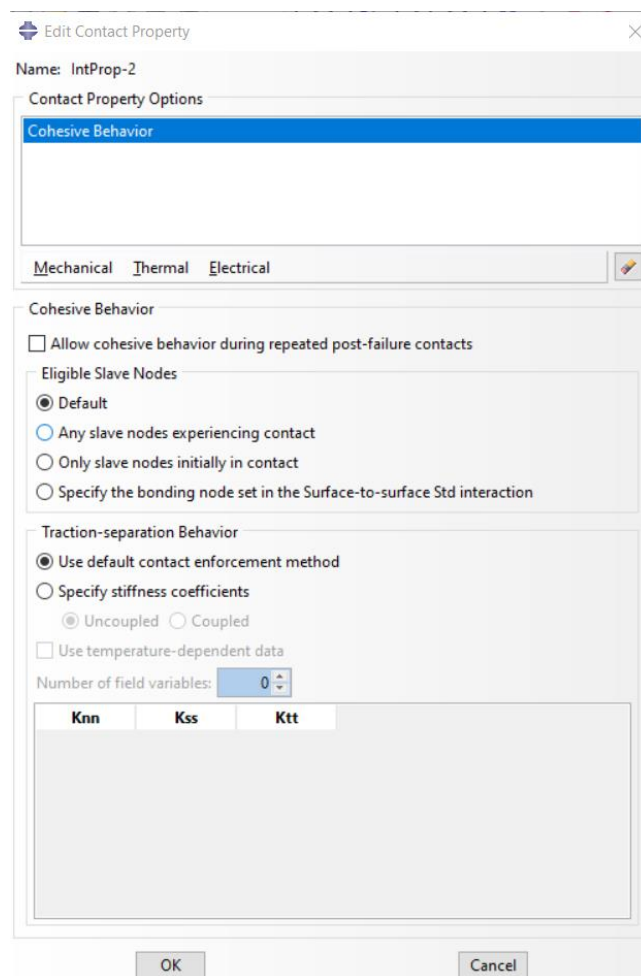


Figure 3. 13 : Cohesive interaction, ABAQUS interface

After the proper definition of Cohesive interaction property, it is implemented in the interaction module on various surfaces in contact with each other. For that purpose, the interaction module is accessed again and on the dialogue box, the masters and slave surfaces are chosen, and the contact iteration property is selected to be cohesive interaction.

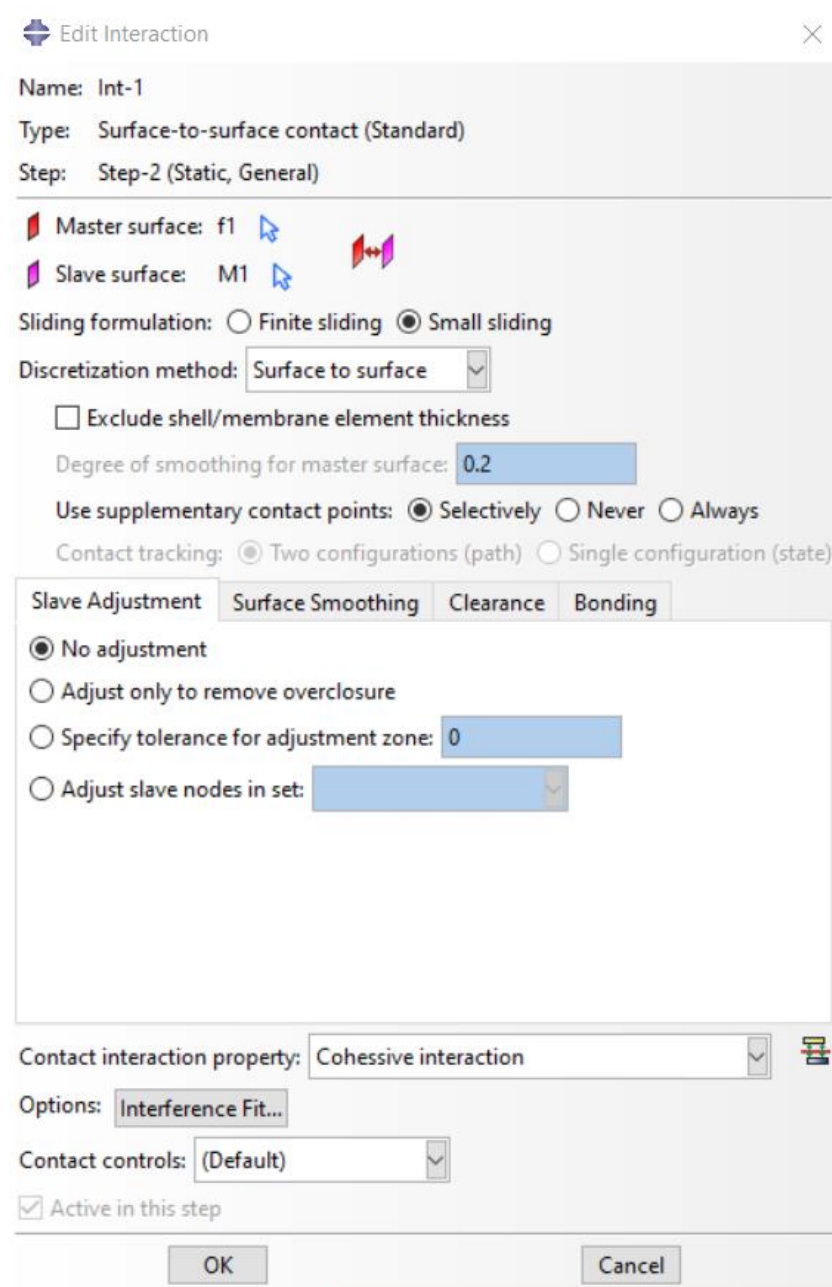


Figure 3. 14 : Cohesive interaction, ABAQUS interface

In order to govern and model the surface based cohesive interaction, various laws and formulae are used in order to properly simulate the crack initiation propagation and failure of material. For this purpose, we use the following laws.

- Damage initiation criteria
- Damage evolution law
- Elastic linear Traction separation law

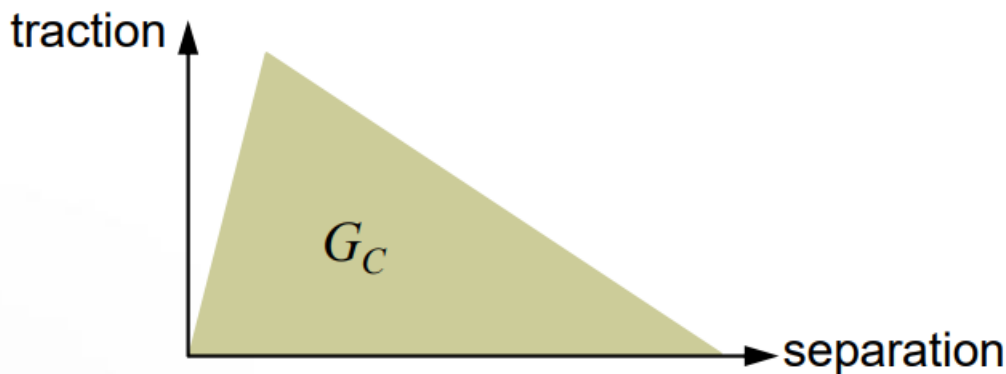


Figure 3. 15 : Linear elastic traction separation law

However, in the case of two surfaces that interact with each other using cohesive law (or even perfect bond) are prone to fail on the basis of interaction properties and is independent on the material properties. Specimen fails as a result of the slippage between two surfaces such that the two surfaces are no longer in contact with each other.

Cohesive elements and cohesive surfaces behave differently under the action of traction separation law. In the case of cohesive elements, separation interpreted as nominal strain and is the ratio of relative displacement between the upper and lower cohesive layer and the initial thickness of layer, and the traction is characterized by nominal stress. In the case of cohesive surfaces, separation is characterized by the contact separation between the two layers and the traction is governed by contact stress which is the ratio between the contact force between two surfaces (as a result of loading conditions) and the contact area in question between two surfaces.

The linear elastic traction separation behavior acts in such a way that it corresponds the normal stress and the shear stress across the surfaces in contact with the normal separations and shear separations along that contact. However, this traction separation behavior is modelled using stiffness constants that act along orthogonal directions

corresponding to the contact surface. As a result, we obtain a stiffness matrix whose diagonal values are of main significance in the ABAQUS.

$$\text{Stiffness matrix} = \begin{bmatrix} k_{nn} & k_{ns} & k_{nt} \\ k_{ns} & k_{ss} & k_{st} \\ k_{nt} & k_{st} & k_{tt} \end{bmatrix}$$

As it is necessary to define the elastic properties of the contact elements, it is observed in figure above, ABAQUS provides user with an option to define the stiffness values, or it may take the default values depending upon the stiffness material properties of the elements included in contact. The stiffness coefficients are set to be uncoupled, if not so, all the non-diagonal terms of the stiffness matrix are needed to be defined.

The damage of specimen under the action of traction separation behavior is independent on the material properties of master and slave surfaces. So, the damage modelling of the surface under the action of cohesive interaction constraint can be modelled using various governing laws, formulae and criteria. The damage criteria are based on the degradation of the contact between various surfaces judged by the comparison of various stresses acting along the surface as a result of the application of load and propagation of the simulation.

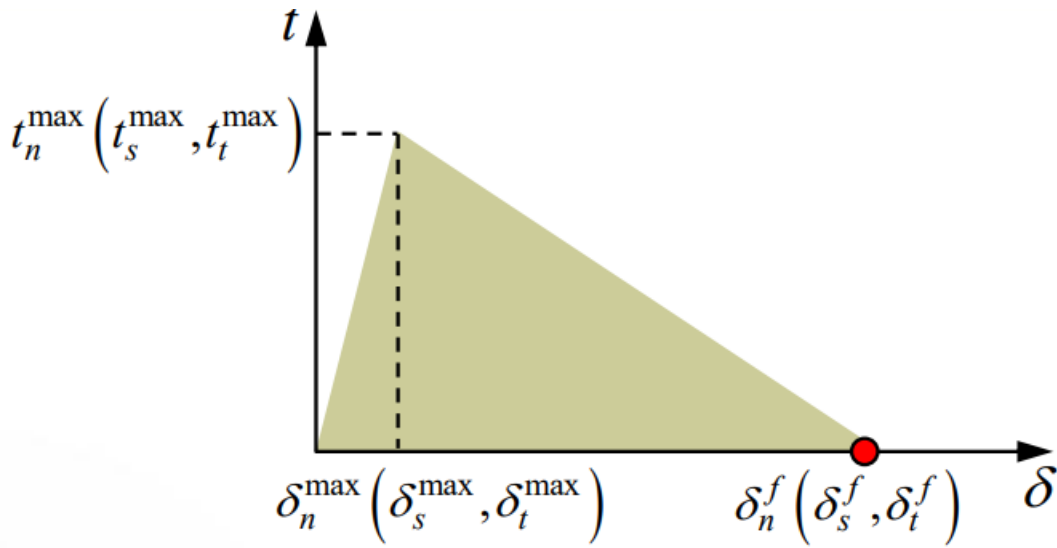


Figure 3. 16 : Damage traction separation response

3.6 Damage initiation criteria

According to the literature, four damage initiation criteria are as follows.

- Maximum stress criterion
- Maximum separation criterion

- Quadratic stress criterion
- Quadratic separation criterion

The maximum stress criterion suggests that.

$$\text{Max} \left\{ \frac{t_n}{t_n^{\max}}, \frac{t_s}{t_s^{\max}}, \frac{t_t}{t_t^{\max}} \right\} = 1$$

The maximum separation criterion suggests that

$$\text{Max} \left\{ \frac{\delta_n}{\delta_n^{\max}}, \frac{\delta_s}{\delta_s^{\max}}, \frac{\delta_t}{\delta_t^{\max}} \right\} = 1$$

Quadratic stress criterion can be expressed as

$$\left(\frac{t_n}{t_n^{\max}} \right)^2 + \left(\frac{t_s}{t_s^{\max}} \right)^2 + \left(\frac{t_t}{t_t^{\max}} \right)^2 = 1$$

Quadratic separation criterion states that

$$\left(\frac{\delta_n}{\delta_n^{\max}} \right)^2 + \left(\frac{\delta_s}{\delta_s^{\max}} \right)^2 + \left(\frac{\delta_t}{\delta_t^{\max}} \right)^2 = 1$$

Where t represents the stresses and δ represents the separations. n points to the normal direction, s corresponds to shear direction and t is the second shear direction. However, if the initial constitutive thickness is equal to 1, then the damage criteria suggest that both the approaches mentioned above are the same.

3.7 Damage propagation criteria

As the process of loading proceeds, the cohesive interaction between the two layers in contact under the governing of cohesive constraint starts to deplete. In order to set a guiding criterion to investigate the damage propagation, the concept of fracture energy is taken into account. So, for that purpose, the total fracture energy needs to be specified.

Now considering the separation-based damage propagation, the damage is expressed as the function of effective separation. This can be expressed as

$$\delta = \sqrt{\delta_n^2 + \delta_t^2 + \delta_s^2}$$

With the propagation of damage, the response of material under the action of loading is no more linear. Depending on the type of material and the loading conditions, the softening response under damage initiation can be linear, exponential, or tabular. This displacement-based evolution in ABAQUS can be found in following dialogue box.

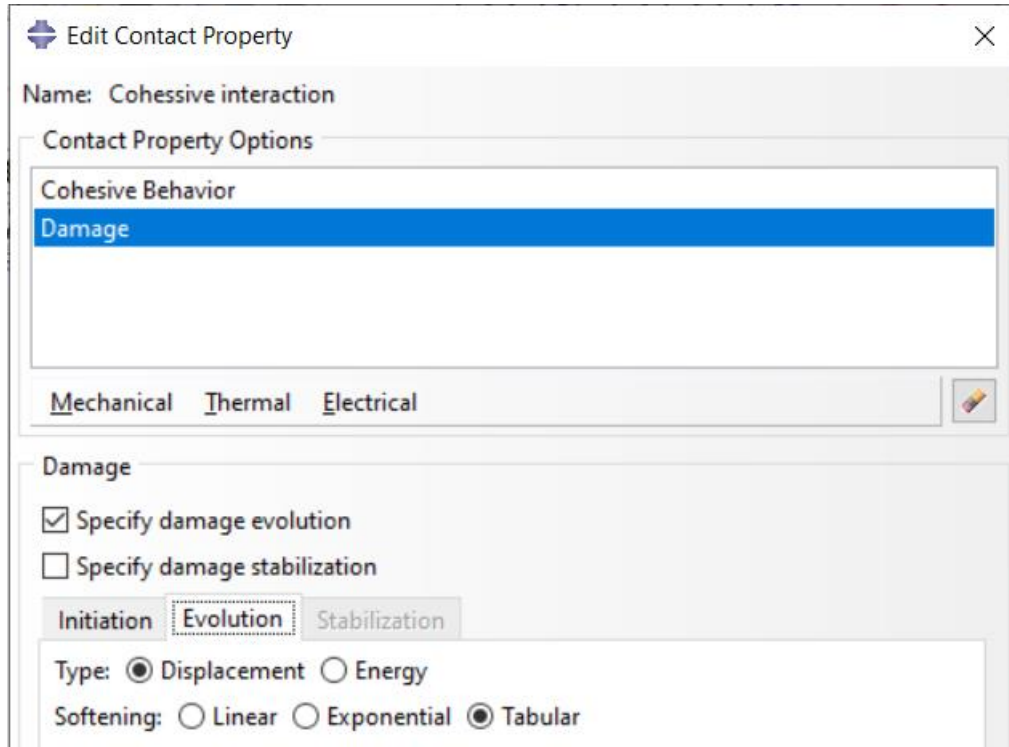


Figure 3. 17: Damage evolution, Separation based

Now the 2nd criteria for governing the evolution depends on fracture energy as discussed before. This criterion can be set using function of mod mix using some analytical form or in the form of tabular data. One of the criteria is known as Power Law and is expressed as

$$\left(\frac{G_I}{G_{IC}}\right)^\alpha + \left(\frac{G_{II}}{G_{IIC}}\right)^\alpha + \left(\frac{G_{III}}{G_{IIIC}}\right)^\alpha = 1$$

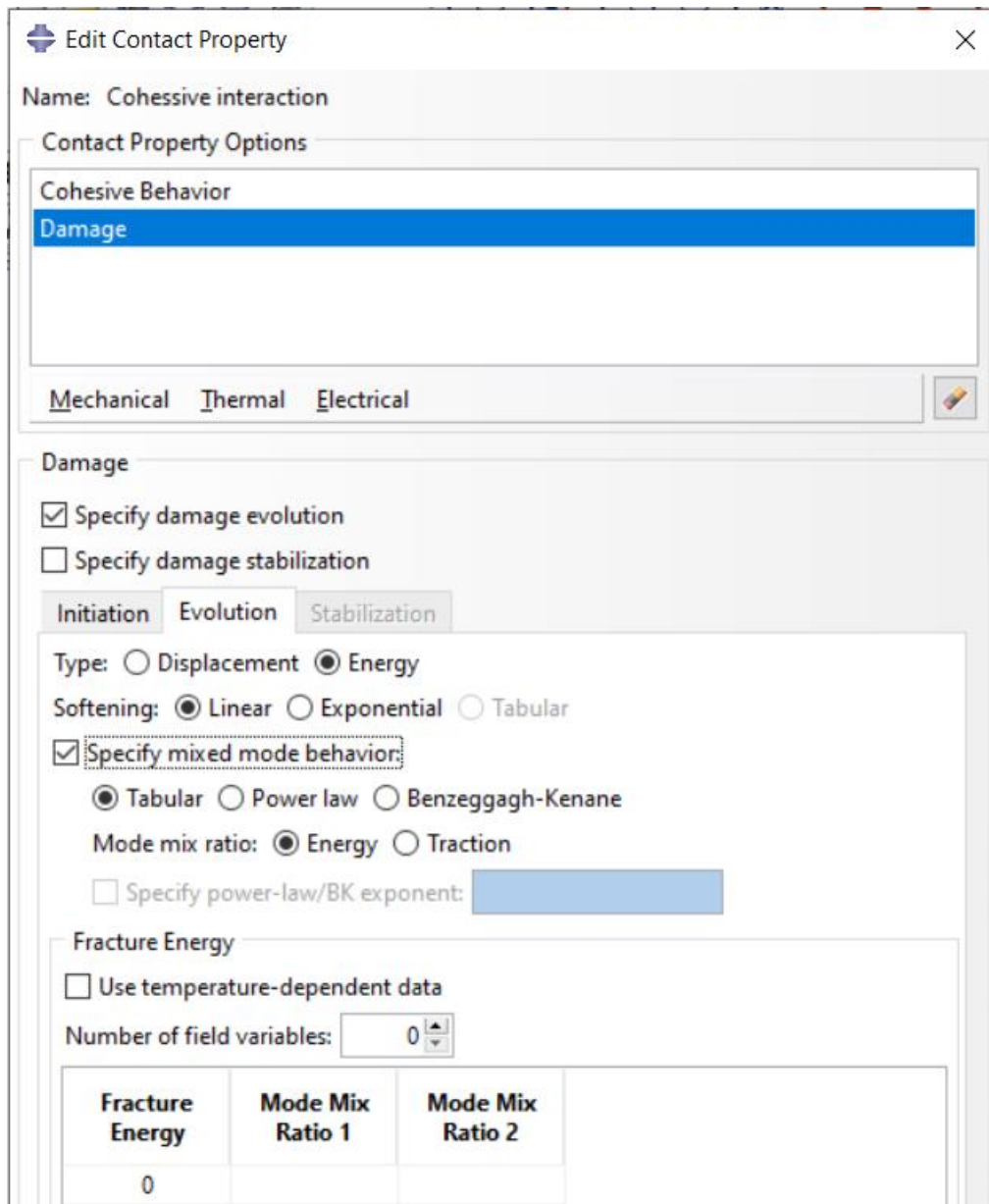


Figure 3. 18: Damage evolution criteria, energy based

3.8 Constraints

After the preparation of assembly of the specimen under study, various constraints can be set. Constraints are positioning tools that help us to tie or constraint two surfaces, surface and a point or various regions etc. together in such a way that their degree of freedom is linked to each other. In the model developed in this thesis, two main constraints have been used, i.e., Rigid Body constraint and Embedded Region constraint, which will be described below.

3.8.1 Rigid Body Constraint

Rigid body constraint requires a reference point. The motion of all the regions or surfaces of the specimen that are selected to be rigid body are constraint against the reference point. As a result of this constraint, the degrees of freedom of rigid body is fixed with respect to the reference point. Under the action of distributed load applied to the element, as the simulation is underway, the motion rigid body is restricted. As a result, there is no deformation (elongation, necking etc.) in the rigid body. However, rigid body movements can be observed. Behavior of specimen (and the rigid body regions) during simulation depends on the orientation of the applied loading conditions.

Considering the rigid body, nodes can be of two types, namely tie nodes and pin nodes. ABAQUS interface gives user the option to choose between two depending on the type of simulation. In the case of pin nodes, the nodes of the rigid body region are tied to the reference point in such a way that their translation degree of freedom is restricted to the reference point. Which means the rigid body is free to move along all three axes. However, in the tie nodes, all 6 degrees of freedom (3 translational and 3 rotational) of the rigid body nodes are restricted to the reference point.

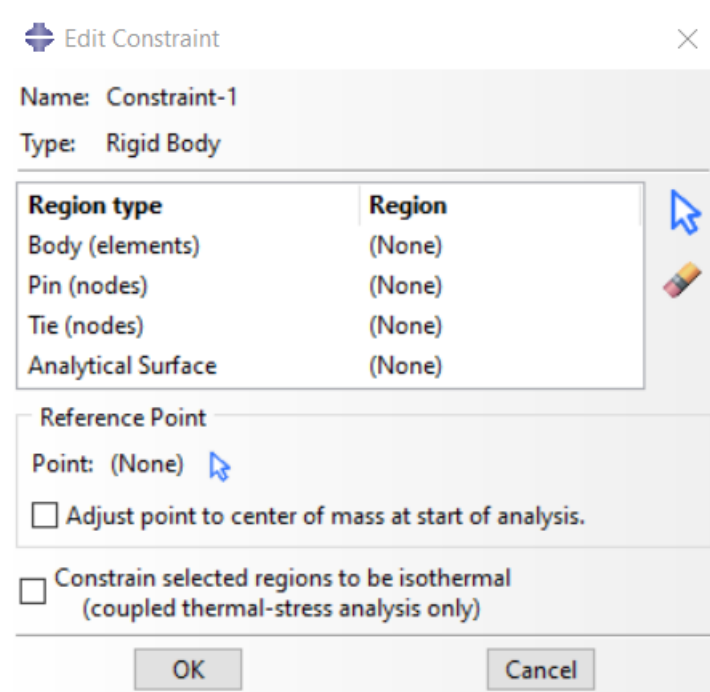


Figure 3. 19 : Rigid body constraint, ABAQUS Dialogue Box

3.8.2 Embedded region constraint

Embedded region constraint requires the definition of embedded nodes and the host nodes. The embedded nodes belong to the surface whose motion is to be restricted with respect to other surface, within a specific tolerance (if specified). While the host nodes belong to the surface to which the embedded surface is embed.

After the definition of embedded and host nodes, ABAQUS looks for the possibility of lying of embedded nodes inside the host nodes. If ABAQUS finds a embedded node inside a host nodes, the translational degree of freedom of the embedded nodes is modified and is restricted to corresponding host node. However, the rotational degree of freedom is not limited. Weight factor roundoff tolerance, Absolute exterior tolerance and fractional exterior tolerance values are set in order to define the tolerance related to the restriction of degrees of freedom.

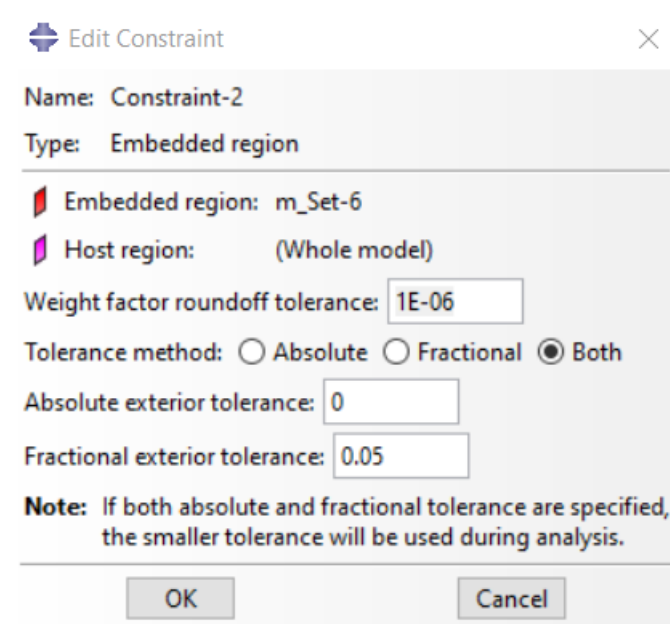


Figure 3. 20 : Embedded constraint, ABAQUS Dialogue box

3.9 Step

ABAQUS is a tool for simulation of linear, nonlinear transient dynamic and quasi-static analyses using FEM Technique ABAQUS has a specialty of allowing the user to use the time history to determine the transient response which is done defining analysis procedures.

ABAQUS is based on the concept of time steps. Each transient FEM problem is discretized in time steps in such a way that the entire time history is divided into smaller and discretized time instances. Within each time step, the process is considered to be static, so the variables under consideration just change the value from one magnitude to other.

The procedure is defined in such a way that on each time step, the dynamic problem and the analysis is defined. ABAQUS provides user with the facility to determine as well as define each time step according to the need. As it is the feature of FEM analysis, each previous time step is updated, going back to time history, according to the features of next step. Thus, any modification or update in next time step is automatically included in the previous step. For example, if the dynamic transient analysis of truss is being done, the loading conditions change in each time step. This change in loading conditions is included in each previous time step.

ABAQUS provides solution to both linear and nonlinear problems. Linear problems are easy and simple to solve. These problems can be solved by ABAQUS by the solution of system of linear equations. In nonlinear problems require the solution of set of nonlinear equations using various incremental and iterative techniques, with the main goal to obtain a convergent solution. In order to solve the nonlinear system of equations, ABAQUS uses two approaches.

According to first approach, the user controls and defines the time increment with all its specifications. The other approach is Automatic control in which the user defines the step and specifies certain tolerance limit. ABAQUS automatically defines the increment size as the response is calculated in the step. The Automatic control approach is more reliable because it is difficult for the user to determine the response ahead of time. In the first step, the user defines the boundary conditions and the initial conditions (if transient).

After the initial step, a different approach is set for each adjacent time step, in which the type of analysis, possibility to modify loading and boundary conditions is defined.

ABAQUS provides user to choose whether to take into account the geometric nonlinearities or not using the NLgeom (nonlinear geometry) feature, the nonlinear geometry effects can be switched on or off.

While defining the steps in the Step module, the ABAQUS provides user with an option to choose between a General nonlinear step or linear perturbation. The first approach takes into account the effects of nonlinearities caused by various factors including material

nonlinearities (Elasto-plastic materials etc.), geometric irregularities (large deformations) and the irregularities caused by irregular contacts. While in the second approach, the linear perturbation actually accounts only for the linear response of the system at the end of the previous nonlinear step but before the linear perturbation step, depending on the base state.

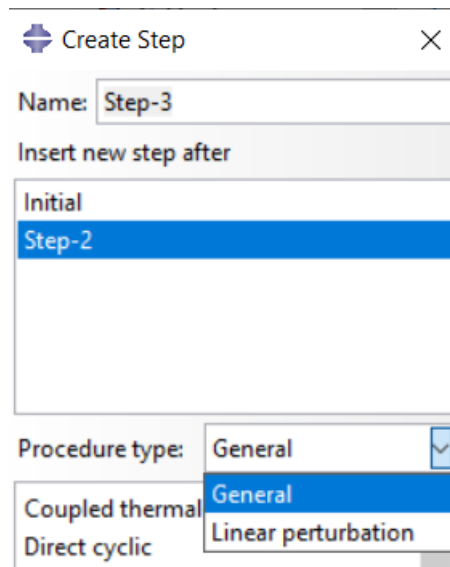


Figure 3. 21 : Step Dialogue Box

General step is defined after the complete definition of initial step. When the problem statement along with its complete initial and boundary conditions is available, the general step is initiated to perform further analysis. Initial dialogue box gives the user to turn off or on the Nlgeom, and the automatic stabilization technique to be adopted. In this step. In the static general step, ABAQUS requires user to determine the time period, and further, the incremental size (minimum, maximum) and maximum number of increments.

3.10 Analysis Procedure

The FEM analysis done by ABAQUS is mostly related to the solution of nonlinear problems with sufficiently large number of variables. As a result, a system of equations is obtained by the discretization. However, as the vast majority of the problems solved by ABAQUS are history dependent, so in order to obtain the solution, a series of small-time increments is required. Two main problems related to time discretization and solution of problem are, the choice of proper increment size and the solution of governing equation on each increment for each node.

Among various techniques used to solve the differentials, ABAQUS uses Newton's method to solve these nonlinear equilibrium equations. The main benefit with Newton's method is that it has better convergence rate than the modified Newton or Quasi-Newton method.

3.10.1 Newton's Method

Newton method can be applied in more than one ways like Taylor's theorem approach or by the quadratic model of the function etc. ABAQUS utilizes the Taylor's theorem for expansion of nonlinear equations, neglecting the higher order terms of the Taylor's expansion. Thus, using this technique, the nonlinear equations are expanded into first order equations, obtaining a linear system of equations, which leads to the Jacobian matrix (matrix containing terms with first partial derivative only). The solution is approximated using the Newton's approach and the iteration continues until the solution converges (entries are sufficiently small).

However, in the case of large and complex FEM problems, the Newton's method is avoided because.

- It is considerably difficult to construct and formulate the Jacobian matrix. So only way around this problem is to do the calculations numerically which is expensive.
- Newton's method is comparatively expensive considering the calculation and formation of Jacobian matrix on each iteration [6].

3.10.2 Quasi-Newton Method

Quasi-Newton method is an advanced technique as compared to Newton's method and offers reliable performance and significant advantages in various complex nonlinear problems, as compared to Newton's approach as it resolves the previously mentioned problems.

According to this technique, the stiffness matrix is updated for iterations rather than formation and factorization of new stiffness matrix in each iteration, thus making it relatively inexpensive. However, this method does not involve the quadratic convergence so may face convergence issues and more number of iterations per increment. In case of nonlinear problems with complex stiffness matrix, the benefit of this technique in

factorization makes it more cost efficient. In short, the quasi-Newton's approach reduces the number of times the Jacobian matrix is factorized.

Quasi-Newton method is also reliable in case of simpler nonlinear problems where the stiffness matrix does not significantly change during iterations. In order to identify the divergence and to update the corrections, line search is used in quasi-Newton method, thus improving the convergence.

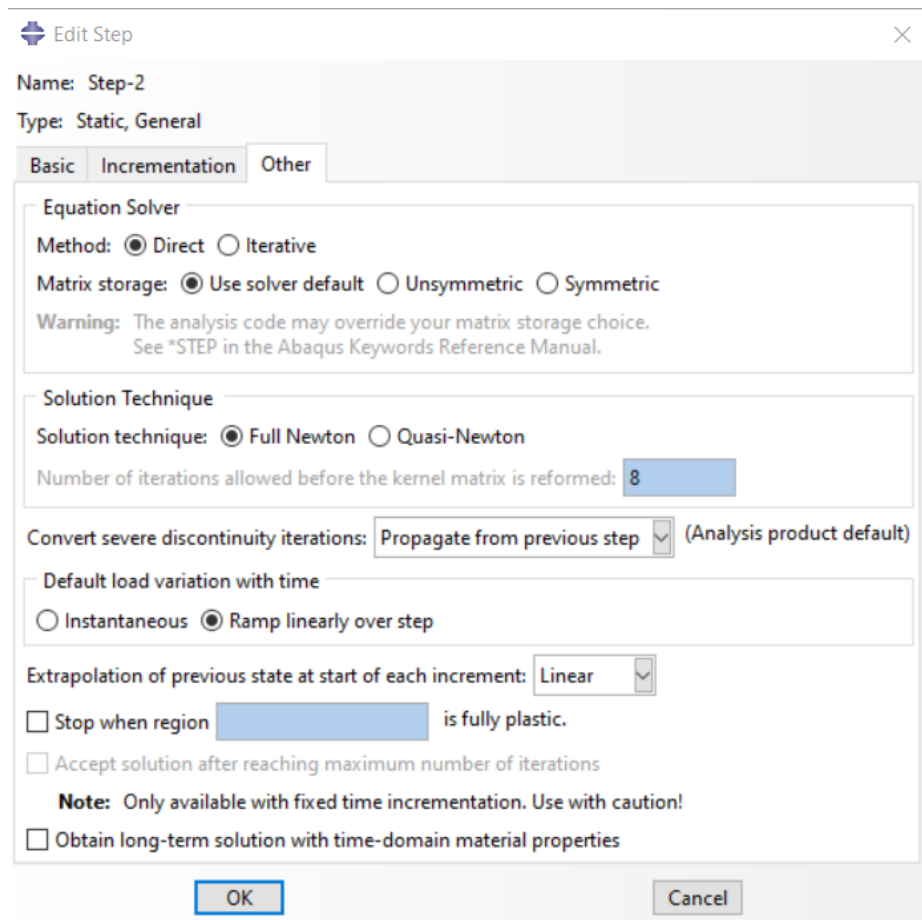


Figure 3. 22 : Step Module, Newton's and quasi-Newton's method

3.11 Mesh

After the completion of all above mentioned modules definition, the last step is the meshing of the assembly (each individual part). For each part related to the geometry, the meshing is done separately. ABAQUS interface provides user with the facility to seed each part according to the sensitivity of application and select the appropriate element type. Seeding provides user with the ability to control the mesh size (approximate global

size), curvature etc. Edges can be seeded separately in order to control their mesh size because generally more dense mesh is required at the edges.

The mesh module in ABAQUS provides user with the ability to define the mesh density at local as well as global level. ABAQUS interface displays different mesh using different colors making it more visible, the mesh type in assembly.

ABAQUS provides user with the ability to select the element type for each element.

Elements can either belong to the part of assembly created by the user or considered as an orphan mesh. After that the mesh quality can be verified using ABAQUS tools

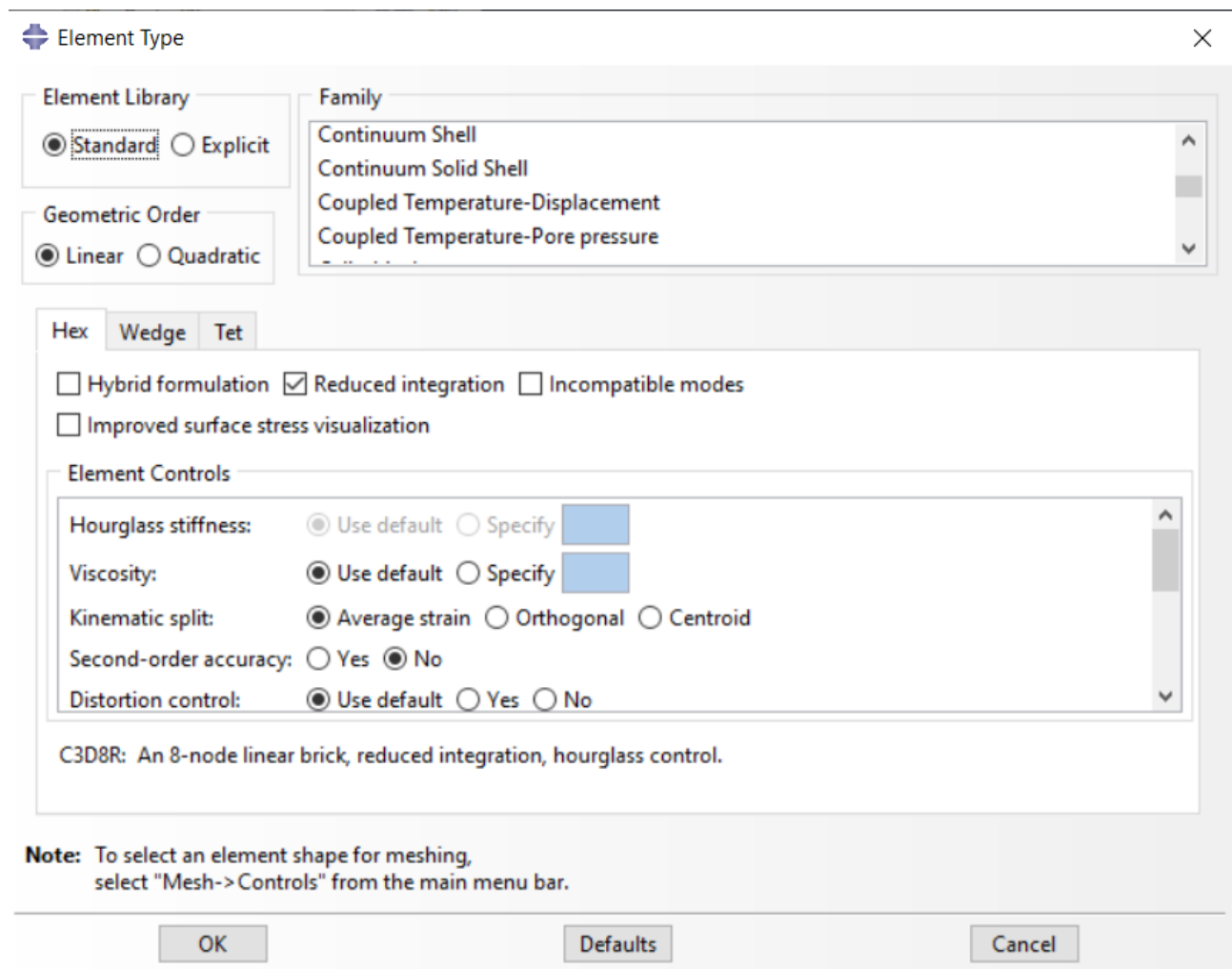


Figure 3. 23 : Element type, Mesh ABAQUS interface

Among number of element types like 3D stress element, cohesive element, continuum shell, continuum solid etc., appropriate element type is selected in order to create the mesh.

ABAQUS provides user with ability to mesh the part manually using structured or swept meshing, or automatically by meshing algorithm adopted by ABAQUS which automatically meshes the part. However, in the latter case, user has the least control over meshing and thus the optimization of meshing can be obtained creating a mesh manually.

The selection of element type depends on the type of model, its shape, aspect ratio, skewness etc. ABAQUS provides user with the facility to choose between various mesh element type like hexahedral, hexahedral dominated, tetrahedral and wedge type. Each mesh type has its own pros and cons. First order tetrahedral elements are basic element type. To obtain reliable mesh using this technique, a very fine mesh size is required. 2nd order tetrahedral elements are more applicable for general applications, but this element type has convergence issues (slower convergence often). Hexahedral elements are more reliable than those mentioned above. However, in the case of complex geometries, hexahedral elements are difficult or in some cases impossible to implement.

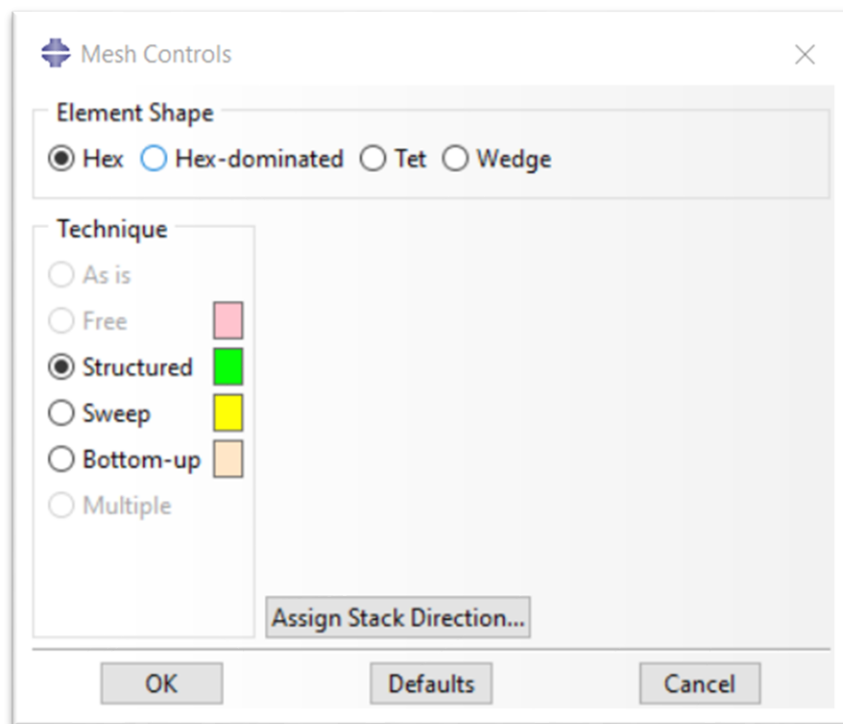


Figure 3. 24 : Element shape, mesh module

In order to optimize the mesh, various meshing rules can be adopted, which operate on the basis of error indicator variables like element energy, maximum equivalent stress, equivalent plastic strain etc. After the selection of an indicator, the ABAQUS automatically does

successive refinement of the mesh on the basis of the solution obtained as a result of simulation. After each iteration of analysis, ABAQUS remeshes the model and selected error indicator is reduced successively.

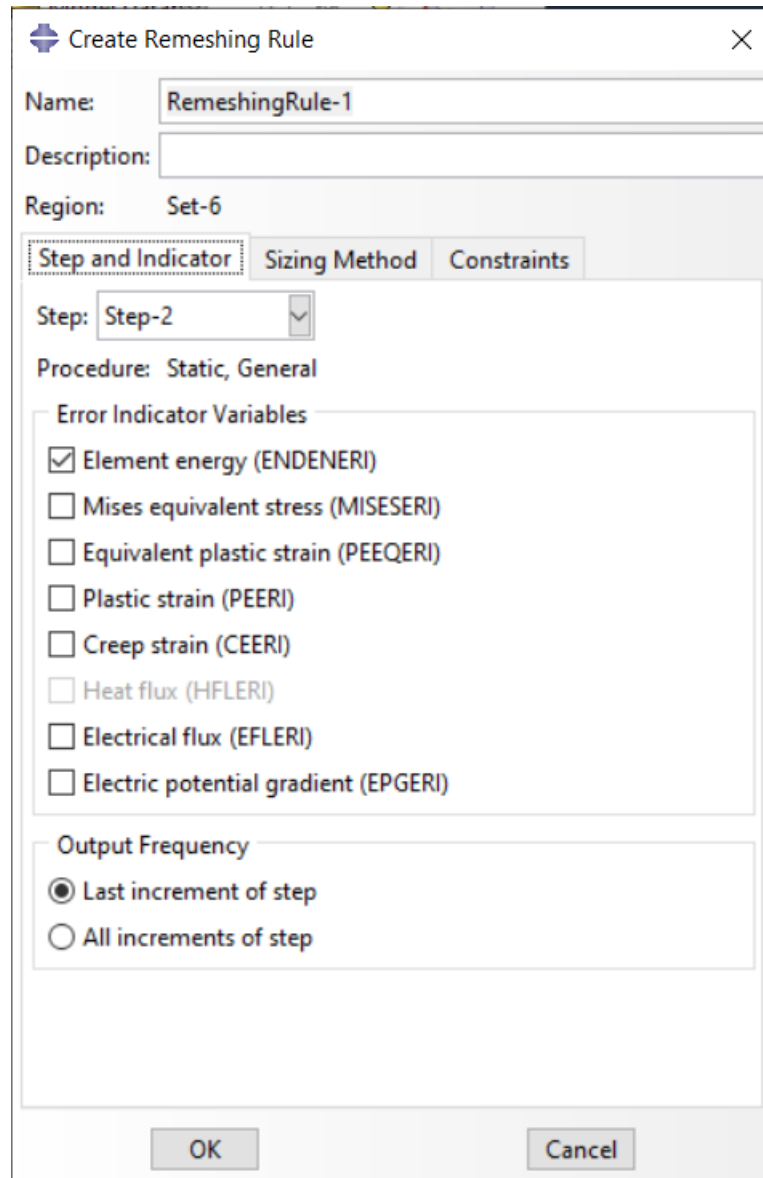


Figure 3. 25: Remeshing rule, mesh module

After the complete definition of mesh. ABAQUS provides the option of mesh verification in which ABAQUS generally analyses the mesh and gives mesh statics and information related to mesh shape and size, characteristics, element failure criteria, aspect ratio etc. Furthermore, the mesh verification tool also does geometry diagnostic in order to diagnose the meshing issues.

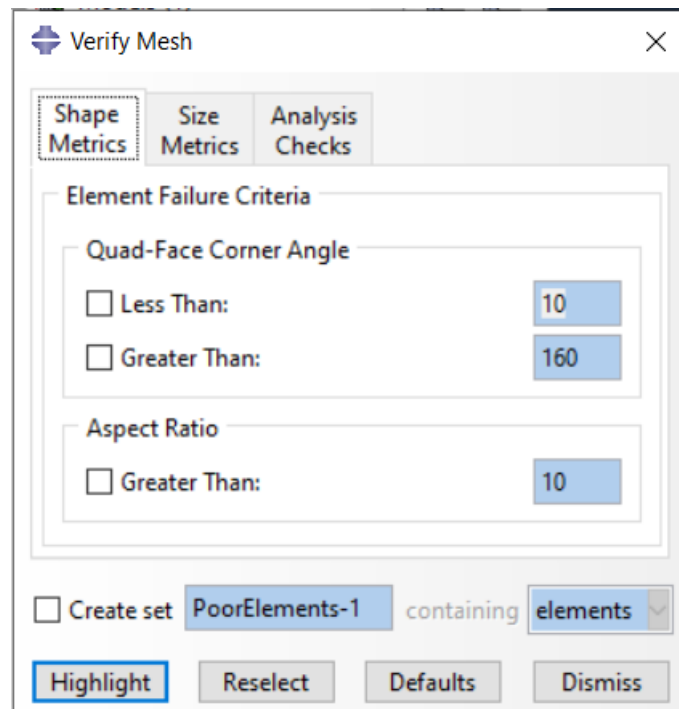


Figure 3. 26 : Verify mesh, mesh module

ABAQUS interfaces provides user with the ease of switching between the mesh display and standard assembly display, using simple **Show native mesh module** icon. The mesh representation can be observed for all independent as well as dependent parts. In the case of orphan mesh or instance which is not associated with any geometry, only the mesh view or orphan part can be view in separate.

3.12 Job

Now after the completion and proper definition of all pre-requisites of the model, the final step is to create the job. In the Job module interface, the user creates a job and then selects the type of job (full analysis, recover or restart a previous job). As the job is submitted for simulation, the ABAQUS does a background check by verifying the geometry, material properties constraints, interactions and meshes. Any discrepancy in any of these modules is communicated to the user in the form of error message. Once the background check is completed, the ABAQUS starts to run the simulation on the model making calculations on each node.

After the completion of the simulation, ABAQUS displays the results which can be accessed by the Result option in the Job drop-down menu. Various results like stresses, strains, modulus etc. can be obtained in graphical form as well as tabular form which can

be exported. User can switch between the initial and simulated graphical results easily. Various display groups can be created in order to better utilize the results using ABAQUS post-processing.

3.13 References

- [1] Paul Barsanescu, Adrian Sandovici, Alexandru Serban (2017), “Gheorghe Asachi” Technical University of Iasi, Romania, Mohr-Coulomb criterion with circular failure envelope, extended to materials with strength-differential effect.
- [2] https://www.instron.com/en-ie/our-company/library/glossary/e/eccentricity-of-loading#:~:text=Distance%20between%20the%20actual%20line,cross%20section%20of%20the%20specimen_
- [3] Tao, Y., & Chen, J.-F. (2015). Concrete Damage Plasticity Model for Modeling FRP-to-Concrete Bond Behavior. *Journal of Composites for Construction*, 19, 04014026. [https://doi.org/10.1061/\(ASCE\)CC.1943-5614.0000482](https://doi.org/10.1061/(ASCE)CC.1943-5614.0000482)
- [4] Gilles Pijaudier-Cabot and Jacky Mazars. Damage models for concrete. In Jean Lemaitre, editor, *Handbook of Materials Behavior Models*. Academic Press, 2001.
- [5] <https://www.technia.com/blog/contacts-surface-to-surface-contact-considerations-part-2-of-3/>
- [6] <https://classes.engineering.wustl.edu/2009/spring/mase5513/abaqus/docs/v6.6/books/stm/default.htm?startat=ch02s02ath14.html>

Chapter 4: Experimental activity

The mechanical characterization of the constituents of TRM materials involves the characterization of mortar specimens as the first step. Variety of mortars can be used. Basic classification of mortar includes organic matrix (Hydraulic natural lime etc.) and inorganic matrices (cementitious matrix etc.). Each matrix type has its own pros and cons. Within the scope of the thesis, the mortar specimen under consideration is natural hydraulic lime based organic matrix that complies with **UNI EN 459-1**. The above-mentioned matrix was selected because of following reasons.

- High breathability
- High workability
- It prevents the formation of mold and condensation keeping the environments healthy.
- Quick and easy to apply either by hand or by plastering machine.
- Compatible with the historic masonry structures and Contributes to the restoration of historic walls.
- Non-reactive in the presence of sulphates contained in the masonry.

Some of the properties of the mortar indicated by the producer are indicated below.

- Temperature of workability 5-35°C.
- pH > 10.5
- Granulometric Interval from 0 to 2 mm (EN 1015-1).
- 2Specific Weight 1800-1900 kg/m³ (EN 1015-10).
- Indicated mixture ratio of 0.19-0.20 l/kg.
- Compression resistance >15N/mm²
- Elastic modulus in compression 15000 N/mm²

4.1 Preparation of mortar specimens

First step in the testing on mortar specimen was the preparation of the samples. So, we need to find the exact amounts and proportions of water and mortar powder to prepare the mortar paste.

The manufacturer indicated a ratio of 0.19-0.20 l/kg. But the water contents are adjusted in the mixture depending on the humidity conditions of the environment. Then we need to find the amount of mixture per specimen which depends on the dimensions of the specimen. The dimensions of the mortar specimen were determined to be 4cm x 4cm x 16cm so the volume is 256cm^3 in accordance with EN 196-1:2016 standard. As 10000cm^3 refers to 18 Kg of the mortar mixture so 256 cm^3 refers to 0.4608 Kg. We take it 0.5kg per specimen approximately.

For 18 Kg of specimen, we need 25 Kg of powder, so for 0.5 Kg we need 0.7 kg of powder. Proportion of water in mixture is taken to be 0.2litre/Kg. So, 0.14litre per specimen of the water content is needed. At a time 3 specimens were prepared in the assembly so for each turn we need 0.42litre of water and 2.1Kg of powder. Now to cater for environmental factors and other external factors, we use a 5% tolerance in our proportions. So according to that, our modified values are 0.441 liter of water and 2.205 Kg of powder.

The exact amount of powder was assured by using accurate weight balance. For the water, graduated cylinder was used to ensure accurate quantity.



Figure 4. 1 : Weight Balance



Figure 4. 2 : Graduated cylinder

After the measurement of water and the mortar according to the appropriate predefined ratio, the mixture was created in a mixing machine. Initially the mortar powder and water are mixed in steel bowl and afterwards the mixture was mounted on the mixing machine. The mixing machine was turned on and the mixture was allowed to blend thoroughly.



Figure 4. 3 : Mortar specimen mold



Figure 4. 4: Filled mold

Then the mold surfaces were coated with thin film of lubricant(oil) for easy removal of specimen. The mixture was filled in the mold and the mold was mounted on a tamper machine which compacts the mixture. These filled molds were given a predefined 60 jerks and then the molds were unmounted from the tamper machine. Then the excess mortar is skimmed off using knife or some flat surface.



Figure 4. 5 : Mold mounted on the tamper machine

Then the specimen mold was left for a day to dry down. After one day, the specimens were taken out of mold by disassembling the assembly and they were immersed in humidity chamber for proper seasoning for 28 days.

4.2 Experimental tests

After the preparation of specimen, the next phase of the mechanical characterization is the determination of type of test the needs to be conducted. Total of 10 specimen were prepared. On these specimens, two types of tests were performed (following BS EN 1015-11-1999). For the mortar specimen, two types of tests are of main significance.

- Compression test, to determine the compressive strength.
- Flexural (3-point bending test) to determine the flexural strength.

Experimental campaign is designed in such a way that each of the 10 specimen is tested for its flexural strength as a result of which these specimen break into two. The data is collected and later on the compression tests are carried out on each of these 20 specimens.



Figure 4. 6: Mortar specimen

4.2.1 Flexural tests

First test applied on the specimen was 3-point bending test. Machine consisted of 3 roller elements, two at the bottom of specimen and one above. The center of upper roller element is exactly in center of the distance between centers of two bottom roller, though at a different height. Upper roller is the loading roller, and the lower rollers are the supporting roller. Load is applied at a rate of 2mm/s and the maximum force is measured. Load is applied gradually without shock. The flexural strength is calculated using the following formula.

$$f = \frac{Fl}{bd^2}$$

In order to carry out the test, all the specimen were mounted one by one on the flexural testing machine and 3 point load is applied until the specimen fails under the load. The dimensions and the weight of the specimen are already known. The main parameters that are obtained by the flexural testing machine are the reaction force and the flexural strength values. These values are obtained digitally from the testing machine in the form of excel file containing the reaction force values. Flexural strength is later calculated using the formula for flexural strength mentioned above.



Figure 4. 7 : Flexural testing machine

4.2.2 Compression test

Compression test is designed to determine the resistance of the specimen under compressive load. Compressive tests are usually carried out using the universal testing machine. The specimen is mounted on the jig and compressive load is applied until the material breaks to failure. As a result of the flexural testing, we have 20 specimens, which are labeled as M3A M3B to M12A and M12B.

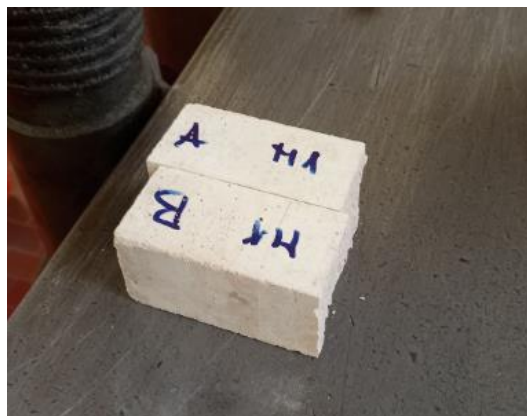


Figure 4. 8 : Specimen of compression test

Each of these specimens were tested and the results were obtained in the form of excel file containing the compressive load values. Compressive strengths of the specimens were calculated using the breaking force/ area dimensions formula.

To determine the compressive behavior and compressive strength of mortar, the machine used was 50KN/s tensile testing machine. The machine consisted of a mounting area where a compression jig was present to mount the specimen. Compression jig is used to properly align the compressive force on the specimen.



Figure 4. 9 : Universal tensile testing machine



Figure 4. 10: Specimen failed under compressive load

Thus, the experimental campaign is concluded in 3 steps, the preparation of the specimen, the flexural testing of 10 specimen and then the flexural testing of the 20 specimens. As a result of this testing, we obtain mechanical properties of mortar specimen under consideration. However, these mechanical properties values are raw values. These values need to be arranged managed and sorted out to get suitable and useful results.

4.3 Results

Experimental campaign for the mechanical characterization of the specimen yield results in the form of data containing reaction forces basically. This data is analyzed and manipulated in order to get the desired results for appropriate characterization of the mortar. In the case of the flexural test, we obtain reaction force which is used to obtain the flexural strength using the formula provided that the dimensions of the specimen are already known. This flexural strength values gives a basic idea about the resistance of the

material under observation, under various bending loads that may act when the material is used various real-life applications.

In the case of the compressive tests, once again we obtain the value of the reaction forces of the material under observation. These values are used to calculate the compressive strength of the material under observation. In the experimentation, the compressive strength is referred to the yield point because technically a material fails to act after the yield point. So, especially in case of structural and masonry applications, the compressive strength for all materials is considered to be yield point. However, in our case the mortar specimen in a brittle material where a material fails at the yield point so there isn't any discrimination.

4.3.1 Results of Flexural test

Results from the testing on each specimen actually generates various values of reaction forces after regular interval (thousands of values). We can actually compute the flexural strength from this reaction force as mentioned above which gives us data in two ways. First of all, we can develop a reaction force vs the displacement graph which exhibits the gradual trend of the specimen under the application of load. Secondly, the maximum value of the strength gives us the idea about the actual flexural strength.

Initially, the performance of some individual specimens can be observed using the load displacement graphs. These graphs are represented as follows.

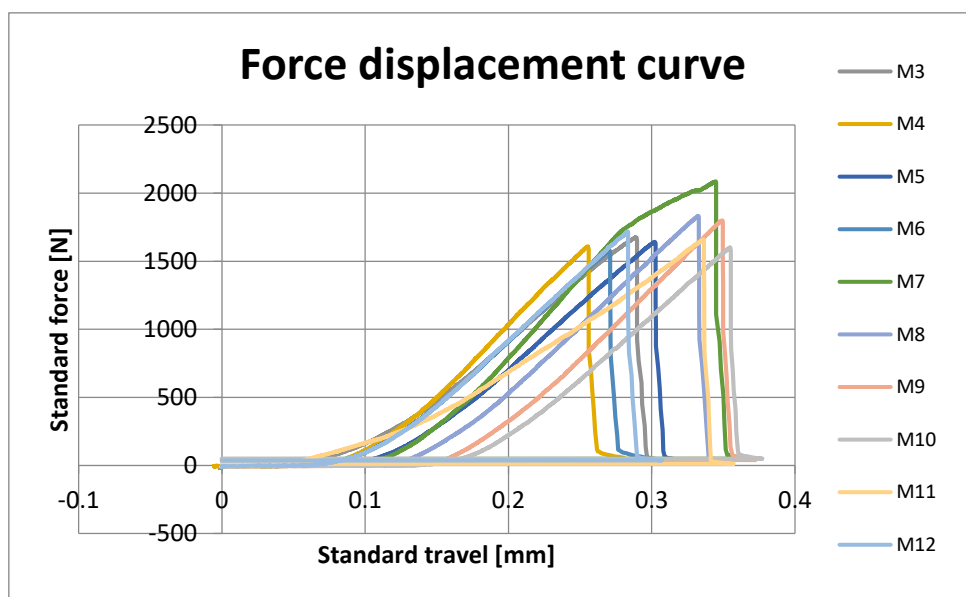


Figure 4. 11: Force displacement Curves from M2 to M12 specimen

Now we need to extract suitable data from the curves. As mentioned before, the flexural strength is determined by the reaction force and the dimensions using the formula of the flexural strength. The following table exhibits the compared flexural strengths of the specimens.

Table 4. 1 : Data from flexural strength test

Specimen ID	a ₀ mm	b ₀ mm	length mm	F _{max} N	Flexural Strength MPa
M3	39,92	39,96	160,0	1677,1	4,21
M4	40,18	40,13	160,0	1607,9	3,97
M5	39,97	39,29	160,1	1641,6	4,19
M6	39,96	39,66	160,0	1578,4	3,99
M7	41,05	40,06	160,2	2085,2	4,95
M8	40,31	39,95	160,2	1831,8	4,52
M9	40,39	40,00	160,1	1799,4	4,41
M10	40,01	39,96	160,1	1601,3	4,01
M11	40,02	39,95	160,1	1659,7	4,15
M12	40,09	40,08	160,1	1719,7	4,27

4.3.2 Compression test

As discussed before, the universal tensile testing machine (50KN/s) is used. The testing machine is used to apply a compressive load until the specimen fails under compressive load. The testing machine actually measures the reaction force related to the displacement.

The main parameter of concern is the compressive strength which can be computed using the dimensions of the specimen. Total of 20 specimen were under observation which were tested. A large number of specimens were used in order to cater for the anomalies in the results. The results from the testing of the specimen are represented below.

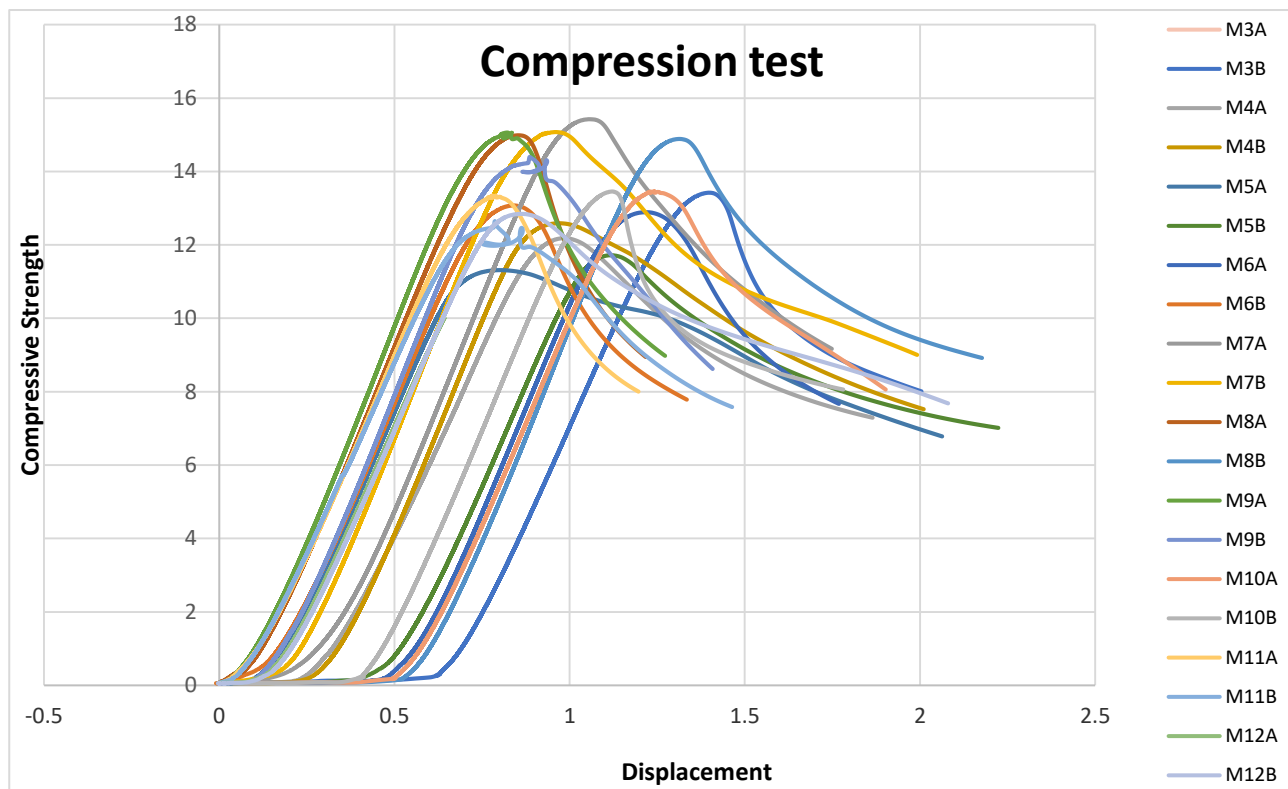


Figure 4. 12 : Trend under compressive load

Table 4. 2 : Data from Compressive tests

Specimen ID	dL at break mm	Compressive Strength Mpa
M3_A	1,99	14,01
M3_B	2,00	12,39
M4_A	1,86	12,18
M4_B	2,01	12,59
M5_A	2,06	10,02
M5_B	2,22	11,31
M6_A	1,77	12,89
M6_B	1,33	13,07
M7_A	1,75	15,42
M7_B	1,99	15,07
M8_A	1,22	14,98
M8_B	2,18	14,89
M9_A	1,27	15,06
M9_B	1,41	14,39
M10_A	1,90	13,46
M10_B	1,78	13,45
M11_A	1,20	13,34
M11_B	1,46	12,65
M12_A	2,85	12,04
M12_B	2,08	12,84

Chapter 5: Numerical Modelling of tensile behavior

After the experimentation, the next possible mean of mechanical characterization of composite material is the numerical modelling of the specimen under consideration. There are numerous drawbacks to practical experimentation such as high costs, time consumption and various factors that affect the accuracy of experimental results. Numerical modeling provides with a cost effective and time saving as well as effective alternative to experimentation.

A sequential numerical modelling campaign must be designed in order to create a perfect and reusable model that can be used later on, on various other specimens having different materials and mechanical properties. The main aim of this part of the thesis is to create an effective numerical modelling strategy by implementation of knowledge from previous research as well as iterative procedures, that can replicate the results from experimentation for any material.

Two different approaches are adopted in order to create the desired material. The details of these approaches are as follows.

- Generating a numerical model on the basis of the data of experimentation obtained from some already established research and experimentation.
- Replicating the numerical model from an already developed numerical model.

In the next few sections, these two approaches will be discussed in detail.

5.1 FEM model from experimental data

In order to follow the first approach, a pre-existing experimentation is needed which has a proper experimentation campaign, following all the rules set by various international standards, as well as authentic and valid results that can be reproduced as a result of simulation of the numerical model.

For that purpose, the research published by Arboleda et al. (2016). The reasons to choose this research are as follows.

- Experimentation campaign follows the international standards set by various institutions
- Experimentation campaign is designed effectively.
- Different clamping systems are tested. As it is already known that the contact between specimen and grip is of utmost importance, so different approaches must be followed.
- It is comprehensive research comprising of 5 different type of fibers.
- Mortars are selected individually for each fiber depending upon the compatibility.
- Mechanical properties of the mortars used in the research are properly mentioned.
- The results from the experimentation campaign depict the effectiveness of the experimentation technique

The details of Arboleda et al. (2016) are already mentioned in the previous sections.

5.2 Development of numerical model

Arboleda et al. (2016) is numerically modeled using ABAQUS CAE as already mentioned. In order to create the model, the main variables of importance are the geometry and material properties which are obtained from the Arboleda et al. (2016) research paper. This research paper actually involves 5 different types of fibers which are as follows

- Polyparaphenylene benzobisoxazole Fiber
- Carbon Fiber
- Coated Carbon fiber
- Glass fiber
- Coated Glass fiber

As mentioned above, mortars are selected individually for each fiber depending upon the compatibility. Arboleda et al. (2016) provides the details of the mortars used for each of the 5 fibers.

5.2.1 Part Module

In order to carry out the numerical modelling, initial step is the preparation of assembly. According to Arboleda et al. (2016), the mortar specimen had a length of 400mm, width of 40mm and thickness of 5mm per layer of mortar. However, in case of the specimen tested with the Clevis gripping, the length of specimen is taken to be 450mm to cater for the clamps. Fiber layer is placed between two mortar layers. Aluminum tabs are provided on both ends in order to facilitate the clamping mechanism. All these three components namely the mortar layers, the fiber and the aluminum tabs are modelled individually. Basically, two parts are created in the ABAQUS CAE interface, the mortar (containing one mortar layer as well as aluminum tab) and the fiber.

The fiber is modelled as 3D deformable shell element, the details of the part model are shown below in the form of image taken out of the ABAQUS interface. Shell element is selected instead of conventional 3d deformable extrusion element in order to model the fiber effectively. Then the 3D model is seeded in order to assign the numerical geometry some predefined nodes. After the seeding, corresponding model is meshed.

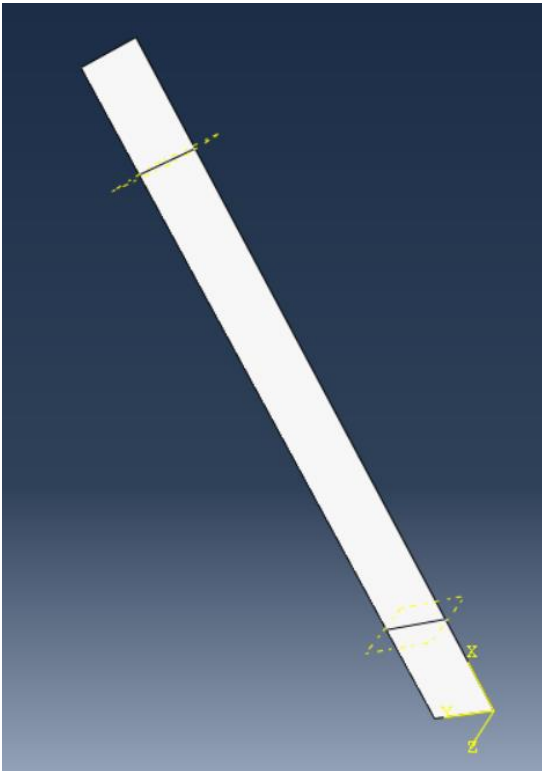


Figure 5. 1 : Fiber Part module

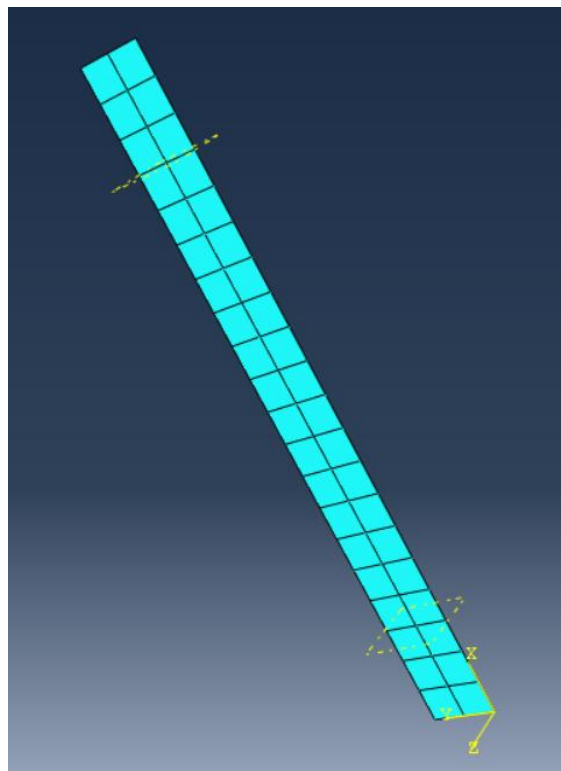


Figure 5. 2 : Meshed Fiber

Second part within the part module is the mortar. The mortar is modelled as 3D deformable solid extrusion element. The dimensions and the geometry of this part is same as that of the fiber part because the aluminum tabs and the mortar are merged into one

another yet. However, as this part is not a shell element so a proper thickness can be observed here. Each of this part represent an individual layer of the mortar specimen, which will be assembled later. After the preparation of the part, the part is seeded in order to assign some nodes to the part. This seeded part is then meshed. The details of the part are represented below by the pictures obtained from the ABAQUS interface.

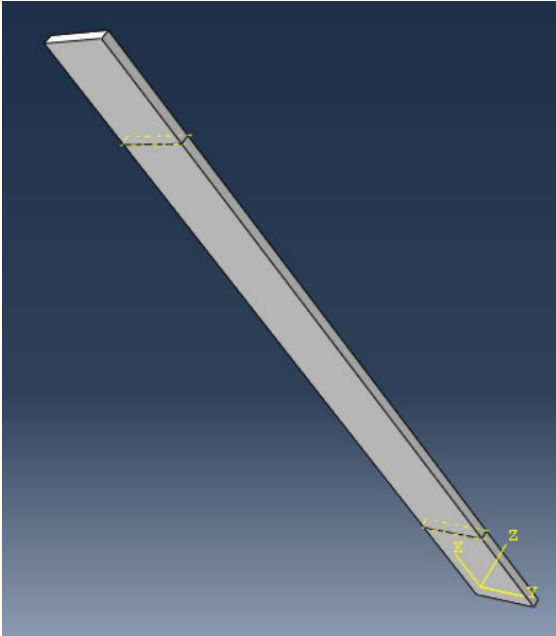


Figure 5. 3 : Mortar part module

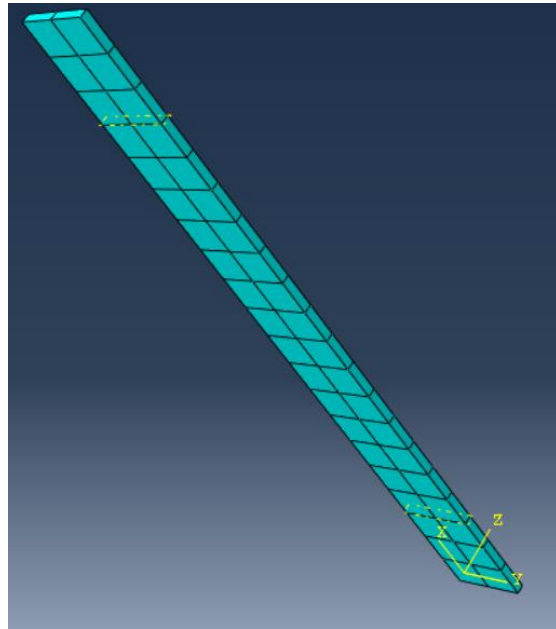


Figure 5. 4 : Meshed mortar

5.2.2 Material Properties Module

Thus, after the definition of the mortar and fiber part, the part module is complete. Now the next module is the materials. But prior to this module, mechanical properties are needed from the Arbodela et al. (2016). So, the mechanical properties obtained from Arbodela et al. (2016) are gathered and manipulated in order to modify them to be used in the model. Following are the details of the material properties that are deduced and manipulated from the model.

Material properties PBO TRM are given in tabular form as below.

Table 5. 1 : Material Properties of TRM materials

Fiber Properties-Elastic	S1-PBO-Clamp	S1-PBO-Clevis	S1-CFRM-Clamp	S1-CFRM-Clevis	S1-cCFRCM-Clevis	S1-GFRM-Clamp	S1-cGFRM-Clamp
G12 (Mpa)	80000	80000	75185	75185	97407	18148	20740
G13 (Mpa)	80000	80000	75185	75185	97407	18148	20740
G23 (Mpa)	332	332	30074	30074	38962	7259	8296
Poisson's ratio	0,35	0,35	0,35	0,35	0,35	0,35	0,35
E1 (Mpa)	216000	216000	203000	203000	263000	49000	56000
E2 (Mpa)	86400	86400	81200	81200	105200	19600	22400
E3 (Mpa)	86400	86400	81200	81200	105200	19600	22400
Shell Thickness (mm)	0,046	0,046	0,047	0,047	0.175	0.036	0.05
Fiber Properties-Plastic							
Yield Stress (Mpa)	3900	3900	1900	1900	1300	1400	1200
Plastic Strain	0	0	0	0	0	0	0
Mortar Properties-Elastic							
Elastic Modulus (Mpa)	6000	6000	7000	7000	7000	5000	8000
Poisson's Ratio	0,19	0,19	0,19	0,19	0,19	0,19	0,19
Mortar Properties-CDP							
Dilatation Angle	31	31	31	31	31	31	31
Eccentricity	0,1	0,1	0,1	0,1	0,1	0,1	0,1
Fb0/fc0	1,12	1,12	1,12	1,12	1,12	1,12	1,12
k	0,667	0,667	0,667	0,667	0,667	0,667	0,667
Viscosity	0,0001	0,0001	0,0001	0,0001	0,0001	0,0001	0,0001
Yield stress comp (Mpa)	27,12	27,12	19,21	19,21	36	8	21,7
Inelastic strain	0	0	0	0	0	0	0
Yield stress tensile (Mpa)	3,8	3,8	2,64	2,64	4	3,2	4
Cracking strain	0	0	0	0	0	0	0
Aluminum Tabs							
Young modulus (Mpa)	10000000	10000000	10000000	10000000	10000000	10000000	10000000
Poisson ratio	0,2	0,2	0,2	0,2	0,2	0,2	0,2

5.2.3 Section Module

In this module we define the sections within the parts that were created in the part module. Parts can be a complex object consisting of several sections. Each section must have a different material. To start with, fiber section is created. Fiber is modelled as continuum shell having a predefined thickness. The thickness is different for each of the fiber within scope of the thesis. These shell thicknesses are already mentioned in the previous material properties section. Thickness integration point is set to be 5. The fiber geometry created in the part module is selected corresponding to the fiber section. Following are the details of the fiber section from ABAQUS interface.

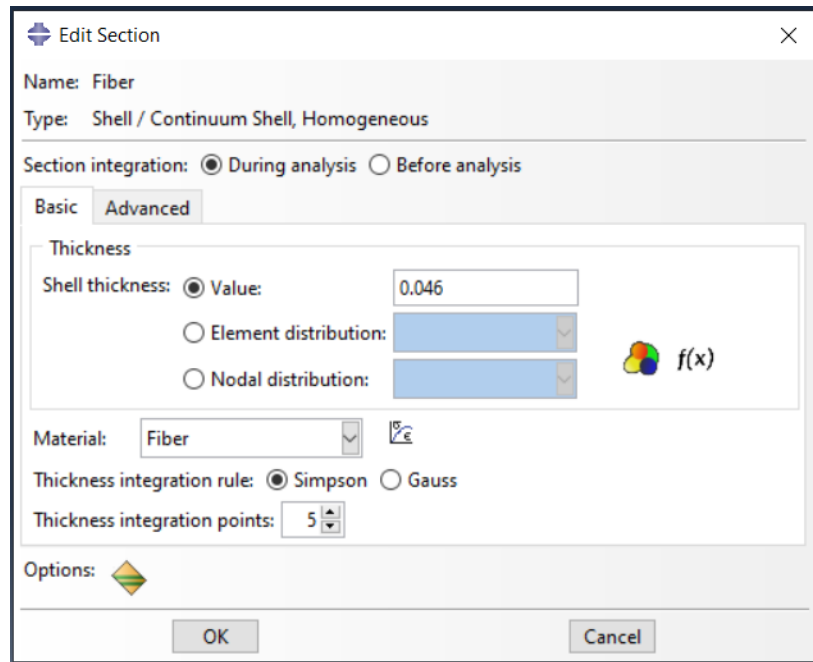


Figure 5. 5: Section module of fiber, ABAQUS interface

Mortar section is created using solid homogenous element. After the creation of the section, the geometry is selected in such a way that the middle part of the mortar part is selected as mortar section however the end parts are selected as aluminum tabs. The mortar is portioned prior to the section creation in such a way that the mortar part is composed of the mortar as well as the aluminum tabs. Planes are created along the length of the mortar part, on both ends. After that, the cell partitioning is done on the mortar part in order to section the part to individually into mortar as well as aluminum tabs. Sectioned part is shown below. Now parts will be assigned individually in the material assignment section.

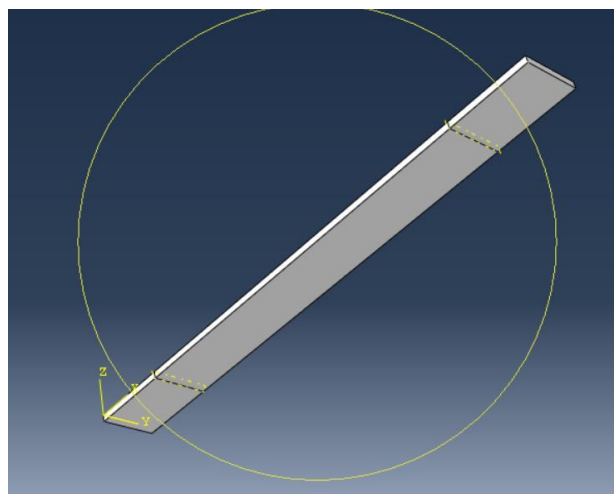


Figure 5. 6 : Section plane on mortar

Now the section assignment part is accessed going back to the part module. Fiber part is assigned fiber section and the mortar part is assigned mortar as well as aluminum tabs section. Now the parts are fully defined, and assembly is ready to be created. Details of the sections are shown below.

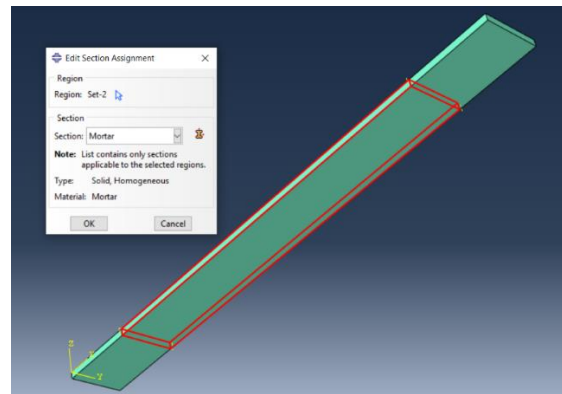


Figure 5. 7 : Mortar Section assignment

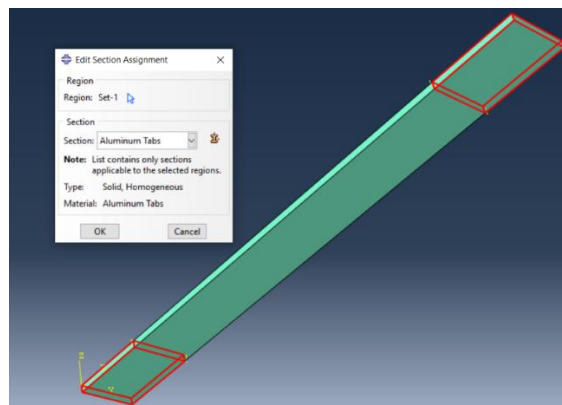


Figure 5. 8 : Aluminum Tabs section assignment

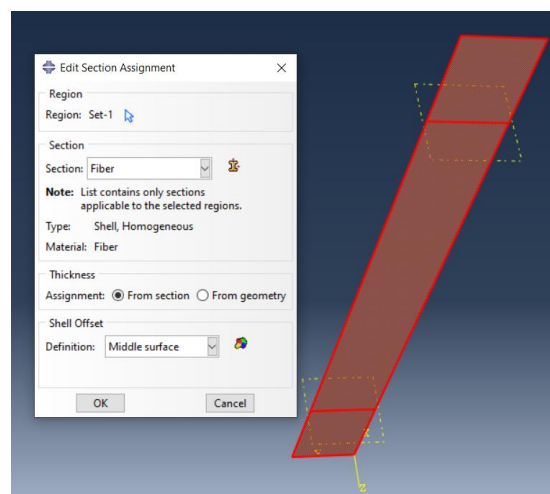


Figure 5. 9 : Fiber Section assignment

5.2.4 Assembly Module

After the preparation of individual parts and definition of sections, the next step is the creation of assembly. ABAQUS provides users with number of tools to assemble the parts. Instance is imported into the assembly module and then various translation and rotational tools are used to assemble the part instances. In the case of specimen under consideration, two mortar instances and one fiber instances are imported in the assembly module window. The fiber part instance is translated to align perfectly the two parts, later on the second mortar part is aligned in the same manner. Finally, the assembly is perfectly constrained.

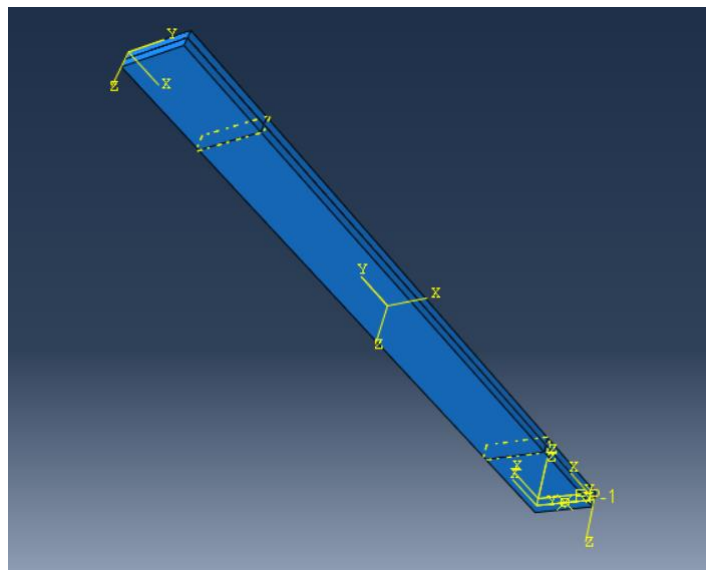


Figure 5. 10 : ABAQUS assembly Module

Material orientation is another important aspect of the ABAQUS model created for analysis. In order to define the material orientation of the specimen, datum system of coordinate must be defined. Two options are available for this purpose, the original principal system of coordinates for which the model is created, and the system of coordinates defined in the assembly module. ABAQUS interface provides user with the possibility to create new system of coordinates which can be defined using the surfaces of the model. So a proper system of coordinates is defined to set a proper material orientation. The following figure shows the defined material orientation.

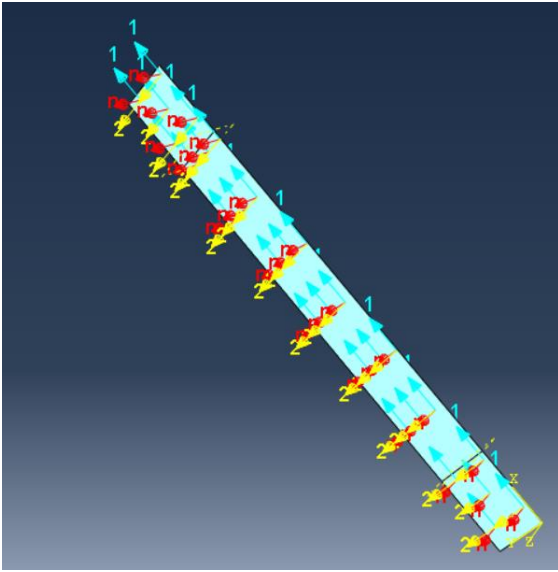


Figure 5. 11 : Material orientation of Fiber

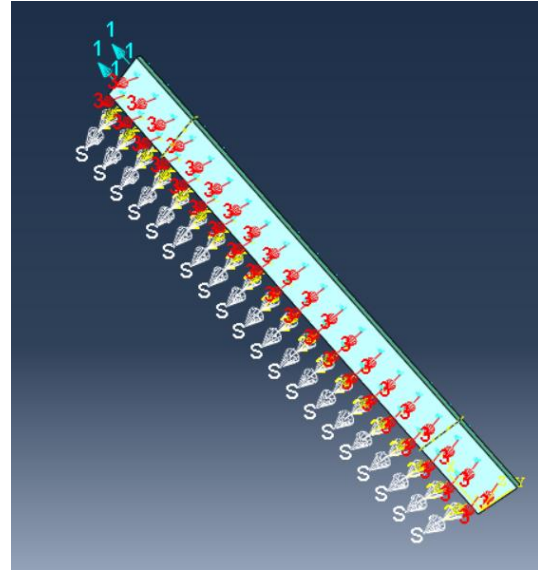


Figure 5. 12 : Material orientation of mortar

5.2.5 Step Module

Next step is the creation of steps in the step module. The first step is the initial step where the initial boundary conditions of the assembly is to be determined. In order to define the initial BC, encaster BC is defined on one end of the specimen in order to replicate the clamping of the specimen into the gripping mechanism of the testing machine. Encaster BC actually fixes one end of the specimen under zero displacement condition, so the material acts as a clamped stationary object. Following figure shows the encaster BC on assembly.

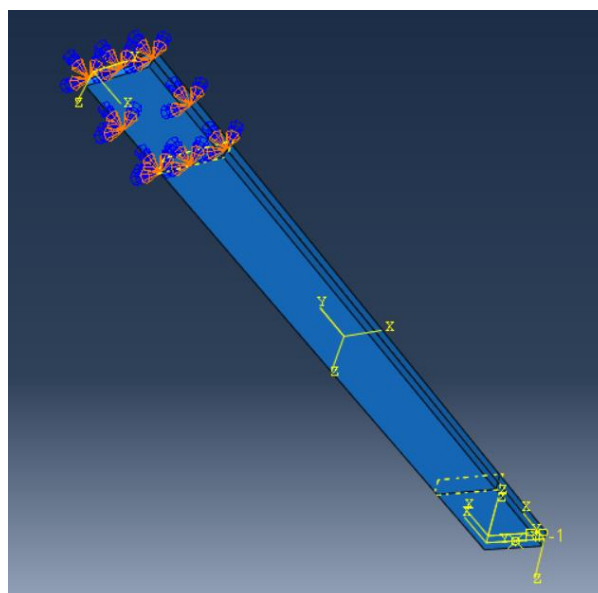


Figure 5. 13 : Encaster Boundary condition

After the complete definition of the initial conditions the next step is to define the Boundary conditions for next steps. The main aim of the numerical model is the testing of the specimen under investigation under the action of load. In this step we replicate the effect of the applied force in the form of Displacement boundary condition. The displacement boundary condition is set on the specimen in such a way that one end of the specimen is still under the action of the encaster BC (propagated from initial step) and the other end of the specimen is under the action of displacement BC (created in this step). The value of the displacement BC is set to be 6 as shown in the figure below.

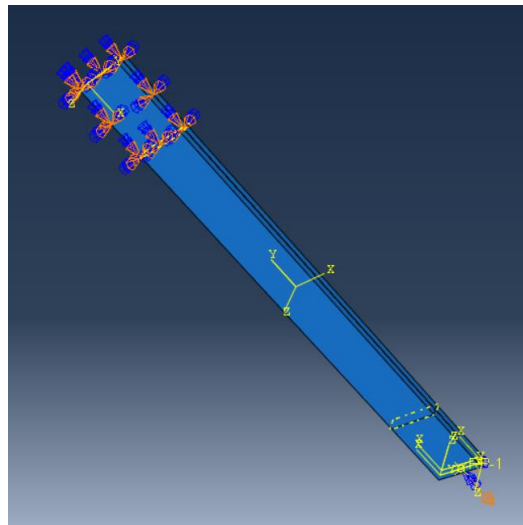


Figure 5. 14 : Displacement BC

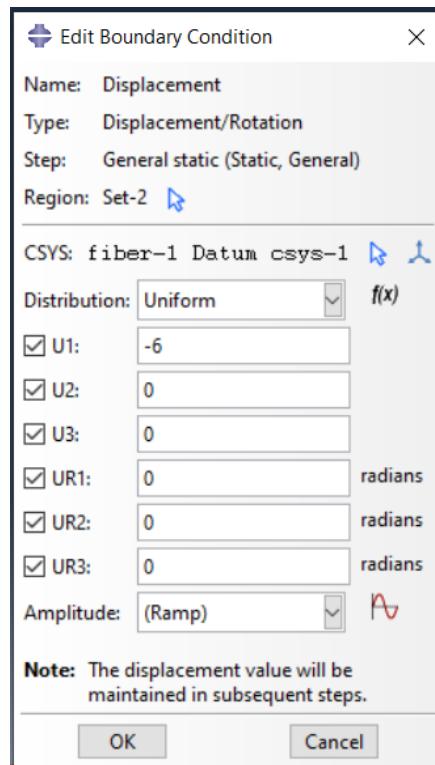


Figure 5. 15 : Displacement BC

5.2.6 Constraint Module

Rigid body constraint requires a reference point. The motion of all the regions or surfaces of the specimen that are selected to be rigid body are constraint against the reference point. As a result of this constraint, the degrees of freedom of rigid body are fixed with respect to the reference point. Under the action of distributed load applied to the element, as the simulation is underway, the motion rigid body is restricted. As a result, there is no deformation (elongation, necking etc.) in the rigid body. However, rigid body movements can be observed. Behavior of specimen (and the rigid body regions) during simulation depends on the orientation of the applied loading conditions.

Considering the rigid body, nodes can be of two types, namely tie nodes and pin nodes. ABAQUS interface gives user the option to choose between two depending on the type of simulation. In the case of pin nodes, the nodes of the rigid body region are tied to the reference point in such a way that their translation degree of freedom is restricted to the reference point. Which means the rigid body is free to move along all three axes. However, in the tie nodes, all 6 degrees of freedom (3 translational and 3 rotational) of the rigid body nodes are restricted to the reference point.

The reference point was previously defined in the assembly module. In this step the rigid body constraint is defined in the end of the specimen where reference node is set in order to apply the load.

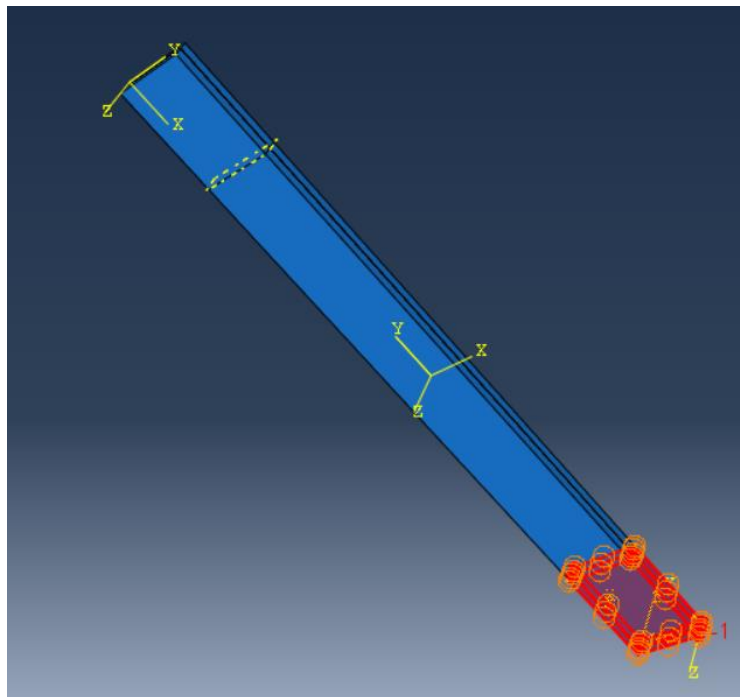


Figure 5. 16: Rigid body constraint

All these boundary conditions can be observed in the Boundary condition module. Now the model is complete. After the completion of the model. The job module is approached, and the Job is create in order to carry out the simulation of the model.

5.2.7 Interaction module

As already discussed, the interaction between the surfaces can be simulated using the perfect bond model as well as the cohesive law. The details of both approaches are described earlier. In order to apply the cohesive law, we need this module. While defining the model, surfaces need to be defined so the fiber surface is set to be the master surface and the mortar surface are set to be the slave surface.

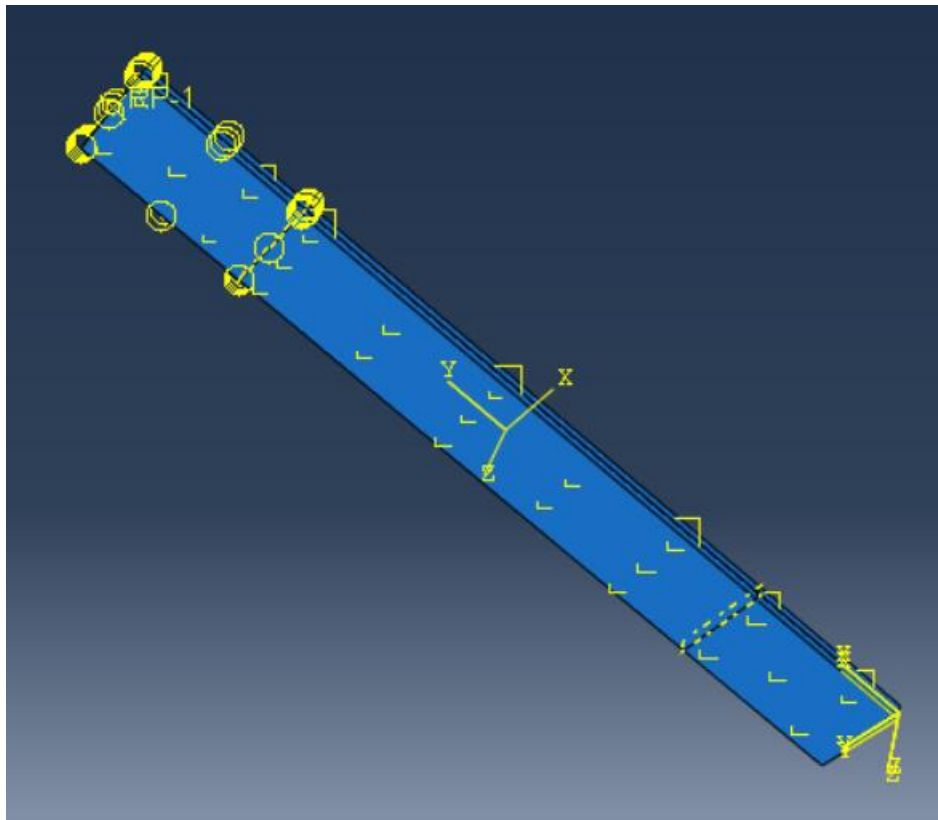


Figure 5. 17 : Interaction-Cohesive law

Cohesive interaction is a simplified approach to model the cohesive behavior. Traction-separation constitutive model is implemented in order to model the interface between two surfaces. The interface thickness is negligibly small. The interface between two surfaces in contact is modelled in such a way that the bond between elements is modelled up to the elastic limit of the tension slip curve.

Edit Contact Property

Name: Cohesive interaction

Contact Property Options

Cohesive Behavior

Damage

Mechanical Thermal Electrical

Cohesive Behavior

☐ Allow cohesive behavior during repeated post-failure contacts

Eligible Slave Nodes

☐ Default

☐ Any slave nodes experiencing contact

☐ Only slave nodes initially in contact

☒ Specify the bonding node set in the Surface-to-surface Std interaction

Traction-separation Behavior

☐ Use default contact enforcement method

☒ Specify stiffness coefficients

☒ Uncoupled ☐ Coupled

☐ Use temperature-dependent data

Number of field variables: 0

Knn	Kss	Ktt
2	2	2

OK Cancel

Edit Contact Property

Name: Cohesive interaction

Contact Property Options

Cohesive Behavior

Damage

Mechanical Thermal Electrical

Damage

☒ Specify damage evolution

☐ Specify damage stabilization

Initiation Evolution Stabilization

Criterion: Quadratic traction

Maximum Nominal Stress

☐ Use temperature-dependent data

Number of field variables: 0

Normal Only	Shear-1 Only	Shear-2 Only
0.24	0.78	0.78

OK Cancel

Figure 5. 18 : Cohesive Interaction properties

Chapter 6: Results and Comparisons

6.1 Comparison between experimental and numerical data by Arboleda et al. (2016)

Finite element analysis (FEA) developed using Abaqus software represents a powerful 3D modeling and characterization tool of the mechanical response of composite materials. The modeling, on Abaqus, of the samples of different fibers, based on a mesoscale, made it possible to simulate the behavior of individual materials constituting the models. The numerical results in terms of load curves deformation were compared with those obtained experimentally, this allowed to identify the parameters that influence the complex mechanical behavior of these composite materials when they are subjected to tensile stress.

Two groups of samples were modeled in the Abaqus software with material subjected to tensile tests during the campaign experimental by Arboleda et al. (2016). These two groups of samples are distinguished according to the type of Clamping (Clamping, Clevis) within the composite. Each group contains numerical models of the nominal size of 10x40x400 mm (In case of Clamping), or 10x40x410 (in case of Clevis) were developed, with each Fiber Material selected by the corresponding Author of Publication. In these models, the layers of fiber are ideally distributed in a manner uniform within each section. The tested specimens of the eccentricities of the fiber fabric which are neglected in the model. The models created for each of the three groups of samples analyzed are distinguished according to the material for the fiber. Numerical analysis allows us to demonstrate the effect on the mechanical properties of various fibers in TRM.

In order to define properly the specimen according to their characteristics, the specimen must be identified according to its specifications via predefined specimen ID. The details of the models created along with the details of dimensions, author, specimen ID etc. are given in the following table.

Within the scope of the thesis, the main aim is to compare the experimental data obtained from the ABROLEDA et al. (2016) with the Numerical data obtained from Numerical Model. The mechanical properties of that need to be implemented in order to create the model to extract the results, are also obtained from the same research. These mechanical characteristics are directly obtained from the research or indirectly computed using

formulae already established. Out of all the established research, Arboleda et al. (2016) was selected because this experimentation campaign follows the international standards set by various institutions and is designed effectively. Different clamping systems are tested. As it is already known that the contact between specimen and grip is of utmost importance, so different approaches must be followed. This comprehensive research comprising of 5 different type of fibers so the effect of these fibers on mechanical properties can be studied. Mortars are selected individually for each fiber depending upon the compatibility. Mechanical properties of the mortars used in the research are properly mentioned, providing ease in extracting the mechanical parameters. The results from the experimentation campaign depict the effectiveness of the experimentation technique. Now, in the next few sections, the comparison is discussed.

Table 6. 1 : Specimen ID

Labels of specimen	Length (mm)	Width (mm)	Height (mm)	Type of test	Type of fibers
S1-PBO-Clamp	400	40	10	Clamping grip	PBO
S1-PBO-Clevis	410	40	10	Clevis Grip	PBO
S1-CFRCCM-Clamp	400	40	10	Clamping grip	Carbon Fiber
S1-CFRCCM-Clevis	410	40	10	Clevis Grip	Carbon Fiber
S1-cCFRCCM-Clamp	400	40	10	Clamping grip	Coated Carbon Fiber
S1-cCFRCCM-Clevis	410	40	10	Clevis Grip	Coated Carbon Fiber
S1-GFRCCM-Clamp	400	40	10	Clamping grip	Glass Fiber

6.2 Comparison with S1-PBO-Clamp

S1-PBO-Clamp is based on single layer of Polyparaphenylene benzobisoxazole Fiber and two layers of Mortar compatible with the fiber. The fiber layer is simulated as sandwiched between two mortar layers. Thickness of each mortar layer is 5mm and the fiber layer is set to be 0.046mm shell element. The Mechanical properties and the dimensions of the specimen are already mentioned as below.

Table 6. 2 : Properties of S1-PBO-Clamp

Type of fiber	Polyparaphenylene benzobisoxazole Fiber
Type of mortar	cementitious mortars
Type of test	Clamping
Type of model	perfect bond
width of specimen (mm)	40
Thickness of specimen (mm)	10
Cross-sectional area (mm ²)	400
Length of specimen (mm)	400

After the completion of the model, the model is simulated. The values are extracted using the ODB field output. The main parameter that needs to be extracted are reaction force and displacement. The numerical data obtained as a result of simulation of S1-PBO-Clamp are given below.

Table 6. 3 : Results from Numerical Model of S1-PBO-Clamp

U2 (mm)	RF2 (N)	Strain	Stress (Mpa)
0	0	0	0
0,6	2375,61	0,0015	593,9025
1,2	3228,9	0,003	807,225
1,8	4080,62	0,0045	1020,155
2,4	4932,35	0,006	1233,0875
3	5784,07	0,0075	1446,0175
3,6	6635,79	0,009	1658,9475
4,2	7487,51	0,0105	1871,8775
4,8	7781,73	0,012	1945,4325
5,4	7781,74	0,0135	1945,435
6	7781,74	0,015	1945,435

In order to extract the numerical values of experimental campaign carried out by Arboleda et al. (2016), the graphs containing the experimental results are analyzed and the values are extracted in order to use them for comparison with numerical model data. Following are the experimental values obtained from the research.

Now we have individual data from the experimental as well as the numerical model. The reaction force and displacement values are extracted using the ABAQUS model. The strain and stress values are obtained from the displacement and reaction force respectively using the dimensions. Now the next step is the comparison between the two. The main properties of interest are stress and strain. Following graph shown the comparison between the two approaches.

Now it is needed to define some parameters related to the stress strain curve corresponding to the three stages of the crack initiation and propagation. For the purpose, some of the importance mechanical characteristics are stiffness, initial and middle stage stress and strain values as well as Ultimate stresses and strains of all specimens. After obtaining the numerical values of these parameters, error between the values obtained by numerical model and the experimental campaign is calculated. All this data is given in the form of following tables.

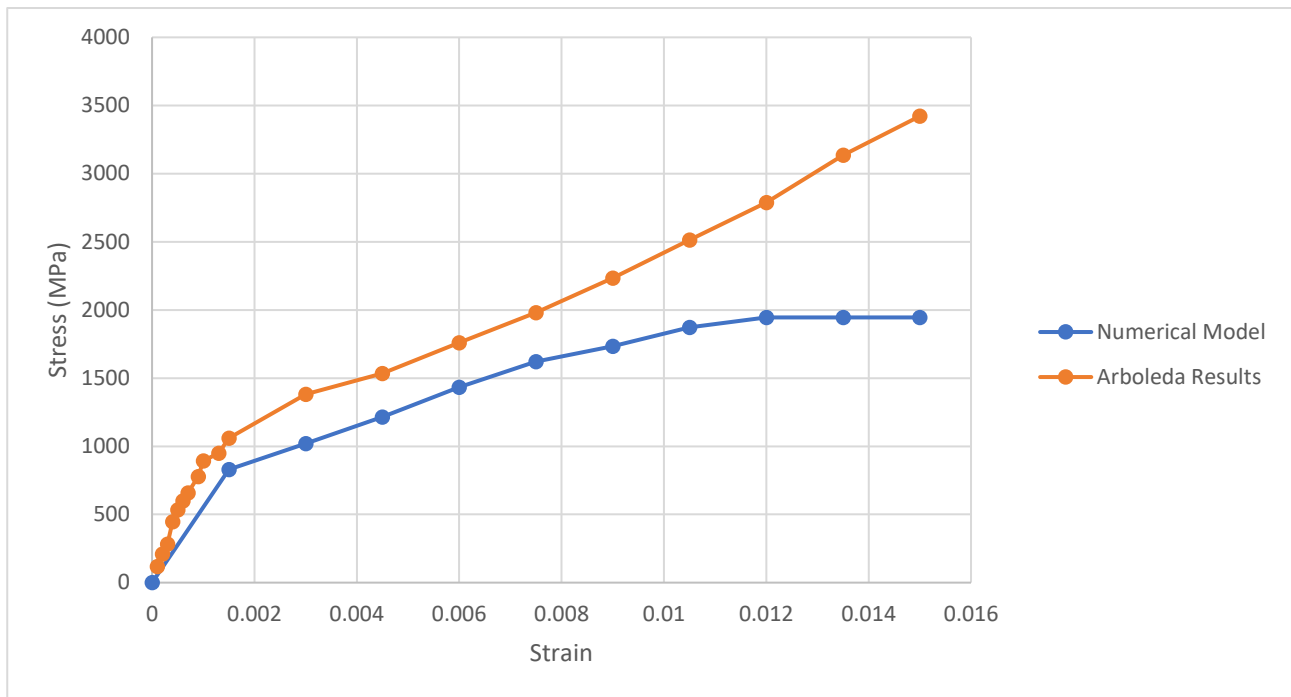


Figure 6. 1 : Stress vs strain comparison for S1-PBO-Clamp

Table 6. 4 : Data from Numerical model

Initial Stiffness (N/mm ²)	554000
First cracking Stress (Mpa)	831
First cracking Strain (mm/mm)	0,0015
Average Second Stage Stress (Mpa)	1458,89
Average Second Stage Strain (mm/mm)	0,00675
Ultimate Stress (Mpa)	1945,43
Ultimate Strain (mm/mm)	0,015

Table 6. 5 : Data From Arboleda et al. along with error

	Percentage error	
Initial Stiffness (N/mm ²)	894200	38,04
First cracking Stress (Mpa)	894,2	7,06
First cracking Strain (mm/mm)	0,001	-50
Average Second Stage Stress (Mpa)	1709,851	14,67
Average Second Stage Strain (mm/mm)	0,00563	-19,89
Ultimate Stress (Mpa)	3421,7	43,14
Ultimate Strain (mm/mm)	0,015	0

6.3 Comparison with S1-PBO-Clevis

S1-PBO-Clevis is based on single layer of Polyparaphenylene benzobisoxazole Fiber and two layers of Mortar compatible with the fiber. The fiber layer is simulated as sandwiched between two mortar layers. Thickness of each mortar layer is 5mm and the fiber layer is

set to be 0.047mm shell element. The Mechanical properties and the dimensions of the specimen are already mentioned as below. Due to clevis gripping mechanism, the aluminum tabs are simulated in the model is such a way that the tabs are a bit elongated.

Table 6. 6 : Properties of S1-PBO-Clevis

Type of fiber	Polyparaphenylene benzobisoxazole Fiber
Type of mortar	cementitious mortars
Type of test	Clevis gripping
Type of model	perfect bond
width of specimen (mm)	40
Thickness of specimen (mm)	10
Cross-sectional area (mm ²)	400
Length of specimen (mm)	410

After the completion of the model, the model is simulated. The values are extracted using the ODB field output. The main parameter that needs to be extracted are reaction force and displacement. The numerical data obtained as a result of simulation of S1 -PBO-Clevis are given below.

In order to extract the numerical values of experimental campaign carried out by Arboleda et al. (2016), the graphs containing the experimental results are analyzed and the values are extracted in order to use them for comparison with numerical model data. Following are the experimental values obtained from the research.

Now we have individual data from the experimental as well as the numerical model. The reaction force and displacement values are extracted using the ABAQUS model. The strain and stress values are obtained from the displacement and reaction force respectively using the dimensions. Now the next step is the comparison between the two. The main properties of interest are stress and strain. Following graph shown the comparison between the two approaches.

Now it is needed to define some parameters related to the stress strain curve corresponding to the three stages of the crack initiation and propagation. For the purpose, some of the importance mechanical characteristics are stiffness, initial and middle stage stress and strain values as well as Ultimate stresses and strains of all specimens. After obtaining the numerical values of these parameters, error between the values obtained by numerical model and the experimental campaign is calculated. All this data is given in the form of following tables.

Table 6. 7 : Results from Numerical Model of S1-PBO-Clevis

U2 (mm)	RF2 (N)	Strain	Stress (Mpa)
0	0	0	0
0,6	2348,9	0,00146341	587,225
1,2	3175,26	0,00292683	793,815
1,8	4000	0,00439024	1000
2,4	4824	0,00585366	1206
3	5649,34	0,00731707	1412,335
3,6	6473,93	0,00878049	1618,4825
4,2	7298,48	0,0102439	1824,62
4,8	8122,9	0,01170732	2030,725
5,4	8708,48	0,01317073	2177,12
6	8715,1	0,01463415	2178,775

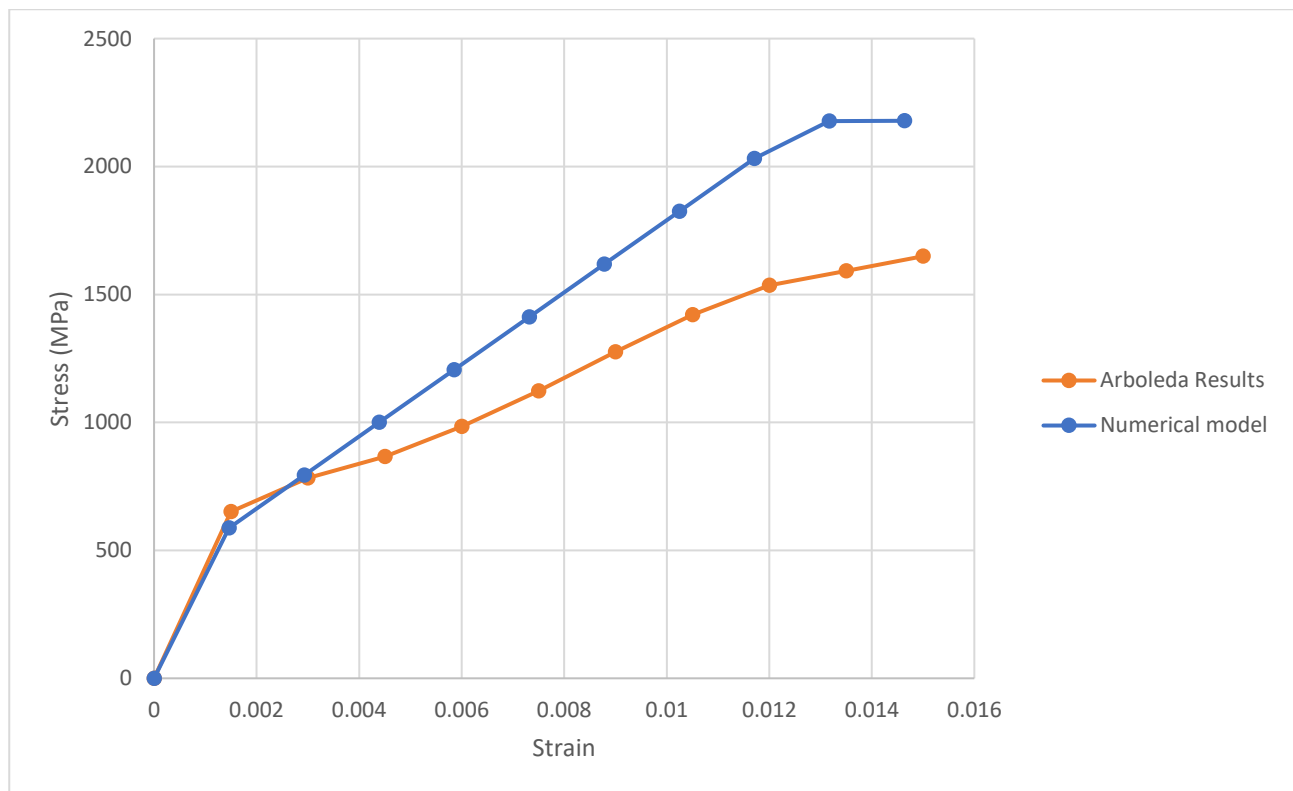


Figure 6. 2 : Stress vs strain comparison for S1-PBO-Clevis

Table 6. 8 : Data from Numerical model

Initial Stiffness (N/mm²)	401270
First cracking Stress (Mpa)	587,225
First cracking Strain (mm/mm)	0,001463
Average Second Stage Stress (Mpa)	1405
Average Second Stage Strain (mm/mm)	0,00658
Ultimate Stress (Mpa)	2178,775
Ultimate Strain (mm/mm)	0,01463

Table 6. 9 : Data From Arboleda et al. along with error

	Percentage error	
Initial Stiffness (N/mm²)	434320	7,6095
First cracking Stress (Mpa)	651,48	9,86
First cracking Strain (mm/mm)	0,00135	8,1
Average Second Stage Stress (Mpa)	1079,92	-30,15
Average Second Stage Strain (mm/mm)	0,00675	2,4
Ultimate Stress (Mpa)	1649,5	32,08
Ultimate Strain (mm/mm)	0,015	2,439

6.4 Comparison with S1-CTRM-Clevis

S1-CTRM-Clevis is based on single layer of Carbon Fiber and two layers of Mortar compatible with the fiber. The fiber layer is simulated as sandwiched between two mortar layers. Thickness of each mortar layer is 5mm and the fiber layer is set to be 0.046mm shell element. The Mechanical properties and the dimensions of the specimen are already mentioned as below.

Table 6. 10 : Properties of S1-CTRM-Clevis

Type of fiber	Carbon Fiber
Type of mortar	cementitious mortars
Type of test	Clevis gripping
Type of model	perfect bond
width of specimen (mm)	40
Thickness of specimen (mm)	10
Cross-sectional area (mm²)	400
Length of specimen (mm)	410

After the completion of the model, the model is simulated. The values are extracted using the ODB field output. The main parameter that needs to be extracted are reaction force and displacement. The numerical data obtained as a result of simulation of S1-CTRM-Clevis are given below.

Table 6. 11: Results from Numerical Model of S1-CTRM-Clevis

U2 (mm)	RF2 (N)	Strain	Stress (Mpa)
0	0	0	0
1,5	3000,09	0,003659	750,0225
3,3	4565,01	0,008049	1141,2525
3,375	4568,46	0,008232	1142,115
3,75	4571,4	0,009146	1142,85
4,315	4575,3	0,010524	1143,825
5,156	4580,49	0,012576	1145,1225
6	4585,16	0,014634	1146,29

In order to extract the numerical values of experimental campaign carried out by Arboleda et al. (2016), the graphs containing the experimental results are analyzed and the values are extracted in order to use them for comparison with numerical model data. Following are the experimental values obtained from the research.

Now we have individual data from the experimental as well as the numerical model. The reaction force and displacement values are extracted using the ABAQUS model. The strain and stress values are obtained from the displacement and reaction force respectively using the dimensions. Now the next step is the comparison between the two. The main properties of interest are stress and strain. Following graph shown the comparison between the two approaches.

Now it is needed to define some parameters related to the stress strain curve corresponding to the three stages of the crack initiation and propagation. For the purpose, some of the importance mechanical characteristics are stiffness, initial and middle stage stress and strain values as well as Ultimate stresses and strains of all specimens. After obtaining the numerical values of these parameters, error between the values obtained by numerical model and the experimental campaign is calculated. All this data is given in the form of following tables.

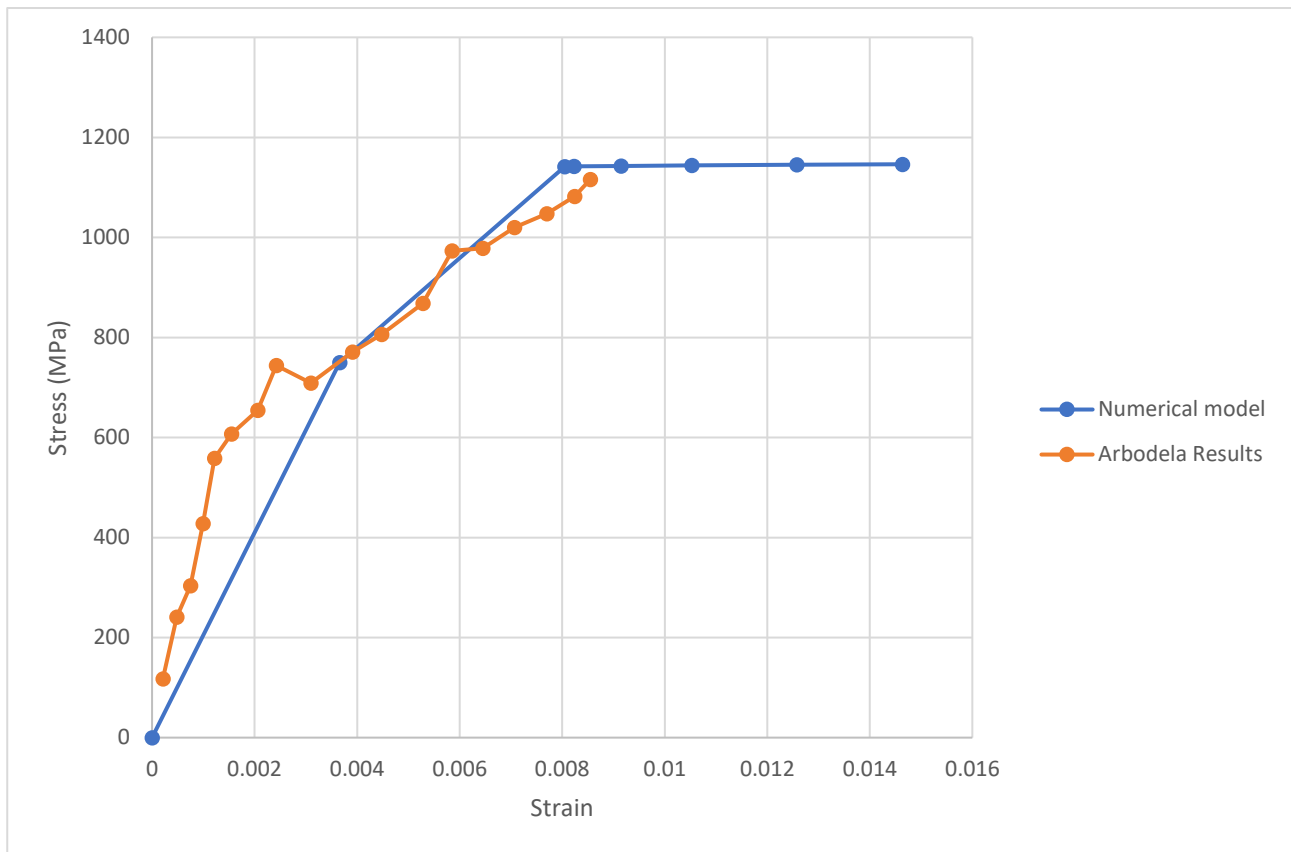


Figure 6. 3: Stress vs strain comparison for S1-CTRM-Clevis

Table 6. 12 : Data from Numerical model

Initial Stiffness (N/mm ²)	205006,2
First cracking Stress (Mpa)	750,0225
First cracking Strain (mm/mm)	0,00365
Average Second Stage Stress (Mpa)	945,63
Average Second Stage Strain (mm/mm)	0,00585
Ultimate Stress (Mpa)	1146,29
Ultimate Strain (mm/mm)	0,01463

Table 6. 13 : Data From Arboleda et al. along with error

	Percentage error	
Initial Stiffness (N/mm ²)	224.535,0000	8,6
First cracking Stress (Mpa)	709,5600	5,4
First cracking Strain (mm/mm)	0,0021	-7,75
Average Second Stage Stress (Mpa)	857,1600	-10,32
Average Second Stage Strain (mm/mm)	0,0048	21,14
Ultimate Stress (Mpa)	1.116,1400	2,7
Ultimate Strain (mm/mm)	0,0086	8,6

6.5 Comparison with S1-GTRM-Clamp

S1-GTRM-Clamp is based on single layer of Glass Fiber and two layers of Mortar compatible with the fiber. The fiber layer is simulated as sandwiched between two mortar layers. Thickness of each mortar layer is 5mm and the fiber layer is set to be 0.036mm shell element. The Mechanical properties and the dimensions of the specimen are already mentioned as below.

Table 6. 14 : Properties of S1-GTRM-Clevis

Type of fiber	Glass Fiber
Type of mortar	cementitious mortars
Type of test	Clamping grip
Type of model	perfect bond
width of specimen (mm)	40
Thickness of specimen (mm)	10
Cross-sectional area (mm ²)	400
Length of specimen (mm)	400

After the completion of the model, the model is simulated. The values are extracted using the ODB field output. The main parameter that needs to be extracted are reaction force and displacement. The numerical data obtained as a result of simulation of S1-GTRM-Clamp are given below.

In order to extract the numerical values of experimental campaign carried out by Arboleda et al. (2016), the graphs containing the experimental results are analyzed and the values are extracted in order to use them for comparison with numerical model data. Following are the experimental values obtained from the research.

Table 6. 15 : Results from Numerical Model of S1-GTRM-Clamp

U2 (mm)	RF2 (N)	Strain	Stress (Mpa)
0	0	0	0
0,6	1245,96	0,0015	311,49
1,2	1433,72	0,003	358,43
1,8	1620,4	0,0045	405,1
2,4	1807,09	0,006	451,7725
3	1993,78	0,0075	498,445
3,6	2180,47	0,009	545,1175
4,2	2367,56	0,0105	591,89
4,8	2553,85	0,012	638,4625
5,4	2740,54	0,0135	685,135
6	2927,22	0,015	731,805

Now we have individual data from the experimental as well as the numerical model. The reaction force and displacement values are extracted using the ABAQUS model. The strain and stress values are obtained from the displacement and reaction force respectively using the dimensions. Now the next step is the comparison between the two. The main properties of interest are stress and strain. Following graph shown the comparison between the two approaches.

Now it is needed to define some parameters related to the stress strain curve corresponding to the three stages of the crack initiation and propagation. For the purpose, some of the importance mechanical characteristics are stiffness, initial and middle stage stress and strain values as well as Ultimate stresses and strains of all specimens. After obtaining the numerical values of these parameters, error between the values obtained by numerical model and the experimental campaign is calculated. All this data is given in the form of following tables.

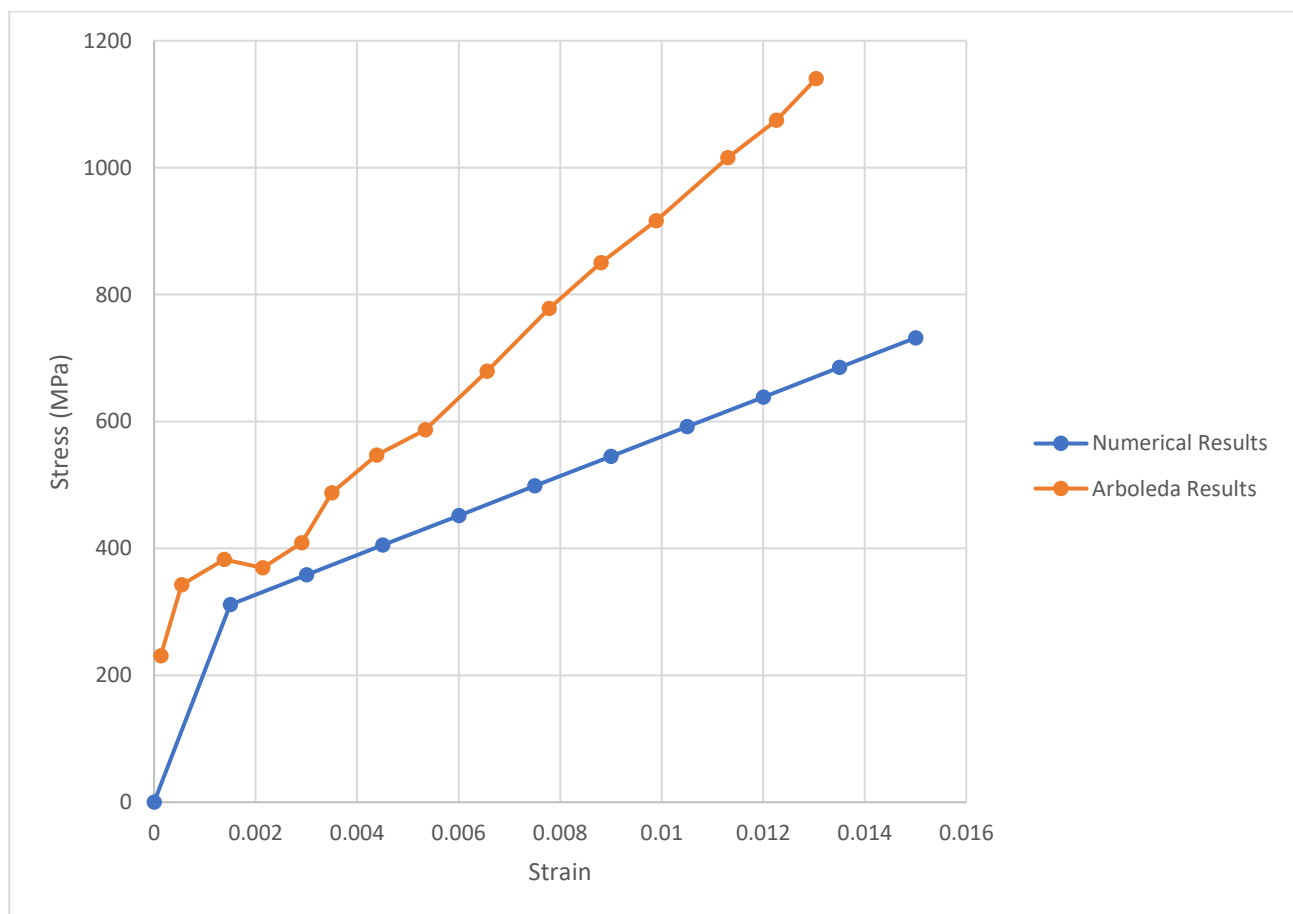


Figure 6. 4 : Stress vs strain comparison for S1-GTRM-Clamp

Table 6. 16 : Data from Numerical model

Initial Stiffness (N/mm²)	207660
First cracking Stress (Mpa)	311,49
First cracking Strain (mm/mm)	0,0015
Average Second Stage Stress (Mpa)	454,12
Average Second Stage Strain (mm/mm)	0,009
Ultimate Stress (Mpa)	731,805
Ultimate Strain (mm/mm)	0,015

Table 6. 17 : Data From Arboleda et al. along with error

	Percentage error	
Initial Stiffness (N/mm²)	288.246,00000	25,09900
First cracking Stress (Mpa)	382,60000	18,58000
First cracking Strain (mm/mm)	0,00138	8,69000
Average Second Stage Stress (Mpa)	674,58000	19,19000
Average Second Stage Strain (mm/mm)	0,00832	8,20000
Ultimate Stress (Mpa)	1.140,03000	35,00000
Ultimate Strain (mm/mm)	0,01304	15,03000

6.6 Comparison with S1-cGTRM-Clamp

S1-cGTRM-Clamp is based on single layer of coated Glass Fiber and two layers of Mortar compatible with the fiber. The fiber layer is simulated as sandwiched between two mortar layers. Thickness of each mortar layer is 5mm and the fiber layer is set to be 0.036mm shell element. The Mechanical properties and the dimensions of the specimen are already mentioned as below.

Table 6. 18 : Properties of S1-cGTRM-Clamp

Type of fiber	Coated Glass Fiber
Type of mortar	cementitious mortars
Type of test	Clamping grip
Type of model	perfect bond
width of specimen (mm)	40
Thickness of specimen (mm)	10
Cross-sectional area (mm²)	400
Length of specimen (mm)	400

After the completion of the model, the model is simulated. The values are extracted using the ODB field output. The main parameter that needs to be extracted are reaction force and

displacement. The numerical data obtained as a result of simulation of S1 -cGTRM-Clamp are given below.

Table 6. 19 : Results from Numerical Model of S1-cGTRM-Clamp

U2 (mm)	RF2 (N)	Strain	Stress (Mpa)
0	0	0	0
0,6	1828,01	0,0015	457,0025
1,2	2052,03	0,003	513,0075
1,8	2274,33	0,0045	568,5825
2,4	2496,63	0,006	624,1575
3	2718,9	0,0075	679,725
3,6	2941,14	0,009	735,285
4,2	3163,34	0,0105	790,835
4,8	3385,53	0,012	846,3825
5,4	3607,69	0,0135	901,9225
6	3809,24	0,015	952,31

In order to extract the numerical values of experimental campaign carried out by Arboleda et al. (2016), the graphs containing the experimental results are analyzed and the values are extracted in order to use them for comparison with numerical model data. Following are the experimental values obtained from the research.

Now we have individual data from the experimental as well as the numerical model. The reaction force and displacement values are extracted using the ABAQUS model. The strain and stress values are obtained from the displacement and reaction force respectively using the dimensions. Now the next step is the comparison between the two. The main properties of interest are stress and strain. Following graph shown the comparison between the two approaches.

Now it is needed to define some parameters related to the stress strain curve corresponding to the three stages of the crack initiation and propagation. For the purpose, some of the importance mechanical characteristics are stiffness, initial and middle stage stress and strain values as well as Ultimate stresses and strains of all specimens. After obtaining the numerical values of these parameters, error between the values obtained by numerical model and the experimental campaign is calculated. All this data is given in the form of following tables.

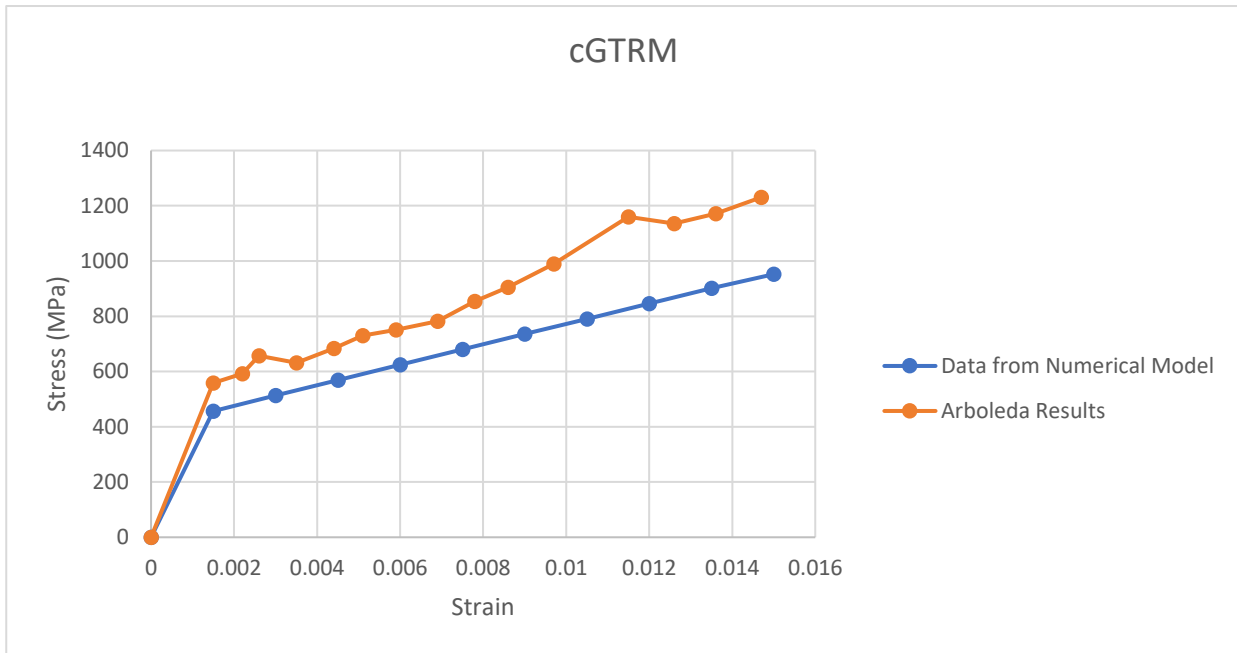


Figure 6. 5 : Stress vs strain comparison for S1-cGTRM-Clamp

Table 6. 20 : Data from Numerical model

Initial Stiffness (N/mm ²)	304668,3
First cracking Stress (Mpa)	457,0025
First cracking Strain (mm/mm)	0,0015
Average Second Stage Stress (Mpa)	706,921
Average Second Stage Strain (mm/mm)	0,009
Ultimate Stress (Mpa)	952,31
Ultimate Strain (mm/mm)	0,015

Table 6. 21 : Data From Arboleda et al. along with error

	Percentage error	
Initial Stiffness (N/mm ²)	358,72200	15,06000
First cracking Stress (Mpa)	502,00000	9,00100
First cracking Strain (mm/mm)	0,00140	7,14000
Average Second Stage Stress (Mpa)	758,78000	6,83000
Average Second Stage Strain (mm/mm)	0,00870	3,34000
Ultimate Stress (Mpa)	1,23100	22,60000
Ultimate Strain (mm/mm)	0,01470	2,04000

6.7 Comparison with S1-CTRM-Clamp

S1-CTRM-Clamp is based on single layer of Carbon Fiber and two layers of Mortar compatible with the fiber. The fiber layer is simulated as sandwiched between two mortar layers. Thickness of each mortar layer is 5mm and the fiber layer is set to be 0.047mm

shell element. The Mechanical properties and the dimensions of the specimen are already mentioned as below.

Table 6. 22 : Properties of S1-CTRM-Clamp

Type of fiber	Carbon Fiber
Type of mortar	cementitious mortars
Type of test	Clamping
Type of model	perfect bond
width of specimen (mm)	40
Thickness of specimen (mm)	10
Cross-sectional area (mm ²)	400
Length of specimen (mm)	400

After the completion of the model, the model is simulated. The values are extracted using the ODB field output. The main parameter that needs to be extracted are reaction force and displacement. The numerical data obtained as a result of simulation of S1-CTRM-Clamp are given below.

Table 6. 23 : Results from Numerical Model of S1-CTRM-Clamp

U2 (mm)	RF2 (N)	Strain	Stress (Mpa)
0	0	0	0
0,6	1864	0,0015	466
1,2	2668	0,003	667
1,8	3471	0,0045	867,75
2,4	4274	0,006	1068,5
3	5077	0,0075	1269,25
3,6	5880	0,009	1470
4,2	6683	0,0105	1670,75
4,35	6884	0,010875	1721
4,4	6940	0,011	1735
4,49	6974	0,011225	1743,5
4,575	6992	0,011438	1748
4,65	6996,25	0,011625	1749,0625
4,78	6997	0,01195	1749,25
4,97	6999,92	0,012425	1749,98
5,26	7002,54	0,01315	1750,635
5,68	7006,01	0,0142	1751,5025
6	7008,38	0,015	1752,095

In order to extract the numerical values of experimental campaign carried out by Arboleda et al. (2016), the graphs containing the experimental results are analyzed and the values

are extracted in order to use them for comparison with numerical model data. Following are the experimental values obtained from the research.

Now we have individual data from the experimental as well as the numerical model. The reaction force and displacement values are extracted using the ABAQUS model. The strain and stress values are obtained from the displacement and reaction force respectively using the dimensions. Now the next step is the comparison between the two. The main properties of interest are stress and strain. Following graph shown the comparison between the two approaches.

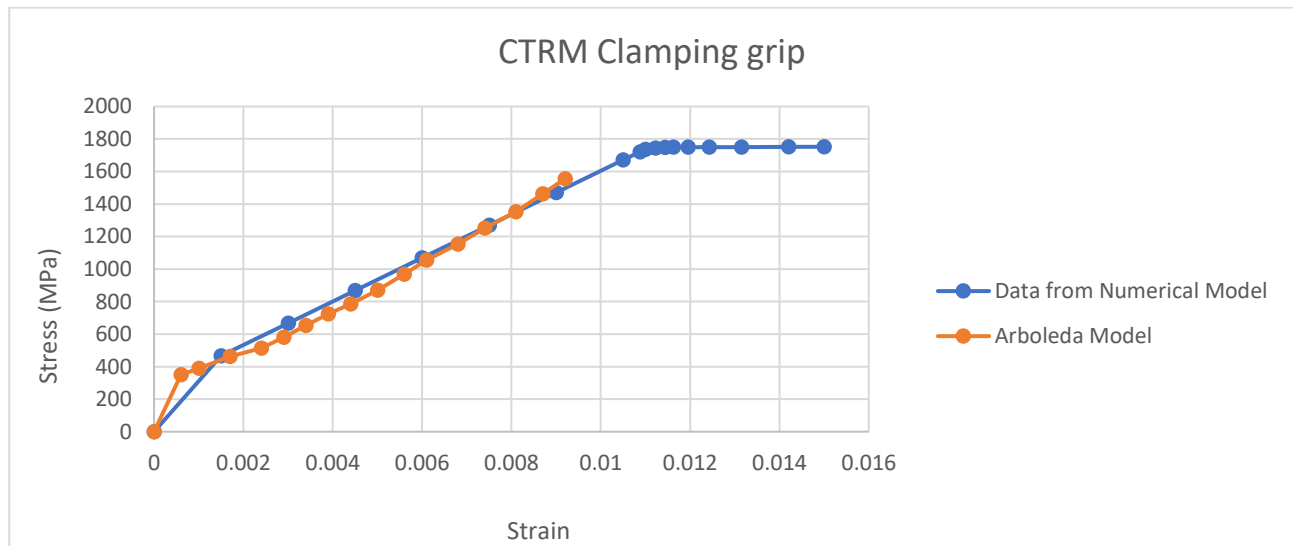


Figure 6. 6 : Stress vs strain comparison for S1-CTRM-Clamp

Now it is needed to define some parameters related to the stress strain curve corresponding to the three stages of the crack initiation and propagation. For the purpose, some of the importance mechanical characteristics are stiffness, initial and middle stage stress and strain values as well as Ultimate stresses and strains of all specimens. After obtaining the numerical values of these parameters, error between the values obtained by numerical model and the experimental campaign is calculated. All this data is given in the form of following tables.

Table 6. 24 : Data from Numerical model

Initial Stiffness (N/mm²)	310666,7
First cracking Stress (Mpa)	466
First cracking Strain (mm/mm)	0,0015
Average Second Stage Stress (Mpa)	831,02
Average Second Stage Strain (mm/mm)	0,00638
Ultimate Stress (Mpa)	1752,095
Ultimate Strain (mm/mm)	0,010875

Table 6. 25 : Data From Arboleda et al. along with error

	Percentage error	
Initial Stiffness (N/mm²)	271352,94	-1,48
First cracking Stress (Mpa)	461,3	1,01
First cracking Strain (mm/mm)	0,0017	11,76
Average Second Stage Stress (Mpa)	910,06	8,68
Average Second Stage Strain (mm/mm)	0,0055333	15,43
Ultimate Stress (Mpa)	1555,56	12,63
Ultimate Strain (mm/mm)	0,0092	18,2

Chapter 7: Conclusions

In this thesis, the mechanical characterization of TRM specimen is analyzed. The study consists of two parts; the first part is the preparation of mortar specimens for their mechanical characterization; the second part is devoted to the development of a FEM numerical model of the tensile response of TRM systems tested in the literature.

The experimental campaign is carried out on specimens of hydraulic lime-based mortar prisms tested under three-point bending and axial compression for determining their flexural strength and compressive strength.

The experimental tests on mortar specimens are as follows.

- **The flexural tests:** these tests are carried out on 10 specimens (from M3 to M12). The flexural strength ranges from 3.99 MPa to 4.94 MPa. The maximum load F_{\max} ranges from 1578 N to 2085 N.
- **The compression tests:** these tests are carried out on 20 specimens (from M3A to M12B). The results range from 10.02 MPa to 15.42 MPa.

The experimental results are in agreement with the mechanical properties of the material provided by the manufacturer and can provide a basis for further experimentation of the TRM specimen containing the corresponding mortar.

The second part of thesis is related to the numerical modeling of TRM specimens and comparison of results in relation to established research. The FEM model is developed in accordance with the predefined standards set by various researches.

The numerical modeling activity is conducted using the finite element software ABAQUS, adopting a modelling techniques in accordance with the methods proposed by several researches available in the literature on this topic. The research work conducted by Arboleda et al. (2016) is replicated through FEM simulations and the comparison between the experimental data and numerical modelling is performed. Mechanical features that are compared include: initial stiffness, first cracking stress and strain, average second-stage stress and strain and ultimate stress and strain. The details of these comparisons are summarized as follows.

- **TRM containing PBO fibers using clamping grips:** the percentage error in the values between the experimental and numerical data is significantly high for initial stiffness and ultimate stress where it is 38.04% and 43.14% respectively. However, the data obtained from the research work shows relatively high strength values for the PBO fibers as compared to other fibers. First cracking stress values have a low error which shows a good numerical adaptation of the experimental activity pointing out a very close to real crack initiation point.
- **TRM containing PBO fibers using clevis grips:** again, we observe the similar trend as witnessed in the case of TRM containing PBO fiber using clamping grips. The percentage error in the values between the experimental and numerical data is significantly high for average second stage stress and ultimate stress (30.15% and 32.08%) while the first cracking stress and strain, average second-stage strain, ultimate strain and initial stiffness values are significantly close, which shows a good numerical adaptation of the experimental activity pointing out a very close to real crack initiation point.
- **TRM containing carbon fibers using clevis grips:** there is a close relationship between the numerical and experimental data with very low percentage error values. Most noticeable error in the comparison is the percentage error in the values of average second-stage strain (21.14%). The rest of the values are significantly closer to each other.
- **TRM containing glass fibers using clamping grips:** in this case a significant variation can be observed between the experimental and numerical model results. Mechanical parameters such as initial stiffness (25.09% error), first cracking stress (18.5% error), average second-stage stress (8.6% error) and ultimate stress (35% error) shows large differences in the values. However, the values of strain all along the stress-strain curve exhibits comparatively low error percentage (8.6%, 8.2% and 15.03% respectively for the three stages).
- **TRM containing coated glass fibers using clamping grips:** in this case, the initial stage shows a similar trend and significantly close values for cracking stress and cracking strain in experimental and numerical model results (9% and 7.14% respectively). Similarly, for the second stage, the percentage error in the values of average stress and average strain is low (6.83% and 3.34% respectively). However,

the big variation can be observed in the case of ultimate stress (with percentage error of 22.62%).

- **TRM containing carbon fibers using clamping grips:** Values related to the initial cracking stress and average second-stage stress are significantly close (1.01% and 8.68% respectively) with a percentage error less than 10% which shows a good numerical adaptation of the experimental activity pointing out a very close to real crack initiation point and the propagation of crack. However, the ultimate stress and strain values vary significantly (percentage error of 12.63% and 18.2% respectively).

The numerical model created within the scope of this thesis performs the simulation quite effectively as exhibited by the results. However, the numerical modelling is a simulation of experimental activity where it is difficult to simulate all the factors and real conditions. Based on the activity developed within this thesis, a few suggestions could be given to improve the numerical model:

- better simulation of the gripping mechanism by creating the model of the clamping mechanism with the interaction at the joint between the clamp and the specimen.
- Improvement of the mesh quality, by reducing the mesh size.
- Improvement of the fiber grid modelling technique, by considering the actual geometry of the tensile strip enclosed within the mortar matrix layers.

Within the scope of this thesis, the numerical model is validated against the experimental results obtained by Arboleda et al. (2016); however, the validation activity can be continued by implementation of the numerical model on a number of other research outcomes on TRM systems as those discussed in Chapter 2.

From the experimental point of view, the research could be continued by conducting:

- tensile tests on bare fibers (single yarns and fiber strips).
- tensile tests of TRM specimens, investigating different clamping mechanisms.

Further mechanical characterization tests of materials (mortar, fibers, TRM composites etc.) performed in laboratory would provide a data base of material properties which would in turn provide us with accurate simulation results, by implementing the tested mechanical features within the finite element model of the TRM specimens.